Lateral Undulation of a Snake-Like Robot

by

Amit Gupta

Submitted to the Department of Mechanical Engineering
in partial fulfillment of the requirements for the degree of

Master of Science in Mechanical Engineering

at the

MASSACHUSETTS INSTITUTE OF TECHNOLOGY

January 2007

Author . . . . . .
Department of Mechanical Engineering
January 19, 2007

Certified b . . . . . .
Hani Sallum
Member Technical Staff, Charles Stark Draper Laboratory
is Supervisor

Certified by . . . . . .
Derek Rowell
Professor, Mechanical Engineering
Thesis Reader

Accepted by . . . . . .
Lallit Anand
Chairman, Department Committee on Graduate Students

Lateral Undulation of a Snake-Like Robot

by

Amit Gupta

Submitted to the Department of Mechanical Engineering
on January 19, 2007, in partial fulfillment of the
requirements for the degree of
Master of Science in Mechanical Engineering

Abstract

Snake robots have been studied by many researchers but historically more on a theoretical basis. Recently, more and more robotic snakes have been realized in hardware. This thesis presents a design process for the electrical, sensing, and mechanical systems needed to build a functional robotic snake capable of tactile and force sensing. Implementing a simple scheme which allows this capability permits the robot to laterally undulate without the use of wheels. The design methodology and implementation is detailed with schematics and a summary of results obtained from the hardware. Through manipulation of the body shape, the robot was able to move in the horizontal plane by pushing off of obstacles to create propulsive forces. It was found that lateral undulation is highly dependent on the actuator torque output and environmental friction.

Thesis Supervisor: Hani Sallum
Title: Member Technical Staff, Charles Stark Draper Laboratory

Thesis Reader: Derek Rowell
Title: Professor, Mechanical Engineering

[THIS PAGE INTENTIONALLY LEFT BLANK]

Acknowledgments

January 19, 2007

This thesis was prepared at The Charles Stark Draper Laboratory, Inc., under contract HR0011-05C-00114 sponsored by DARPA.

Publication of this thesis does not constitute approval by Draper of the findings or conclusions contained herein. It is published for the exchange and stimulation of ideas.

Amit Gupta

Contents

List of Figures

List of Tables

Chapter 1

Introduction

1.1 Snake Robots

For the purposes of this thesis, one should distinguish between snake-like robots and other robots. Snake robots generally exhibit many degrees of freedom; it is not uncommon for a snake robot to have over 10 degrees of freedom, some have 30 or more. For these robots, actuation always occurs at least in the horizontal plane but many robots also assert control in the vertical plane as well. The robot link mechanism is modular and scalable often allowing the robot to be easily lengthened or shortened up to critical values without the loss of capability. Additionally, snake-like robots are free moving unlike manipulators that are fixed at a base point. These traits provide benefits that make snake-like robots appealing while simultaneously adding complexity that makes them difficult to design and control.

1.2 Motivation

Snake robots have the potential to revolutionize many areas of robotics. Snakes are possibly the most versatile of all animals so far as locomotion is concerned as there is virtually no naturally occurring environment that snakes cannot traverse. They are able to travel over slippery surfaces, through thick brush, across boulders and even up trees. Snakes can navigate through pipes, small holes and across gaps. Certain

species of snakes have been witnessed climbing up a smooth vertical metal pipe in order to raid bird houses. Their gaits are so adaptable that greasing the poles is often insufficient to protect those bird houses. No other animal exhibits this degree of adaptability to its environment. Successfully emulating even a portion of a snake's behavior would therefore be a significant advancement in robotics.

The applications for a robot capable of traversing such a wide range of terrain are broad. A snake-like robot could potentially navigate through rubble from a collapsed structure to locate survivors. This same vehicle could be used to inspect the inside of oil or sewer pipes for damage. If the robot was small enough, it could replace endoscopes in medical procedures. The manufacturing industry could use them to inspect or manipulate objects in hard to reach places. Robots with these capabilities could even be used in military reconnaissance operations. Since the vehicle is low to the ground it would be difficult to detect and its ability to crawl through fences would increase its effectiveness. There are many uses for a robot that can mimic the movement of a snake but the research done in the field still leaves much to be discovered.

1.3 Problem Statement and Goals

This project will focus on the design and construction of a multi-segment high degree of freedom snake-like robot. The goal of this vehicle is to mimic the serpentine form of locomotion called lateral undulation without the use of wheels. All forward propulsive forces will be generated by manipulating the body posture to contact and then push off of obstacles in the environment. This robot would provide a unique platform for the development of a force based controller as, to the author's knowledge, no other snake-like robot provides tactile and force sensing capabilities. The success of the design will be shown by demonstration of a lateral undulation gait that leverages obstacles in its path.

1.4 Chapter Outline

Chapter 2 of this thesis includes a detailed background that covers snake biology and modes movement as well as previous snake robotic work as it pertains to lateral undulation. Chapter 3 discusses the detailed design of the electrical system starting with the functional requirements, through component selection to circuit design and PCB layout. Chapter 4 covers the mechanical design which includes FEA of important features, design rational behind particular components and the actuator selection. The testing of the actuators and sensors and the results of a lateral undulation gait are covered in Chapter 5. This thesis is concluded in Chapter 6 with a discussion of the design evaluation, improvements and future work.

Chapter 2

Background

There is a significant amount of research that has been done on serpentine biology, locomotion and robotics. Studying all three of these areas allows one to better understand how snakes exist in nature and how the field of serpentine robotics has evolved. Dowling published a good overview of these topics in his dissertation [12] but much has been done since then, specifically with regards to lateral undulation. As there is no single text that provides a comprehensive up to date summary of the existing research, this chapter though, will attempt to do so. Particular attention will be paid to lateral undulation.

2.1 Biology and Locomotion of Snakes

Over the course of evolution snakes have developed traits that vary wildly between species. A fully grown thread snake, for example, can measure only 11.5 cm long and have a diameter of a quarter of a cm while an adult anaconda can grow up to 10 meters long and measure up to 85 cm around. Despite such a large gamut covered by various species of snakes, they still exhibit striking similarities in their skeletal structure, sensing capabilities and modes of locomotion.

2.1.1 Structural Anatomy

The skeletal structure of a snake is mainly composed of a series of vertebrae each with a pair ribs. Just as snakes can have greatly different lengths, the number of vertebrae between species can vary from below 100 to over 400 [29]. The vertebrae serve many purposes; they provide housing for nerve tissue, provide connection points for muscle and limit joint movement.

Nerve tissue that runs through the vertebral column is secured to and protected by the surrounding bone. In order to minimize the strain on the nerve tissue, the spine is very inelastic to longitudinal tension and compression. The structure of the vertebrae restricts the degree of lateral and ventral movement between two adjacent joints. Typical values for lateral articulation across species are 10-20 degrees while ventral freedom is limited to about 10-15% of that. The structure, while allowing movement along those two axes, prohibits rotational displacement between vertebrae greater than about two degrees. It is thought that this is to prevent damage to the nervous tissue while allowing required flexibility during particular gaits [28]. Examining Fig. 2.1.1 one can see the cavity towards the center of the vertebrae, labeled as nine, through which the nerve tissue runs. The labels three and four refer to the skeletal features which limit torsion; features six and seven limit the ventral flexing.

The tendon and muscle system interconnect various ribs and vertebrae as well as vertebrae and skin. This allows a snake to actuate its skin with respect to its vertebrae which is important for rectilinear motion as discussed in §2.1.3. The skin is composed of overlapping smooth scales. The scales serve a dual purpose of aiding in protection and in locomotion. Since the scales are hard and smooth they allow the snake to slide along with ground with minimal friction while protecting against sharp or rough protrusions in the environment. Studies done by Gray show that coefficient of friction between a grass snake and various substrates can vary from μ=0.2 to μ=0.4 [16]. He also showed that a snake's belly scales exhibit a directional dependence on the coefficient of friction. It was found that μ was lower in the longitudinal direction (along the snake going from head to tail) than in the lateral direction (perpendicular

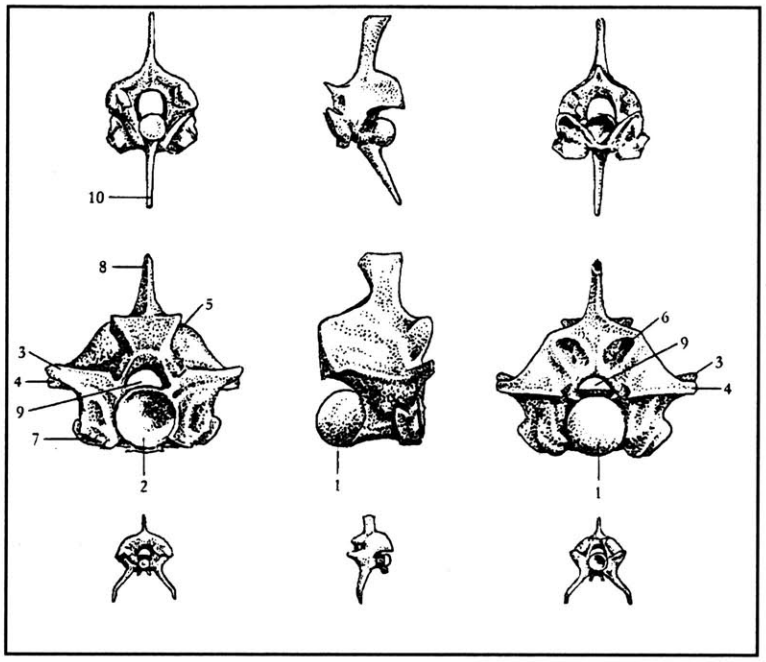

Figure 2.1.1: Snake vertebrae limit joint articulation while providing an anchor for muscles and protection for nerves. Figure from [12].

to the longitudinal direction). According to his measurements the difference is rarely greater than a factor of two; additionally, μ for the lateral direction is not greater than 0.4. This data is supported by Moon [30].

2.1.2 Sensing and Control

In order to give the snake maximum power and control over its body, a single vertebrae is linked to many different other vertebrae and ribs. A particular vertebra can be connected to as many as 40 different muscles. This allows several different muscles to act on a specific area of the body thereby increasing the available maximum force. This also relaxes the strain requirement on any single muscle which reduces fatigue and energy expenditure [29]. Additionally, this highly redundant interconnectivity allows a snake to have great control over its body posture, the force distribution between its body and the environment as well as the force distribution within its body. Control of all this allows snakes to locomote via position control, impedance/force control or a hybrid control dominated gaits. Two of the most common gaits observed in snakes are sidewinding, which is mainly a position controlled mode of locomotion,

and lateral undulation that is predominantly force controlled [18].

The vast amount of feedback a snake gets from its skin and muscles assists its ability to control itself. A snake's skin is very pressure sensitive thereby giving the snake full tactile sensing. When a portion of a snake is in contact with the environment, the snake is able to sense where the contact is and the reaction force at that location. Since a snake's vision is generally very poor, the feedback required for the gaits is provided almost exclusively through tactile sensing. While this seems to be generally accepted there is some dissention as to the reliance snakes have on vision regarding locomotive tasks [31] [41].

2.1.3 Gaits

Snakes are able to locomote via a variety of gaits, the four primary gaits are sidewinding, lateral undulation, concertina and rectilinear. Other less frequent modes of transport include slide-pushing, saltation, and "flying". Use of these gaits depends on the terrain, the physical characteristics of the snake and the presence of dangers or other motivations. All of these gaits are discussed below with the exception of lateral undulation which is covered in §2.2.

Sidewinding

While sidewinding, a snake will lift up sections of its body and place them along the direction of motion as illustrated in Fig. 2.1.2. As can be seen, the motion is periodic with each body segment performing the actions of those segments anterior to it. The placement of the head determines the direction of travel, with any changes to the periodic motion originating at the head and then propagating down the body. Burdick reported that snakes generally establish three ground contact points but may briefly only have two [7]. The motion dynamics were described on a basic level by Hirose as two sine waves propagating along the body; one in the vertical plane and one in the horizontal plane. The gait can be controlled by varying the amplitude, phase offset, and frequency of these two waves [18].

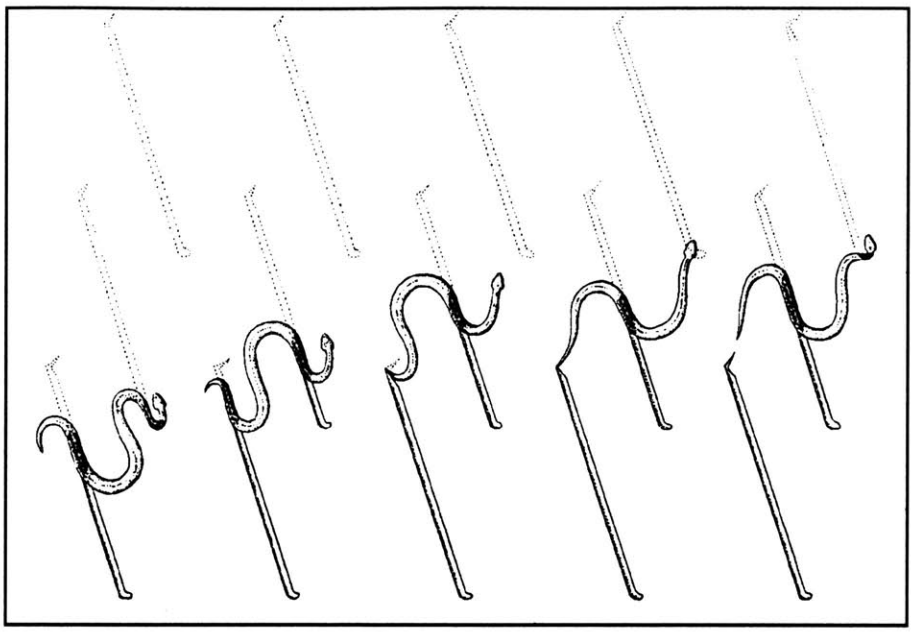

Figure 2.1.2: Sidewinding results from wave propagation down the body of the snake in both the horizontal and vertical planes. Figure from [12].

Sidewinding relies on static contact with the ground but is ironically used most often in environments with slippery flat surfaces. As stated above, sidewinding relies on two to three points of static contact with the ground. The body weight is distributed among these few points thereby increasing the maximum frictional force at those locations. This allows the snake to exert a greater force on other segments of its body and therefore move faster. It is thought that different modes of locomotion are chosen for their efficacy in a particular environment and the energy used. The energetic costs of various modes of locomotion though, are still in debate as there have been many studies that counter each other [45]. For example, snakes can laterally undulate through sand yet they typically sidewind instead. It is thought that sidewinding may be more energy efficient but other factors may play a role as well. While in the desert, snakes may prefer sidewinding motion as it reduces the amount of body surface in contact with the hot sand therefore minimizing the head absorbed from the environment. In other settings where big rocks are present or the sand has large grains and is very loose, snakes will laterally undulate. The best conclusion drawn from these observations unfortunately is that gait selection has many factors.

Concertina

When snakes are in areas too tight for sidewinding they will usually resort to concertina locomotion. A snake in a narrow channel will press segments of its body against the sides of the channel which increases the normal reaction force and therefore the static frictional force. It will then either extend out its body length ahead of this section or pull up the length behind it. By progressively alternating this pushing and pulling, a snake can even move through slippery channels. Snakes may even slightly lift the sections of body that are being pulled or pushed to decrease the friction of that segment, a process called sinus lifting. To conserve energy those segments are rarely lifted completely off the ground surface, rather a portion of the segment's weight is supported by the joints that are pressed against the channel. An illustration of this progression is displayed in Fig. 2.1.3. The last frame of this figure shows the snake starting to push laterally against the channel near its head. Snakes will establish a secure new hold before the previous one is released. This enables the snake to continuously progress forward [13].

Rectilinear

Rectilinear motion has been the target of much misunderstanding over the years. While performing this gait, the snake is usually laying straight and moving in the direction of the head. There is little or no visible vertical movement of the body. The snake appears to be slowly "walking" forward one body segment at a time. For this reason it was once thought that the ribs were actuated and acted as legs slowly walking the body forward. That is not what happens though and this motion is actually similar to concertina. Instead of the snake body pushing against the walls of a channel though, it pushes against the ground. As in concertina, the snake will actuate certain segments at a time and the weight of these segments is partially supported by the adjacent ground contact points. Then, utilizing the muscles that connect the skin to the ribs and vertebrae, the snake will move its skin forward with respect to the vertebrae and ground. In this manner the snake can advance.

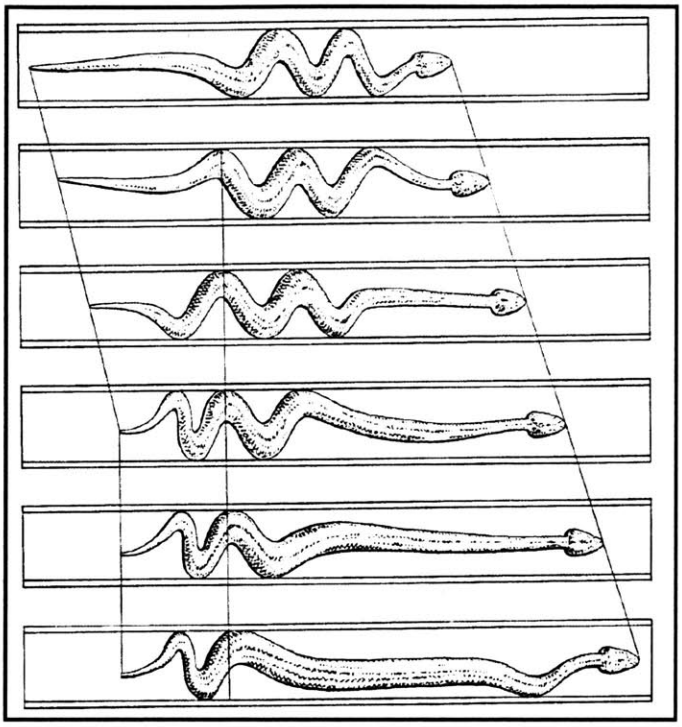

Figure 2.1.3: Concertina resembles an accordion motion and is used in narrow areas. Figure from [12].

This gait is often used in very tight channels where the walls are very close to the sides of the snake and the accordion-like posture required for concertina is not possible. It is also used more often by larger snakes as the limited amount of motion opposing gravitational forces minimizes energy expenditure. Gaits such as sidewinding can be very taxing for large snakes. Additionally most of the larger snakes such as anacondas exist in tropical areas where wide open spaces, the ideal terrain for sidewinding, is not present. [13]

Other Gaits

Slide pushing occurs when the body of the snake vigorously undulates from side to side in an effort to push the body forward. Slide pushing most often occurs when a snake is on a smooth surface and gets startled. Because this gait is not an effective means of escape, as it is slow and very energy consuming, a snake will often soon change to a different gait. Slide pushing can have some benefits though when used in conjunction with other gaits. Gray observed that when snakes are laterally undulating

over a slippery surface studded with unevenly spaced vertical pegs, portions of the body could undergo slide pushing in an effort to increase the forward thrust while the rest of the body would continue laterally undulating [16].

Other less common forms of locomotion include saltation and "flying". During saltation a snake will coil its body and then rapidly extend it out. In this manner a snake can effective jump. This movement is energy intensive and has not been found in the larger snakes. Though snakes are not known for their aerodynamics some species can glide though the air. This behavior has been found in certain tree snake whereby they spread out their ribs and their belly becomes a very rudimentary parafoil and the snake undergoes a controlled fall to its destination.

2.2 Lateral Undulation

Lateral undulation, sometimes called serpentine motion, is perhaps the most interesting of all the modes of locomotion snakes can perform because of its complex mechanics. Motion via lateral undulation requires a delicate balance of multiple force vectors and intricate manipulation of body posture. Unlike most forms of movement performed by animals or robots where obstacle avoidance is important, the exact opposite is true about lateral undulation. During legged or wheeled locomotion, obstacles such as rocks and trees must be navigated away from as they can impede or completely disrupt motion. Snakes employing lateral undulation, however, leverage those very obstacles to provide forward propulsive forces. By steering towards obstacles, snakes are able to move faster and more efficiently than if they did not.

During lateral undulation, a snake's body is in sliding contact with the ground. As Gray found, though snakes exhibit a directionally dependant coefficient of friction, this difference is small. While this difference makes it possible for a snake to move forward over smooth ground, progression would be slow and less efficient than other gaits. If however, the snake were able to push off of protrusions in the environment the maximum possible speed and efficiency both increase. When a snake pushes on an object, the force the object pushes back with can be broken down into two com-

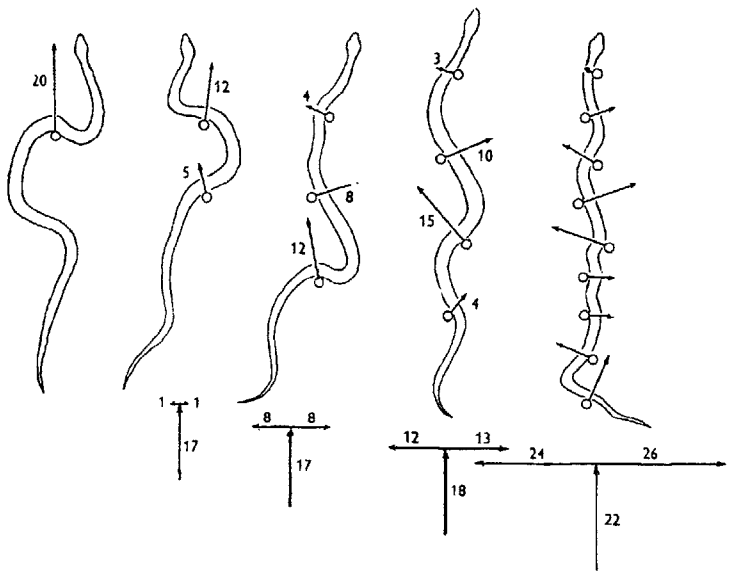

Figure 2.2.1: As a snake contacts more pegs its body straightens out but the forward pointing force vector remains relatively constant.

ponent vectors, a component tangent to the desired direction of motion and another component perpendicular to that direction. The vector that is tangential provides the propulsive force while the perpendicular one is canceled out by friction and other reaction forces. These results were found by Gray and are illustrated in Fig. 2.2.1. [16]

Gray was one of the first to study lateral undulation in depth and publish his results. He found that snakes undulating through an array of vertical pegs would create reaction forces such that the tangential component was relatively constant with respect to the number of pegs in contact whereas the normal component would increase dramatically. These reaction components are illustrated at the bottom of Fig. 2.2.1 where the measured normal reactions vary from 1-26 gram-force but the tangential reactions range from 17-22 gram-force. This seems to say that the forward speed is independent of the number of contacts between the snake and its environment. Bennet, however, showed a correlation between the two by measuring speed while varying the spacing between the pegs and body length of the snake. He found that as the ratio of body length to peg spacing decreased, so did forward speed [6]. It is thought that contact with multiple pegs prevents lateral slippage thereby allowing all

the movement to contribute to forward motion.

During lateral undulation, the body of snake follows a single path therefore all body segments contact the same obstructions at the same angles. The head of the snake determines the direction of travel by setting the path for the body. During tests done with a snake pushing against a single peg, Gray found that the force exerted on the peg during the entire motion was relatively constant as shown in Fig. 2.2.2. This indicates that as snakes undulate, the force distribution on the environment does not change. While the snake progresses, points of contact are propagated down to the end of the body until they are no longer within reach. As the head encounters new obstacles, the angle and force of contact is determined by these lost points of contact. Because of the discontinuous nature of this gait, transitory periods of acceleration are experienced but tend to be minimized. For a particular environment, a snake's body will travel over the ground at approximately a constant speed.

One trait to note from Fig. 2.2.2 is the large degree of curvature of the body immediately anterior to the peg. Moon found that a higher degree of curvature is indicative of larger forces being exerted. In these cases, he also found that the force component normal to the desired direction was small. This same characteristic can be confirmed from Gray's results as well by examining Fig. 2.2.1. This behavior is not surprising. In order to create a reaction force parallel to the desired direction of travel, the body's tangent vector at the point of contact must be normal to the direction of motion. Because of the differential skin friction, the body's longitudinal axis is more or less aligned with the desired direction to minimize frictional forces. However, in order to subtend the angles required to create the tangent vector at the correct location, many vertebrae must be part of the curvature. During tests performed by Moon [30], there were 22-59 vertebrae contributing to the body curvature around a single peg. Since each vertebrae can have 10-20 degrees of lateral freedom, a large degree of body curvature is possible over 59 joints.

In his book [13], Gans states that the body curvature sometimes required by lateral undulation makes it ill suited for larger snakes. Large snakes such as constrictors tend to have a higher body diameter to body length ratio. The higher aspect ratio

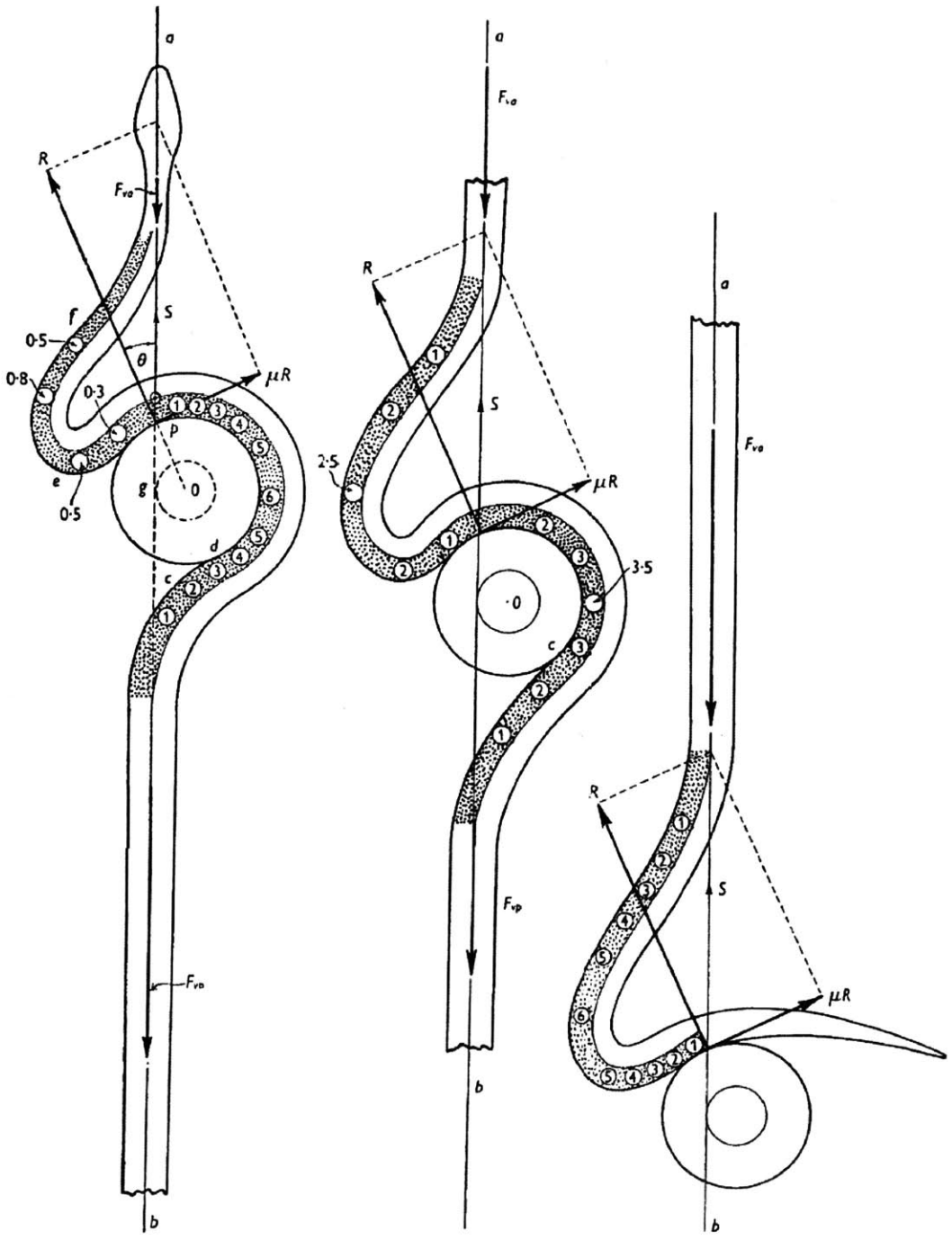

Figure 2.2.2: As an obstacle moves down a snake's body, the force and angle of contact remain constant.

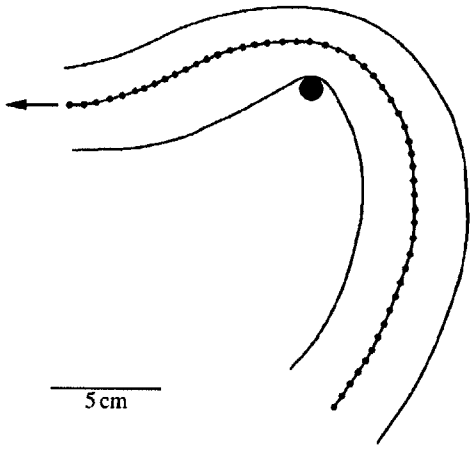

Figure 2.2.3: The body of the snake locally deforms when the snake pushes against a peg.

combined with the number of vertebrae required to subtend the ideal body curvature does not allow the freedom needed by the remaining body length to effectively undulate. When concerned with robots however, this claim does not apply. Snake-like robots can easily be constructed to allow 90 degrees or more of lateral actuation between two joints. This permits large body curvature to take place over relatively few vertebrae thereby eliminating one problem associated with high aspect ratio snakes.

Despite all the research done on snakes, there is some debate regarding certain aspects of lateral undulation. The biggest point of contention regards the fundamental mechanics of lateral undulation. Gasc claims that navigation around a single peg involves different mechanics than movement through an array of pegs [14]. Moon, however draws a parallel to a cam follower mechanism and claims that the basic motion is identical [30]. The second debate involves deformation of the body wall when pushing against a peg. Moon observed this and provided the illustration found in Fig. 2.2.3. He suspected that this deformation contributed an important factor to the dynamics of lateral undulation. It is not clear from his data whether this deformation changes the direction of the reaction force from perpendicular to the general body curve to perpendicular to this local deformation. It is possible though, that this deformation is the unavoidable result of the body's elasticity and plays no significant role in lateral undulation.

2.3 Previous Snake-like Robots

Robots capable of imitating snake-like locomotion are of great interest to many people because of their wide range of applications. There have been several robots that exhibited some form of snake like motion and they run the gamut in their mechanical complexity, sensor integration, and control methods. For the purpose of placing the present research in the context of prior achievements we will concentrate mainly on snake-like robots and control techniques that have been implemented in hardware for laterally undulating vehicles. These vehicles are best separated by their construction, wheeled and non-wheeled, as the hardware configuration and control methods greatly affect each other.

2.3.1 Wheeled Robots

Some snake robots are actuated in only the horizontal plane and employ passive wheels, similar to the diagram in Fig. 2.3.1. Laterally undulating with passive wheels provides significant benefits but also limits the robot's range of application. The wheels provide an idealization of the frictional properties exhibited by a snake's skin. Gray found that their skin shows a directional dependence on coefficient of friction which he postulated played an important role in lateral undulation. The wheels provide this difference but to a much larger degree than actually found in snakes. While laterally undulating, snakes get the majority of their propulsive force by pushing off of obstacles in the environment. Wheels act as these obstacles by providing reaction forces perpendicular and tangential to the desired direction of motion. With wheels acting in this manner, obstacles need not be sought out and reaction forces are more easily controlled. Issues such as maintenance of contact between the robot and obstacle do not arise. Additionally the wheels tend to cause smoother movement and allow the controller ignore many frictional forces. Unfortunately wheels also limit the robot to hard smooth surfaces in a fairly uncluttered environment. Despite some of the profound differences between wheeled robot locomotion and snake locomotion, much has been learned from them.

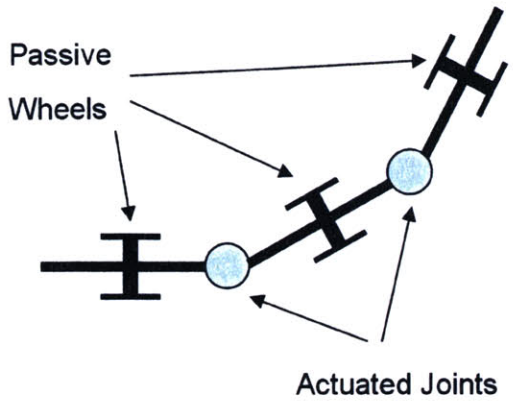

Figure 2.3.1: Top view of a typical wheeled snake robot. The wheels are passive and the rotational actuation takes place in the plane of the page.

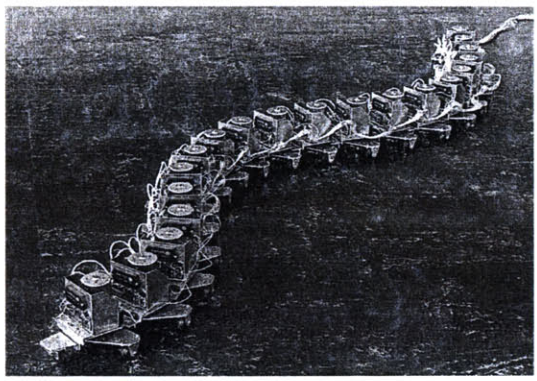

Figure 2.3.2: The ACM was one of the first snake robots and utilized wheels to mimic snake locomotion.

Hirose

Some of the first work on snake robots was done by Hirose and Umetani. They coined the term ACM, or active cord mechanism, for their robot. Hirose's work concentrated on lateral undulation and the robot presented in his comprehensive text [18] was designed to achieve this gait. The robot was based on his analysis of real snakes and the design framework he developed. This framework outlined actuator and joint requirements based on gait parameters such as the wavelength and speed desired and their effect on minimum actuator torque and power. Using these guidelines Hirose developed the robot in Fig. 2.3.2.

On the ACM robot, Hirose implemented lateral undulation via the serpenoid curve discussed in §2.2. Since the only feedback was joint angle, the control loop was

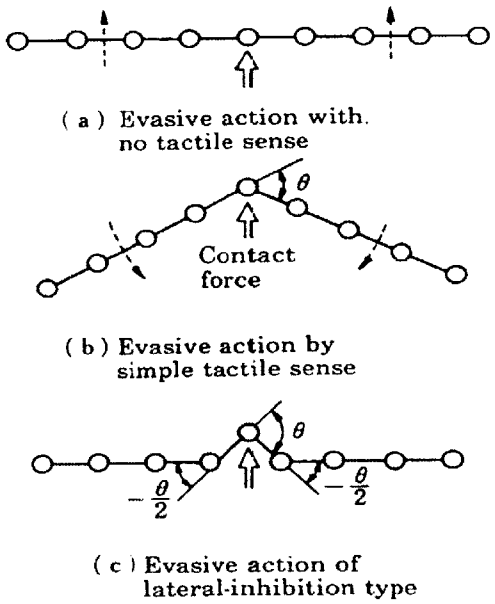

Figure 2.3.3: Hirose implemented lateral inhibition on the ACM which allowed it to hug objects and traverse a maze.

around position. The desired angular position was calculated at the head module and then propagated towards the tail. By regulating the propagation delay, Hirose was able to control the speed of forward motion. Steering was accomplished by adding a bias to the desired position fed to the head unit. A constant bias would produce circular motion of constant velocity. Therefore steering to a desired direction could be effectively achieved by adjusting the amount of bias and the time the bias was applied. In his robot, steering was controlled by a human operator. Though lateral undulation lends itself better to force control, he was able to demonstrate the efficacy of controlling body posture to attain undulating locomotion.

The next design iteration included limited tactile feedback in the form of binary on/off switches. The new control scheme incorporated lateral-inhibition whereby when joint i encountered a tactile sensation, joint i, i+1 and i-1 reacted in a manner to move joint i away from the input therefore eliminating the contact [44]. The basics of this control scheme are depicted in Fig. 2.3.3.

Hirose and Umetani were able to achieve some remarkable results using this seemingly simplistic scheme. Ironically, the lateral inhibition controller which meant to

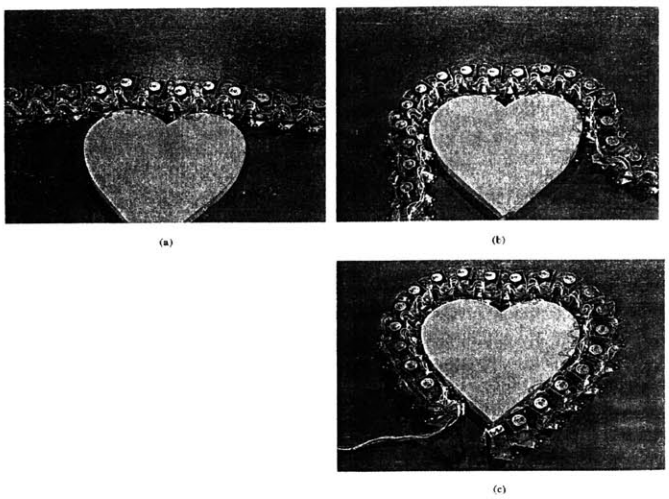

Figure 2.3.4: The tactile sensors and new control scheme allowed the ACM to coil around arbitrarily shaped objects.

avoid contact, enabled the ACM to coil around and hug objects it encountered. Figure 2.3.4 depicts the ACM wrapping itself around an arbitrarily shaped object. Though this may seem counter intuitive for a scheme meant to avoid contact, the benefit makes more sense when put in another context. When the ACM was placed in a narrow channel maze, it was able to hug the walls and produce forward propulsive forces. The combination of "evasive" action overlaid on the previous position control loop allowed the ACM to navigate autonomously through the channel. The tactile sensors at the head would determine the body shape bias which would then be sequentially sent down the body. A picture of this experiment is shown in Fig. 2.3.5. [17]

For the previous two tests, the wheels were replaced by omni-directional ball casters. In the case of maze traversal though, casters are essentially the same as wheels as far as propulsion is concerned. The maze walls prevent sideslip and only allow displacement in the tangential direction, exactly like wheels. Since all the joints are in contact with walls and the channel is roughly the width of the ACM, the reaction forces are very similar to the free moving wheeled case. This did represent important progress though as it showed forward propulsion was possible without strict adherence to the serpenoid curve. It is important to note though that all the maze sections had a roughly sinusoidal shape similar to the serpenoid curve. One

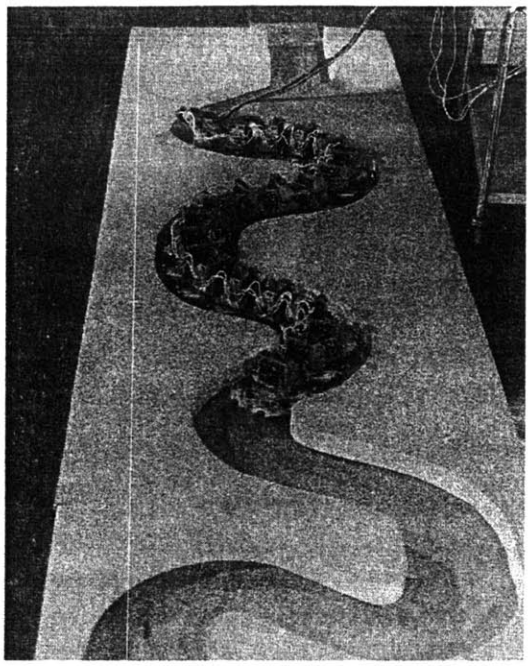

Figure 2.3.5: The ACM traverses a narrow channel maze using ball casters instead of wheels.

interesting observation Hirose made was the existence of a minimum required speed for maze traversal. If Hirose lengthened the control signal's propagation delay too much, the propulsive action would cease and the ACM would be stuck.

Shan

Much of the work done by Yansong Shan was completed by 1995. His first snake robot, the MS-1, employed ball casters and sharpened pins that were actuated in the vertical plane. The solenoids that activated these pins could drive them into the ground surface to provide an anchor point for the robot [39]. An image of this robot is displayed in Fig. 2.3.6. At first glance it may seem that the robot is laterally undulating but as pointed out by Dowling [12], this gait is a form of concertina. This author believes it is more appropriately a hybrid of concertina and rectilinear. By examining the motion of the robot as illustrated in Fig. 2.3.7, one can see that the body shape and movement of body waves is similar to concertina. However, since the reaction forces are provided by the ground and not the walls of a channel, the gait also closely resembles rectilinear motion. It is important to make this distinction since

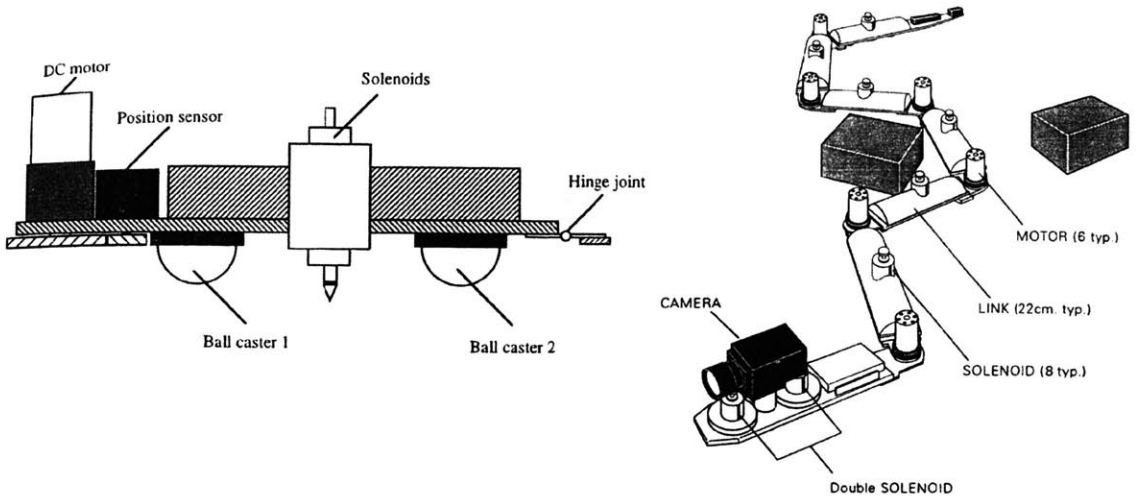

Figure 2.3.6: Shan's MS-1 uses solenoid driven pins to provide a point of action for reaction forces.

concertina motion generally requires stronger actuators with better force control.

Like Hirose's ACM, the head module of the MS-1 determined the new joint angle required which was then sequentially sent down the body. The MS-1 was however equipped with a video camera which enabled it to seek a target goal and autonomously guide itself towards that goal. This was a significant step forward from Hirose's work where all target directed steering was done by an operator. Another important contribution made by Shan was the concept of obstacle accommodation [40]. Shan developed a framework of motion planning for fixed base multiple degree of freedom (DOF) manipulators. This work was largely founded on inverse kinematics. This work allowed the manipulator to encounter an obstacle and proceed with the task while obstructed at unknown points on unspecified links. The results were demonstrated in simulation for a two DOF manipulator. Though the methods are computationally intensive for a snake robot with much greater than two DOF with further development it could provide a good platform for motion planning of a lateral undulation gait in an unstructured environment.

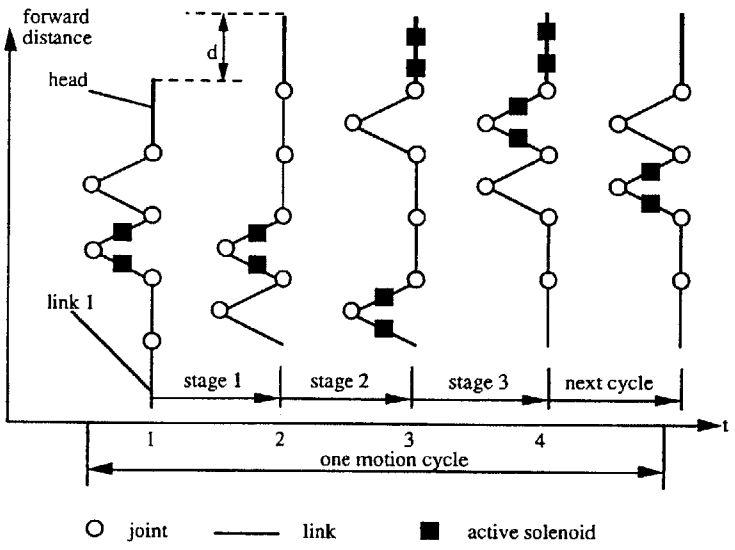

Figure 2.3.7: The MS-1 exhibits a concertina-rectilinear hybrid motion.

Ma

Some of the most recent work on wheeled lateral undulation was done by Shugen Ma. His work directly extended Hirose's and built off of all the same principals. Ma reformulated some of Hirose's basics though by proposing a new body posture for lateral undulation called the serpentine curve. He showed this curve to be more efficient for lateral undulation based off of snake muscle models he derived. Using those models he was able to predict the force a body segment could exert given its curvature and muscle structure. This force could then be broken down into its components which are normal to and tangential to the direction of motion. Ma defined efficiency as the ratio of tangential force over normal force. On this basis he found that the serpentine curve could be twice as efficient as the serpentine curve while only using 20% more power. Ma then implemented this control scheme in both simulation and hardware. His robot's basic construction architecture was similar to Hirose's as was his implementation of propagating control signals down the body segments. The important outcome of his robot was proof that the serpentine curve could be realized in hardware. [24] [25] [26]

2.3.2 Non-Wheeled Robots

Much of the past work on non-wheeled lateral undulation has been done mainly in simulation. More recently, specifically within the previous four years, this work has transitioned to hardware. The work done in simulation present very good theoretical controllers to perform lateral undulation but are generally not realizable in hardware. The simulations typically assume perfect knowledge of contact with obstacles and the force of interaction with the environment and other joints. Many of the simulations also assume perfect control over interaction forces which would require infinite resolution on joint angle. Moreover, many of the controllers devised are very computationally intensive as found in [3] where a 12 segment robot was modeled and each iteration step required over 70 hours. While this is definitely the exception and not the rule, even calculation times longer than a few seconds may prevent useful results as Hirose reported an minimum speed required for his robot to successfully laterally undulate through the maze. For completeness a comprehensive survey of simulation studies can be discovered in [1] [2] [3] [4] [5] [10] [11] [15] [26] [27] [35] [38] [43] but these will not be discussed. Rather implementations that involve hardware are presented below.

Nilsson

Most of Martin Nilsson's work concentrated on the design of snake robot joints, but he also studied snake locomotion and gait generation based on surface friction. He approached the task from a mechanical design driven view whereby control methods were dictated by the axes that were actuated. Additionally he emphasized the need for torsion free joints in order to maximize torque transfer from joint to joint. Some of the most significant work relevant to this section was on control of gaits without the aid of directional dependant friction. He tested his robot under these conditions while controlling the body shape to be a moving wave of circular arcs. He showed that forward progress was possible though it was occurred at approximately one quarter the speed than in the case where directional friction was present. He also noted that

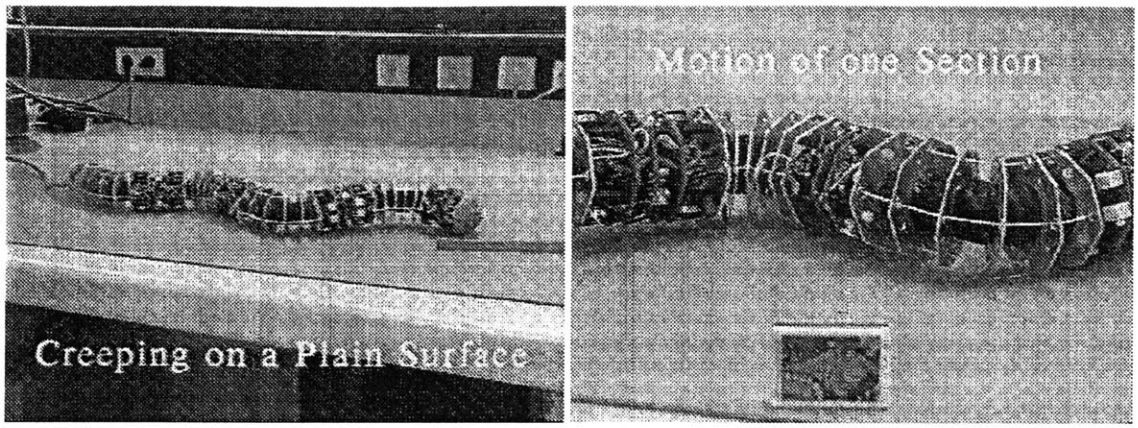

Figure 2.3.8: The GMD robot uses a cable pulley system to emulate muscular actuation. The body segments are connected by rubber joints which results in a smooth body curve.

the direction of progress was dependant on the ratio of tangential to normal friction. [32] [33]

GMD

The GMD-snake was a project in Germany to develop a non-wheeled snake. Their robot was very novel in its design. The robot was composed of many metal plates that acted as the vertebrae. The vehicle was divided up into six sections where all the vertebrae in one section were connected together by cables. These cables were attached to pulley and acted as muscles by providing a tension force on the metal plates. Each metal plate was attached to the body by flexible rubber joints. This construction allowed the body shape to be a fairly smooth curve even in the presence of external forces that deformed the body shape [34]. The controller employed a set preprogrammed motion primitives that would be assembled together by a higher level controller to achieve the desired gait. Using this method the team was able to achieve a basic creeping form of movement [46]. This robot was significant in that it most closely mimicked the actuation methods and body structure found in snakes. An image of the GMD has been provided in Fig. 2.3.8.

Lewis

The most recent work done on non-wheeled lateral undulation was performed by Sam Lewis. He built a servo based 11 segment robot from sections of PVC. The head module had infrared range sensors which were used to detect obstacles. Gait generation was performed by the head unit and then the position commands were shifted to the other links. His robot successfully navigated through a field of evenly spaced pegs using the data gathered by the infrared sensor. The vehicle would steer towards obstacles with the intent of leveraging them for forward propulsion. From examination of his results it is doubtful that this was ever achieved. The robot appears to propagate itself forward based on joint movement and ground friction instead of from forces provided by the obstacles. While this claim cannot be completely confirmed from his work, the reported results are unclear at best. [23]

Saito

Masashi Saito and his team approached the problem of non-wheeled lateral undulation from a modeling perspective. They formulated models of the friction and body dynamics for simulation purposes as well as controller development. They were the first to address this problem in a modeling, analysis and controller synthesis framework. Feedback sensors included local joint angle sensors as well as an overhead camera to detect body orientation and forward heading. Body posture was determined by the serpenoid curve but the serpenoid curve parameters were based off simulation values to maximize efficiency given the friction and body model. Using the simulation, they were able to derive optimal gait parameters for different ratios of tangential friction and normal friction between the snake and the ground. In this manner, their approach was not limited to merely a single configuration of robot or environment but was applicable to many different scenarios. Their experimental results confirm their ability to control to a desired velocity concurrent to a desired direction. Though the system exhibits an oscillatory error to both controlled outputs, the mean output is remarkably correct. Because of the completeness of their approach and their amazing

results, this work is perhaps the most important and pertinent to non-wheeled lateral undulation. [37]

Chapter 3

Electronics

The electrical subsystems of this vehicle replace the nerves, brain and sensing capabilities of a real snake and therefore are arguably the most important part of the robot. Many times one can compensate for mechanical design flaws within the electronics and controls but not vice versa. This difference highlights the importance of the electrical design. The entire design process is discussed in this chapter starting with the requirements, going through the sensor selection and circuit design to the component selection and finally ending with the printed circuit board layout. Improvements to the electrical design will be discussed in §6.2.

3.1 Functional Requirements

Each joint of the robot must have certain capabilities for lateral undulation to be possible. Broadly, the joints must be able to support sensing, communication, processing, and actuation functions while minimizing the board area, cost and maximizing flexibility for development. These functions should allow the robot to operate at a mechanical frequency range of 0.1Hz to 1Hz.

3.1.1 Processor

The processor's role in the robot can vary greatly depending on the control implemented. If all the desired states are externally calculated and then transmitted to each joint, then the local joint processor does not have to do much calculation. In this case the processor controls the joint to the desired state but it is mainly a communications controller. If the controller is implemented at a joint local level, the calculation requirements will be much higher. This implies the processor will likely need to handle signed floating point numbers, carry out many calculations, support many variables and possess built in higher math functions. For the purposes of this robot though, control will be done mostly off board to simplify the system architecture and implementation.

With some of the processing requirements lifted off of the microcontroller, it is best to examine the other attributes desired. Firstly, the processor must be fast enough to allow communication at the speeds required. For maximum flexibility, the processor should permit transmission speeds up to 0.5Mbps. Assuming each joint's state is 32 bytes and there are 16 joints, this would allow a maximum sampling rate of 1KHz. With a body frequency of 1Hz, a three decade difference in sampling frequency should be more than adequate for control. If all other processes on the microcontroller happen much faster than 1KHz, then this sampling rate is achievable.

The microcontroller must have enough input/output pins to interface with all the sensors and communication lines. Size and power consumption should not become a driving force for board size or battery selection. Ideally the microprocessor would be easy to implement in hardware and software. According to Paul Horowitz [19], it is often best to use a processor that has a large amount of documentation and support. He also recommends using the same processor that one's peers use to facilitate implementation and troubleshooting.

3.1.2 Sensing

Knowledge of obstacles in the environment is vital for lateral undulation. The scope of this project will be limited to the manipulation of known obstacles. The ability to search for new obstacles and sensors that would assist with that task are left for future versions. In order to best leverage obstacles, the robot must sense the location of contact and the force of interaction. This information in conjunction with body shape data, such as joint angle, is vital to propagate the obstacle along the body. The joint angle sensor should be accurate to within the output resolution of the actuator. The tactile sensors must be able to sense location of contact to approximately ± 0.25cm and force to ± 1N. This degree of accuracy limits the force output measurement error to approximately 10% of the lowest estimated friction between a joint and the test environment.

As the control methods for snake robots evolve, the gait should be optimized to manipulate the external forces between the robot and environment as well as the internal forces. Therefore, one should design the vehicle such that the torque created from link to link is measurable. These measurements would allow one to better characterize the interaction between the robot and its surroundings. If the vehicle moved between areas with different friction such as from a tile floor to a carpet, the transition would be indicated by a rise in the internal torque measurements. By sensing a change in its environment, the robot could adjust its body posture and desired torque values to accommodate the new conditions. The sensitivity of this torque sensor should also be about 10% of the estimated friction. At full range, it should be able to detect the maximum torque the actuator is able to output.

One of the metrics for robot performance is efficiency. This can be determined from the ratio of power out to power into the system. For locomotion a more meaningful metric often used is the ratio of distance traveled to power into the system. Both of these require a measurement of power into the system. Since all the power consumed is sourced from a battery, the easiest characterization of power in is Power = V*I, which requires knowledge of battery voltage and current draw.

In order for lateral undulation to be a useful form of locomotion, the robot must be able to sense its directional heading. Joint angles give the relative displacement of links with respect to each other but data of body orientation relative to a fixed reference is needed to determine direction of movement. If the orientation of one link is known, then the orientation of the entire vehicle can be discovered. While it would be biomimetic for the head to perform this function, this sensing can occur anywhere along the body. To reduce the introduction of error, this sensing capability can be redundant with orientation determined at the head and tail, or at other points on the vehicle.

3.1.3 Communication

Certain forms of communication will be required by the vehicle no matter what type of control is used. The joints will need to receive individual as well as group commands from the head module. For this, the head module will need to communicate with any particular joint without interfering with the other joints. Under some situations though, the joints may need to move synchronously and therefore react as a group to a signal received from the head module. The communication should take place fast enough that it does not limit the motion of the vehicle. All locomotion in snakes takes place by the propagation of body waves. These waves are low frequency, generally under 1Hz. Therefore a communication cycle for the vehicle must be able to occur at a minimum of 10Hz.

The modules must be able to communicate with external devices for the purposes of control and data retrieval. For example, to communicate with a controller written in C or Matlab, the head module should be able to support a standard communication interface. Considerations include necessary voltage levels, noise immunity, handshaking capabilities and buffer requirements. Depending on the standard chosen, all or some of these must be implemented on a hardware level or be capable of being implemented on a software level. This project will interface with Matlab because of its availability and ease of use. Additionally, Matlab includes packages that use common communication standards so the selection of Matlab does not prevent one from

interfacing the snake with a different platform at a later time.

Each module must also communicate with all of its sensors fast enough and often enough to send all the required data to the head module. It must be able to access each sensor reading at any desired moment without affecting the sensor value. This data should be stored either locally on the joint or centrally by Matlab. A limited amount of feedback should be provided to the user as well. This feedback should occur during motion to inform the user of errors and provide the programmer with easily accessible flags.

3.1.4 Power Source

Every joint will need to be supplied with a maximum of six amps, three for each motor. The power source should be able to maintain a minimum voltage required for the other components to function. The power source should be small and light enough to be carried on the vehicle. An external power source could provide better performance would but also tether the vehicle. Any batteries should be rechargeable and able to provide full power for at least 10 minutes. It is estimated that a test run should not last more than one minute and it is desirable to run at least 10 tests between charging cycles. Additionally the battery should be situated for easy access when charging is needed.

3.1.5 Physical Considerations

The cost of the printed circuit board is driven by its size and therefore it is desirable to minimize the board area. Cost is a secondary motive though; as the board size is a driving factor of link size, a smaller board means a smaller link. The board should be large enough to accommodate any heat sinking required by high power areas. Heat can be dissipated through conduction to the ground plane or by convection through a heat sink. All of the circuit traces should be sized to handle at least twice the maximum possible current to prevent traces from burning out.

There will be many connection points on each joint in order to communicate with

all the sensors, other links and actuators. A failure at any connection point can disrupt the desired motion and in some cases cause the vehicle to become unresponsive. It is therefore vital that the connection points be as robust as possible. Unfortunately the vast number of connections can scale the cost of each link significantly so the connector-cable combination cost must kept low. The connectors must maintain the signal integrity despite repetitive flexing and movement of its cable. All connections should be able to withstand vehicle vibration and impact shocks between the robot and the environment.

3.2 Electrical Overview

A block diagram of the electrical system is shown in Fig. 3.2.1. Each subsystem is discussed below in detail. Broadly, the analog to digital converters (A/Ds) allow the processor to read analog voltage levels. The processor controls the servo motors' position by outputting a pulse width modulated signal. The tactile sensors detect whether the joint encounters any obstacles and transmit this data at the processor's request through the A/D. The processor maintains communication with the head module to receive the control signals. The head module can then calculate the desired states locally or via Matlab. A record of each joint's variable state is transmitted to the local EEPROM for later analysis.

3.3 Tactile Sensing

There are many technologies commercially available that sense force and location of contact. Each technology has varied benefits from sensor size, cost, accuracy, robustness, signal processing requirements, linearity, ease of implementation to repeatability. Unfortunately none of the sensors are exceptional in all the categories. The technologies surveyed for this application will be discussed below on the basis of their fundamentals and advantages. The chosen technology will then be discussed in further detail including its circuit design.

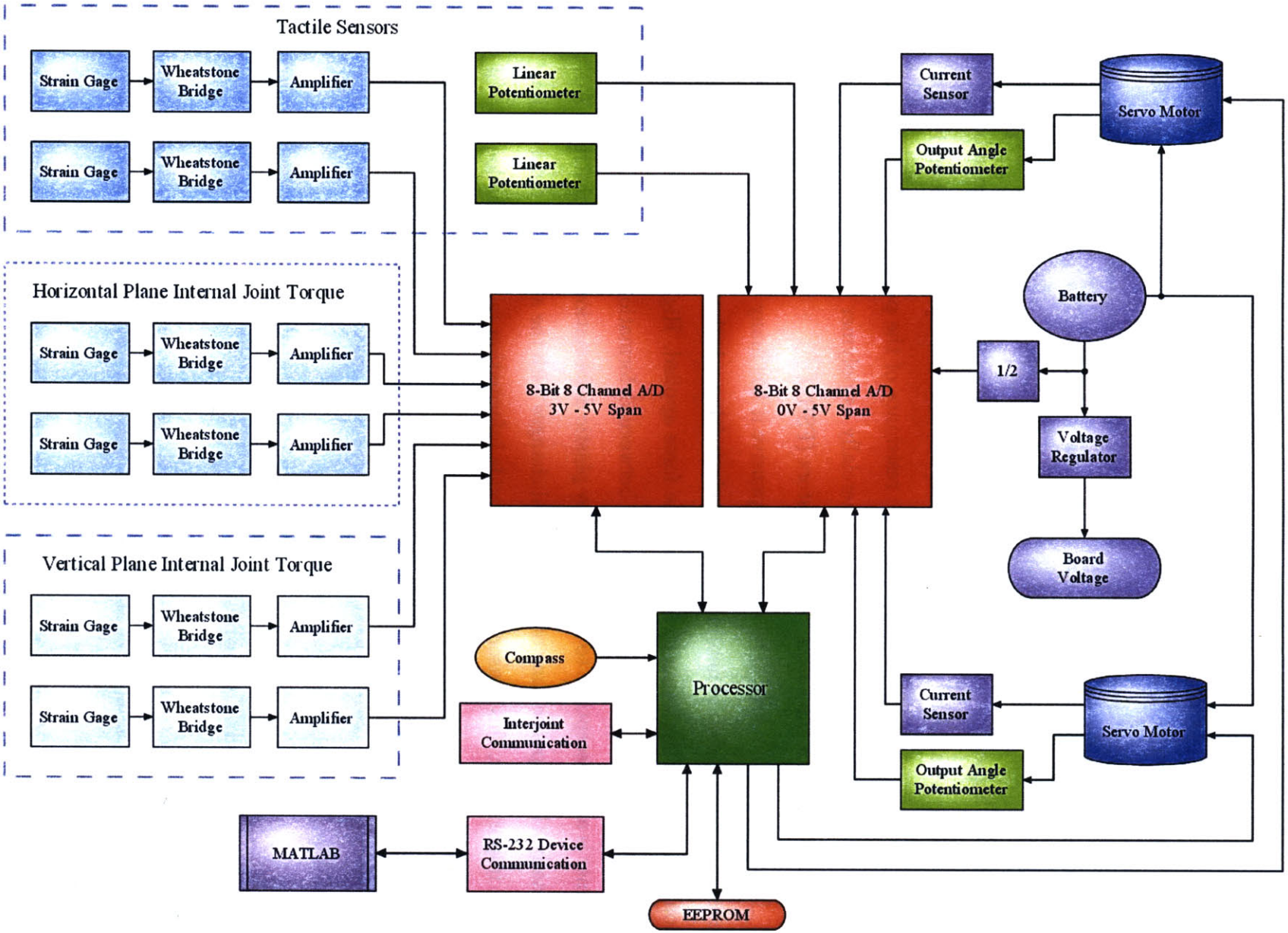

Figure 3.2.1: Block diagram of the electrical system.

3.3.1 Tactile Sensor Selection

Resistive Elastomers

Resistive elastomers measure force based on the resistance change of a polymer substrate. A nonconductive polymer is typically doped with carbon blacks or carbon nanotubes that percolate into the nonconductive structure. The addition of the carbon increases the conductivity of the polymer. The higher density of the doped agent is the higher the conductivity of the substrate will be. When the substrate, usually made of a foam or rubber, is deformed, the density of the carbon in that region increases causing a reduction in the resistance of the polymer. This is shown in Fig. 3.3.1. These sensors are sold commercially as polymer sheets or as individual components often called force sensing resistors (FSRs).

While this technology is relatively inexpensive it has many drawbacks. The force-resistance relationship is nonlinear and requires either a lookup table with interpolation or complex algorithms to calculate the force applied. Higher quality elastomers exhibit a strictly exponential relationship between deformation and resistance. The polymer is also susceptible to drift caused by plastic deformation of the substrate. Additionally, the response time of this material changes with the amount of deformation. Most importantly, this sensor does not provide information regarding the location of applied force. Location can only be determined by using an array of individual FSRs and determining which sensor is registering the force. An array arrangement requires each component to have individual signal lines. This becomes problematic because of the implied wiring and connection issues.

Quantum Tunneling Composites

Quantum tunneling composite (QTC) based force sensors are very similar to resistive elastomers in their capabilities and limitations but work off of fundamentally different principals. These sensors are made from a flexible silicone composite that is impregnated with small bits of metal. As the material is deformed the resistance across the composite can drop from approximately 10MΩ down to a few Ohms. Unlike the

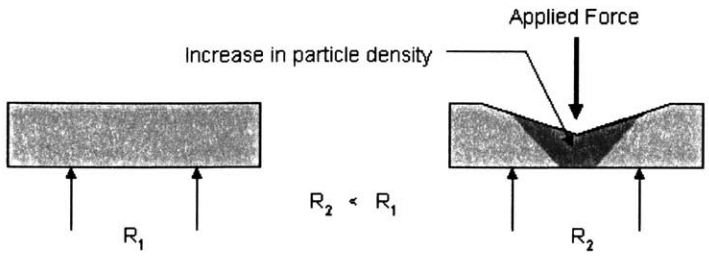

Figure 3.3.1: As the material deforms, the carbon density increases causing the resistance to decrease.

resistive elastomers that depend on carbon percolation to conduct current, QTCs rely on the electrons leaving one metal piece, "tunneling" through the silicon compound, and flowing to another piece of metal. An important note on this process is that the metal bits are always electrically insulated from each other. The current flow is based on the quantum probability of an electron exhibiting wave-like properties which allow it to penetrate the insulating silicone barrier.

Similar to the elastomers, these composites exhibit an exponential relationship between the force applied and the resistance drop. QTCs also do not yield location of force without utilizing an array formation of discrete sensors. These sensors do offer significant benefits over their elastomer counterparts. Since they are silicone based, they provide a higher degree of compliance thereby simulating a skin-like elasticity. Because of the excellent mechanical properties of silicon, the composite is highly resistant to plastic deformation. Also, measurement errors caused by drift or material creep are largely eliminated.

Capacitive Arrays

Capacitive based tactile sensors are generally packaged as MEMS or micro-machined based arrays. The sensor's design is similar to a variable capacitor. A capacitor's capacitance is determined by the surface area of the plates, the distance between them, and the dielectric strength of the material between the plates. In a variable capacitor, generally the last two properties are held constant while the surface area of the plates is varied. Since it is the area of overlap between the plates that matters,

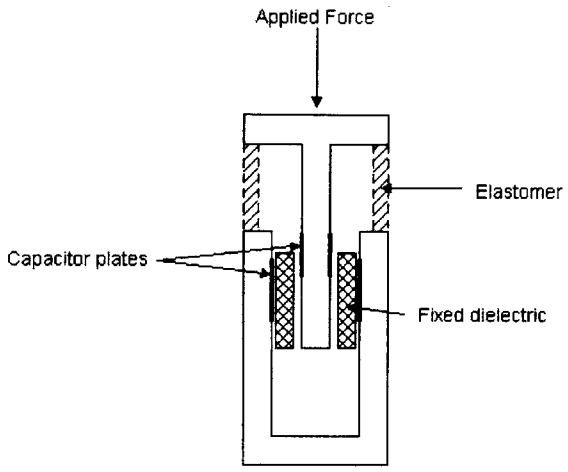

Figure 3.3.2: As the spring-like elastomer deforms, the overlapping area of the capacitor plates increases thereby increasing the capacitance.

one plate is moved parallel to the other. This changes the area of overlap and thus the capacitance. If the capacitor is designed such that a predetermined force is required to move the plates, one can measure the capacitance and then determine the force required to cause that measurement. In Fig. 3.3.2 this force member is represented by a spring-like elastomer. As the applied force increases, the elastomer deflects more thereby increasing the surface area of the capacitive plates.

Since these sensors generally come packaged as arrays, force location can be determined by the position of the activated capacitors in the array. Unfortunately, like all arrays, a large number of connecting signal wires is required. Moreover, measurement of the capacitance is typically performed using a precise current source and then measuring the time based rate of change of the voltage across the capacitor. This process is much more computationally intensive than required for the resistive elastomers. Another consideration involves system noise. The circuitry needed to support these sensors requires particularly careful design as stray capacitance can significantly corrupt sensor data.

Optical Fibers

There are many types of optical based tactile sensors and they are mainly differentiated by their method of sensing. The two classes are intrinsic sensors, which modulate the properties of the light to determine force and contact location, and extrinsic sensors that keep the light properties constant but rely on the deformation of the fiber optic cable as input. The intrinsic sensors are not suitable for this application as they require advanced detection equipment and processing to determine phase shifts and polarizations. Extrinsic optical sensors operate with a light source at one end of the cable and a reflective surface at the other. When a point force is applied to the cable, a portion of the light traveling through the cable gets blocked thereby reducing the amount reflected back. This action is conceptually similar to pinching a garden hose; as one pinches the hose harder, the amount of water spraying out is further reduced. By measuring this change in light intensity, the force and location of contact can be discovered. While these sensors offer many benefits in their accuracy, weight, robustness and ease of installation, they require too much processing overhead to be used on a self-contained vehicle and are generally prohibitively expensive.

Strain Gages

Strain gages detect the force on a rigid member by measuring the strain on the surface they are bonded to. Any force applied to an object with a measurable elastic range will cause a strain profile to exist throughout that body. A strain gage is a thin flexible resistive element that is rigidly mounted on that object. The strain within the member is transferred through the connection to the gage. Generally, strain gages consist of a resistive element that is deposited on a thin laminated film. This film will stretch or compress based on the strain, this change of length causes the resistance to respectively increase or decrease. Over their operating ranges, the gages will exhibit a linear relationship between applied strain and output resistance. By measuring this resistance and multiplying by a constant, one can recover the applied force.

These gages are simple to use if the geometry of the strain bearing member lends

itself to easy strain calculation and if the location of the force is known. In the case of a cantilevered beam, only the applied torque can be determined without knowledge of the force's location. If this location could be discovered, then strain gages would fit the application very well. The circuitry required to support strain measurement is minimal and the calculations necessary are not processor intensive. With proper installation and use, noise and drift can be largely eliminated or compensated for. For example, use of either braided wire or cable that prevents wires from moving relative to one another can greatly reduce sensor noise. Drift can be minimized by ensuring proper mounting using an inelastic glue. Additionally, temperature effects can be compensated for by choosing a gage that expands and contracts at the same rate as the substrate.

Strain gages offer many of the same benefits as the other types of sensors without the detriments, so if position could be measured as well the needs of this application would be satisfied. One method was reported by Yan-Bin Jia [21]. Jia used a metal structure composed of a "wrist" and "jaw". Forces applied to the jaw are picked up by strain gages mounted to the wrist. The arrangement of the strain gages allows them to sense in two perpendicular axes as shown in Fig. 3.3.3. With known wrist-jaw geometry, one can calculate the position and force of the contact as derived by Jia with the equation

$$\frac{\sigma_2}{\sigma_1} = -\frac{d}{32h}. \tag{3.3.1}$$

Here, σ_1 and σ_2 are the stresses gathered from the sensors S_1 and S_2 respectively, d and h are dimensions as defined in Fig. 3.3.3. Though strain gages measure strain, there is a linear relationship between stress and strain so one can calculate stress from a strain measurement. If the wrist and jaw are constructed from a stiff material such aluminum, h can be considered a constant and the equation can rearranged to yield d, the location of contact, as a function of the measured strains. Further manipulation of the strain readings yields the magnitude of the force. This method achieves force-position detection however as described in Jia's presentation requires a fair amount of calibration. After the calibration, the results reported are accurate

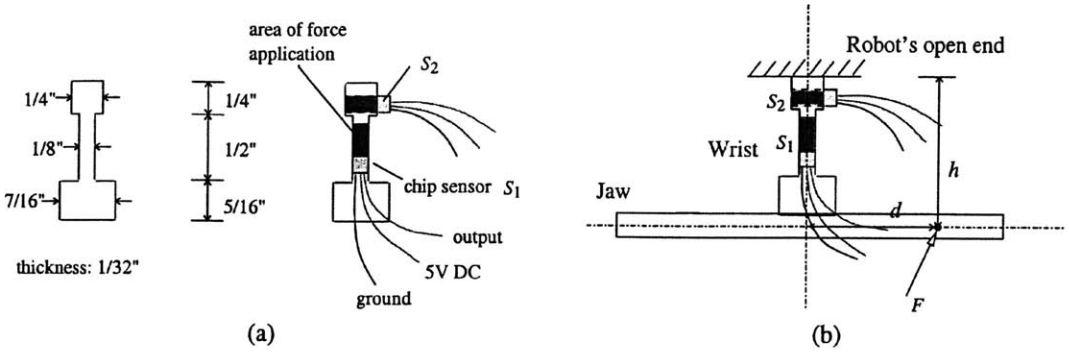

Figure 3.3.3: A force F applied at distances d and h from the neutral axes can be read by the strain gages S_1 and S_2.

to within bounds acceptable for application on this snake robot.

Another configuration using strain gages utilizes a unique potentiometer to determine position. In the case of the cantilevered beam discussed earlier, position is needed to differentiate force from applied torque. To understand this, one can briefly review beam theory. When a force is applied to a cantilevered beam, a bending moment is created within the member and can be expressed as $M = -F(L - x)$ with the variables as described in Fig. 3.3.4. From basic mechanics it is known that the stress within the beam is related to the bending moment by

$$\sigma = -\frac{My}{I} \tag{3.3.2}$$

where σ is the stress, y is the distance to the neutral axis, and $I = bh^3/12$ is the moment of inertia of the beam [36]. Hooke's Law, $\sigma = E\varepsilon$, relates the stress in the beam to Young's modulus of elasticity, E, and the strain, ε. Combining these equations we see that

$$\varepsilon = \frac{F(L - x)y}{EI}. \tag{3.3.3}$$

Since torque can be defined as $T = Fd$, the above equation shows that the strain is linearly proportional to the torque applied to the beam. Therefore by measuring the strain and location of applied force, one can determine the magnitude of the force.

In order to determine the position of the force, a unique type of linear poten-

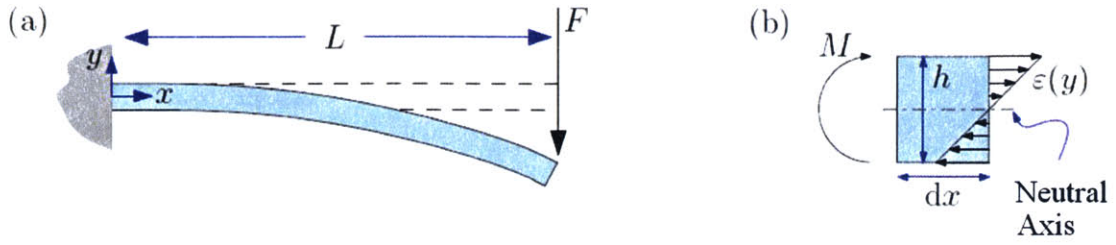

Figure 3.3.4: Diagram of a cantilevered beam. (a) Beam of length L, thickness h, depth (into the page) b, with force F applied at $x = L$. (b) Free-body diagram of beam element of length dx with strain $\epsilon(x, y)$, and moment $M(x)$. Note that y is defined zero at the neutral axis.

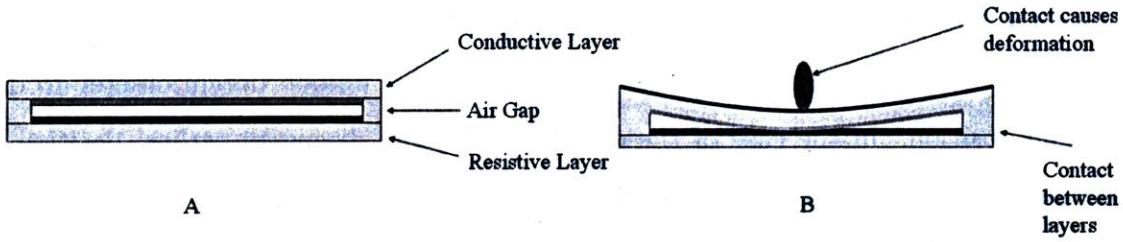

Figure 3.3.5: Unlike conventional linear potentiometers, the SoftPot relies on a compliant conductive surface to sense position.

tiometer was used. The SoftPot^{TM} made by Spectra Symbol is not a traditional linear potentiometer in that it is a compliant mechanism as illustrated in Fig. 3.3.5. This component consists of two parallel flexible substrates, one is conductive and the other is resistive. A voltage difference is applied across the full distance of the resistive layer creating a linear voltage drop across its span. The conductive layer acts as the wiper. When it is brought into contact with the resistive layer, the voltage at the point of contact is conducted to the wiper output pin. Since the voltage drop is linear across the resistive layer, the voltage on the wiper is directly proportional to the location of contact.

This method of tactile sensing was determined to be most efficient as it required the minimal number of connections, sensors, assembly effort and calibration. Additionally the potentiometer dimensions and resistance can be customized which allows for maximum flexibility with the rest of the vehicle design.

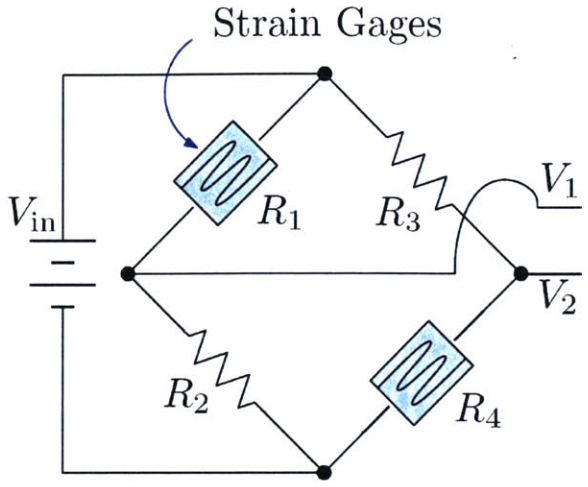

Figure 3.3.6: The voltages V_1 and V_2 vary as the resistance of the strain gages change.

3.3.2 Tactile Sensor Circuit Design

Wheatstone Bridge

Use of a Wheatstone bridge is a common way to read the input from strain gages. This circuit as pictured in Fig. 3.3.6 allows one to change the voltage at the output by changing the resistor values. The equation describing the output of the bridge is

$$V_1 - V_2 = V_{\text{in}} \left[\frac{R_1 R_4 - R_2 R_3}{(R_1 + R_2)(R_3 + R_4)} \right] = V_{\text{out}}, \tag{3.3.4}$$

where all the variables are as shown in Fig. 3.3.6. The placement of the gages in the circuit depends on their location on the beam. The design for the tactile sensor incorporates a linear potentiometer on the outside face of the strain bearing member, therefore the gages should be placed on the inside surface. Placement in this location also helps protect the sensor from damage. Placing both gages on the same surface means they will be subjected to the same strain and therefore the same changes in resistance. Given the placement of the gages, configuring them as shown in the bridge allows them to amplify the output by a factor of two.

Commonly, the resistors R_2 and R_4 are chosen to match the values of the resistances of the strain gages R_1 and R_3 (350Ω). In this case, under zero strain $V_1 - V_2 = 0$.

This is an ideal situation though where the resistances can be matched exactly to the gages. In reality, resistors tolerances vary from 0.1% to 20%. The highest precision resistors found in the desired surface mount form factor were 357Ω with a tolerance of 1%. This has the effect of biasing $V_2 > V_1$ which must be taken into consideration at the amplification stage.

If resistances lower than the nominal gage voltage were chosen then the bias would be reversed such that $V_2 < V_1$. This creates a potential problem because of where the strain gages are bonded. As determined above, the gages should be attached on the inside surface of the strain bearing member. When an external force is applied to the member, this surface is compressed causing a negative strain. Negative strains cause the resistance of a strain gage to decrease. If their resistance dropped more than 2Ω to below 348Ω, the closest 1% resistor value, the numerator of Eqn. 3.3.4 would change sign thereby making $V_2 > V_1$. This is would create a problem with the next amplification stage unless the circuit was designed to handle negative voltages. It is not important that $V_2 > V_1$ or vice versa, just that the relationship is constant.

To determine exactly how the bridge acts one must first know more about the strain gages. Gages are generally characterized by a specified value called the gage factor. The relationship between the resistance of the gage and the applied strain is given by

$$\frac{dR}{R} = GF\varepsilon, \tag{3.3.5}$$

where GF the constant gage factor, R is the nominal gage resistance, dR is the change in resistance, and ε is the applied strain. As the applied strain increases, the quantity $V_{\text{out}} = V_1 - V_2$ will change. The nature of this change can be found by differentiating Eqn. 3.3.4 with respect to R_1 and R_4 to yield

$$V_{\text{out}} = V_{\text{in}} \left[\frac{R_1 R_2}{(R_1 + R_2)^2} \left(\frac{dR_1}{R_1} \right) + \frac{R_3 R_4}{(R_3 + R_4)^2} \left(-\frac{dR_4}{R_4} \right) \right]. \tag{3.3.6}$$

Since the strain gages are mounted next to each other, their strains are equal but their relative positions in the bridge cause them have to opposite effects on output voltage hence $dR_1 = -dR_4 = dR$. Also, the relationship between strain and voltage

can be seen by substituting Eqn. 3.3.5 for dR/R above to yield

$$V_{\text{out}} = V_{\text{in}} \left[\frac{R_1 R_2}{(R_1 + R_2)^2} (GF\varepsilon) + \frac{R_3 R_4}{(R_3 + R_4)^2} (GF\varepsilon) \right]. \tag{3.3.7}$$

The above equation holds true for all strains created by pure bending moments. V_{out} is a small value, for this application it is typically 0.04V. In order to detect such a small reading, it must be amplified enough that system noise does not drown the signal. The strain gages selected are the Omega SG-7/350-LY13. This model matches the thermal expansion characteristics of aluminum thereby eliminating modest temperature changes as a source of error. Also, this package includes two parallel strain gages side by side so both sensors are installed simultaneously under the same conditions.

Voltage Amplification

Amplification is commonly done using operational amplifiers, or op-amps for short. The signals are wired into the inverting and non-inverting input terminals and their difference is then amplified. Since the signal fed into the inverting terminal, V_-, is subtracted from the non-inverting signal, V_+, it is important to ensure that $V_+ > V_-$. Unless the system is able to support negative voltages, failure to comply with this would cause the op-amp output to remain at zero volts. This is why the bridge bias, discussed above, must be kept constant. As long as the bias does not change, the relationship $V_+ > V_-$ will hold and the op-amp will function properly.

The amplification factor is determined by two gain setting resistors as shown in Fig. 3.3.7. These resistors connect between the input and output and between the input and ground. Since these are connections between the input and ground, the op-amp's input impedance is significantly lowered. High input impedance is important as it increases accuracy; therefore the amplification is typically performed in three different stages. The first stage is strictly differential with unity gain while the second and third stages perform the amplification. A two stage amplification is preferable because op-amp performance decreases with increasing gain. For example,

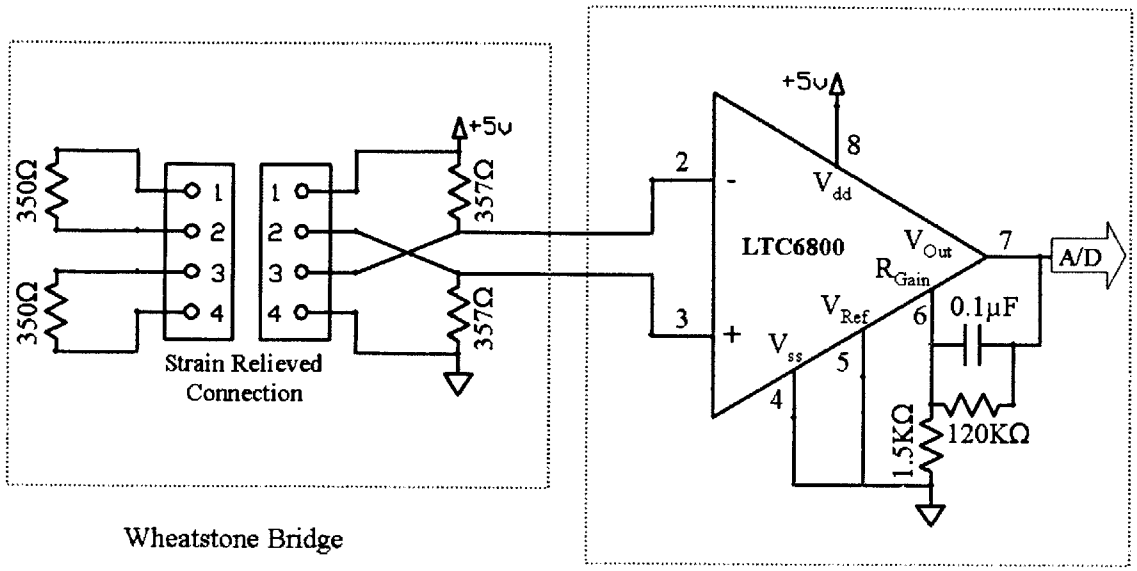

Figure 3.3.7: Schematic of the Wheatstone Bridge and Amplifier. $V_{Out} = 81(V_+ - V_-)$

the common mode rejection ratio (CMRR) decreases and the input offset voltage increases with higher gain. Implementing a dual stage gain maximizes the amplifier performance. Luckily all these stages come prepackaged as a unit called an instrumentation amplifier. These components allow for high gain without loss of performance characteristics.

The gain should be determined by the maximum amount of strain expected and the effect of resistance tolerances. Firstly, the nominal value of V_{out} is 45.5mV as determined from Eqn. 3.3.4. Because of resistor tolerances, this nominal voltage can vary by $\pm$7mV. The maximum strain occurs when the actuator is at stall torque. Assuming that the reaction torque is applied externally on the strain member, the maximum strain is found by substituting Eqn. 3.3.3 into Eqn. 3.3.7 and letting the quantity $F(L - x)$ be equal to the stall torque. A stall torque of 2.8N-m[1], a gage factor of $GF = 2$, and $V_{in} = 5$V leads to $\Delta V_{out} = 8.1$mV.

The maximum value for V_{out} occurs at full strain when resistance tolerance errors cause the nominal voltage to be 52.5mV; this yields $V_{out} = 60.6$mV. After amplification, the signal will be routed to an analog to digital converter which uses 5V as

[1]the actual stall torque of the actuator is 1.4N-m but it goes through a 2:1 gearing

its full scale voltage reference. In order to make full use of this scale, V_{out} should be amplified to 5V yielding a gain of 82.5. Using common resistor values, it is easy to achieve a gain of 81. The minimum value of $V_{out} = 38.5$mV and occurs under no load. With an amplification of 81, the minimum voltage output is 3.12V. This defines the desired active range for the analog to digital converter.

With the gain determined, we can now determine the voltage at the output of amplifier as a function of resistances and applied strain. Because of the bridge bias discussed earlier, $V_2 > V_1$, V_2 is wired to the non-inverting input terminal and V_1 to the inverting terminal. The relationship between the input and output is given by

$$V_{\text{out,Amp}} = \left[1 + \frac{R_6}{R_5}\right](V_2 - V_1), \tag{3.3.8}$$

Where R_5 and R_6 are the gain setting resistors. Now, by re-examining Eqn. 3.3.7 we see that $R_1 = R_4$ and $R_2 = R_3$. Simplifying and substituting for $-V_{out} = V_2 - V_1$ above yields

$$V_{\text{out,Amp}} = \left[1 + \frac{R_6}{R_5}\right] V_{\text{in}} \left[-2\frac{R_1 R_2}{(R_1 + R_2)^2}(GF\varepsilon)\right]. \tag{3.3.9}$$

Applying Eqn. 3.3.3 gives

$$V_{\text{out,Amp}} = \left[1 + \frac{R_6}{R_5}\right] V_{\text{in}} \left[-2GF\frac{R_1 R_2}{(R_1 + R_2)^2}\frac{F(L-x)y}{EI}\right]. \tag{3.3.10}$$

The strain measurement is taken on the compression side of the beam thereby yielding a negative strain. Because of the coordinate system chosen, this is reflected by $y < 0$. The sign of y negates the sign change caused by $-V_{out} = V_2 - V_1$ therefore yielding a positive output voltage.

The instrumentation amplifier selected is the LTC6800. This component allows rail-to-rail output swings which is important because the amplifier and the analog to digital converter reference the same voltage. If the output had a limited voltage range, the full scale of the conversion would not be used and resolution would be lost. The physical size of this component was also important. One amplifier is needed for each strain measurement yielding a total of six amplifiers. These units are available

in MSOP form factor which is much smaller than other standard package sizes such as SOIC. This diminished size prevents the amplifier from having a significant impact on board size and simplifies the printed circuit board design.

3.4 Joint Angle

Fortunately the sensors available for joint angle are much simpler to choose from than for tactile sensing. Though there is a dizzyingly broad selection of sensors available, they can be easily grouped together by their operating principles. Conveniently, the sensors in each one of these groups that are suitable for this application share similar properties as far as resolution, cost, size and ease of installation is concerned. The sensors examined can be categorized as optical, magnetic and resistive.

3.4.1 Joint Angle Sensor Selection

Optical

The most common type of optical angle encoders sandwich an encoder wheel between a light source and light sensor. The encoder wheel alternatingly permits and prevents light from passing through it. The light sensor picks up these changes and outputs digital pulses corresponding to the transmission of light. By counting the number of pulses output from a known position, one can determine the angle of the shaft. Direction of travel is determined by quadrature encoding in which the encoder wheel is divided into two parts which transmit and block light at the same frequency but different phases. This configuration not only allows one to determine the direction of travel but also increases the encoder resolution.

Optical encoders can be very accurate and commonly offer resolutions under 0.1 degrees. This resolution comes at a price though as the three parts of the optical sandwich can make a bulky package which complicates the mechanical design. Additionally the support circuitry is more complicated than that for other sensors. Optical encoders are usually wired to a decoder chip which communicates to a counter. To

obtain the joint angle, the counter must transmit its data to the processor where the count is converted to a useful form. Though optical encoders can yield good measurements, there are other sensors that are better suited for this application.

Magnetic

Another class of sensors relies on the detection of either magnetic or electric flux. The output shaft is equipped with a certain configuration of magnets or current carrying wires which cause either a changing magnetic or electric flux respectively. This change is then detected by a specific IC. The resolution of these sensors depends on a number of configuration specifics but can vary from one degree to 0.001 degree. In the simplest form, this sensor requires only one magnet and an IC so the package can be fairly small. However this setup is highly sensitive to shaft misalignment or external magnetic fields. Moreover depending on the chip, the magnetic decoder IC can output either a count proportional to angle or two sine wave proportional to angle. In the latter case, the processor must execute trigonometric functions to determine the angle. While magnetic encoders can be an acceptable option, they are not as convenient as resistive based options.

Resistive

A hollow shaft potentiometer was chosen to measure the joint angle. Hollow shaft components rely on an external shaft to be inserted into them to provide the rotational actuation. This property was desirable as it would allow the potentiometer to mount directly to the output shaft thereby simplifying the mechanical design. Moreover, by measuring the angle directly at the output, true output position can be determined despite nonlinear effects such as backlash. Potentiometers either provide a continuous signal over a limited angle range or a discontinuous signal in a continuous rotation configuration. The discontinuity is a dead band in the output; in the sensor selected the dead band is 27 degrees. Although the joints will have a limited range of motion, all the hollow shaft potentiometers found were continuous rotation. Since a continuous rotation component is the only option, the dead zone must be addressed. At a

minimum, the output pin will need to be tied to a pull-up resistor to prevent the signal from floating while in the dead zone. With the exception of this area, the potentiometer provides a continuous analog signal so the resolution is determined by the digital interface quantization.

3.5 Direction Sensing

Direction is most easily sensed by an electronic compass. These modules are solid state components that measure the direction of the earth's magnetic field. Some of the commercially available packages are built for high end use and offer great accuracy, fast response time, and tilt compensation. This vehicle is not intended to head in a very precise direction so accuracy to within a few degrees is acceptable. Even among the slowest compasses, response time is rarely above 50ms. While this limits sampling to 20Hz, the vehicle body frequency is well below that so control should not be hindered by this limitation. Since the error can become large for angles greater than 10 degrees out of plane, tilt compensation can be important if the sensor is taken out the horizontal plane. Unfortunately tilt compensated compasses are generally large and expensive so one without this feature will be incorporated into the design. One module sold by Parallax not only fits the required specifications but is design to be serial peripheral interface (SPI) compatible. As this is a common form of device communication, this sensor would be simple to interface with the processor.

3.6 Torque and Current Sensing

As covered above, strain gages offer the ability to sense the torque applied to a member. The torque the actuators apply to each joint is best measured by strain gages since they are accurate and simple to implement. Since the circuitry to support them already needs to be designed, choosing these sensors presents limited electrical complications. This does impact the mechanical design though as the strain members have to lend themselves to good readings and easy gage installation.

One important consideration though comes from examination of Eqn. 3.3.3 and Fig. 3.3.4. Strain gages measure applied torque if the location of the x-y origin is known. For example, a vertical torque applied at joint x could lift up joints $x+1$ and $x+2$ or instead could lift up joint x and $x-1$. The outcome depends on body orientation and environmental conditions. This has the effect of moving the x-y origin depending on which segments move. Picture someone trying to push a car. If the car is in neutral the vehicle will move and the person's feet will be the anchor point. However if the car's brake is engaged and person pushes hard enough, their feet will slide on the ground while the car's wheels are the anchor point. The same line of thought applies to this robot; as the anchor point moves, so does the x-y origin. By installing a strain gage at each end of the beam though, one can determine where the support is and thus get a more accurate vehicle torque profile.

Current at any location can be measured by using a current sensing IC. These chips are installed in series with the location to be measured and have an output voltage proportional to the current sensed. The voltage can then be read by the processor through an analog to digital converter. The system voltage can be read directly by the processor through the converter as well.

3.7 Support Circuitry Design

3.7.1 Analog to Digital Conversion

Conversion of an analog signal to digital form is commonly done using successive approximation methods whereby each digital bit is calculated and transmitted in series. The number of bits the A/D breaks the signal into corresponds to the resolution of the conversion. An A/D compares the input signal to a reference range; the broader the reference range is the worse the resolution of the A/D will be. For example, a reference range from 0V-5V for an 8-bit conversion would yield a resolution of 19.5mV. Some A/D's allow a differential input with reduced range. This allows one to obtain the full bit-wise resolution for an arbitrarily adjusted reference range. The A/D

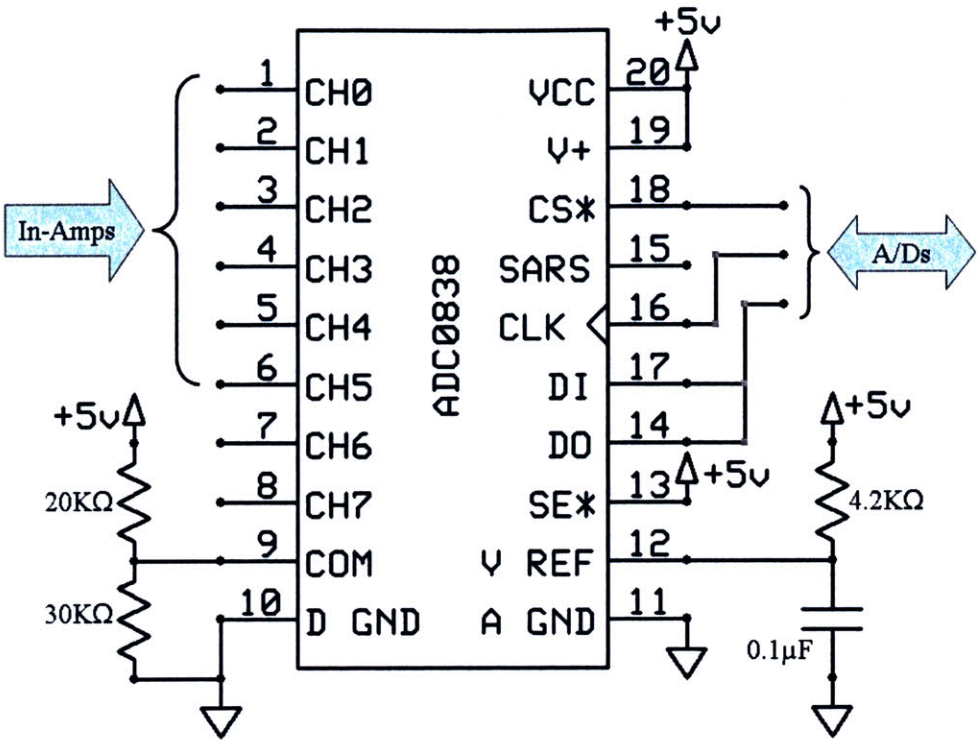

Figure 3.7.1: This configuration provides the full 256-bit resolution over a 3V-5V range.

output is a truncated integer given by

$$AD_{\text{out}} = (2^n - 1)\,\frac{V_{\text{in}} - V_{-\text{ref}}}{V_{+\text{ref}} - V_{-\text{ref}}} \tag{3.7.1}$$

where n is the number of bits the A/D uses, V_{in} is the signal voltage, V_{-ref} and V_{+ref} are respectively the lower and higher end of the reference voltage range. For an 8-bit A/D, the output can vary from 0-255.

Given the amplifier output range calculated above, an 8 bit A/D would yield a resolution of 7.8mV. The maximum applied torque causes a voltage swing of 656mV at the output of the amplifier, or 84 digital values at the A/D output. This yields a measurement error of 0.0285N-m. Referencing the mechanical design, this means the maximum error in sensed force is 0.34N which is within the tolerance specified in §3.1.2.

Each of the analog signals needs to be converted to digital form for the processor.

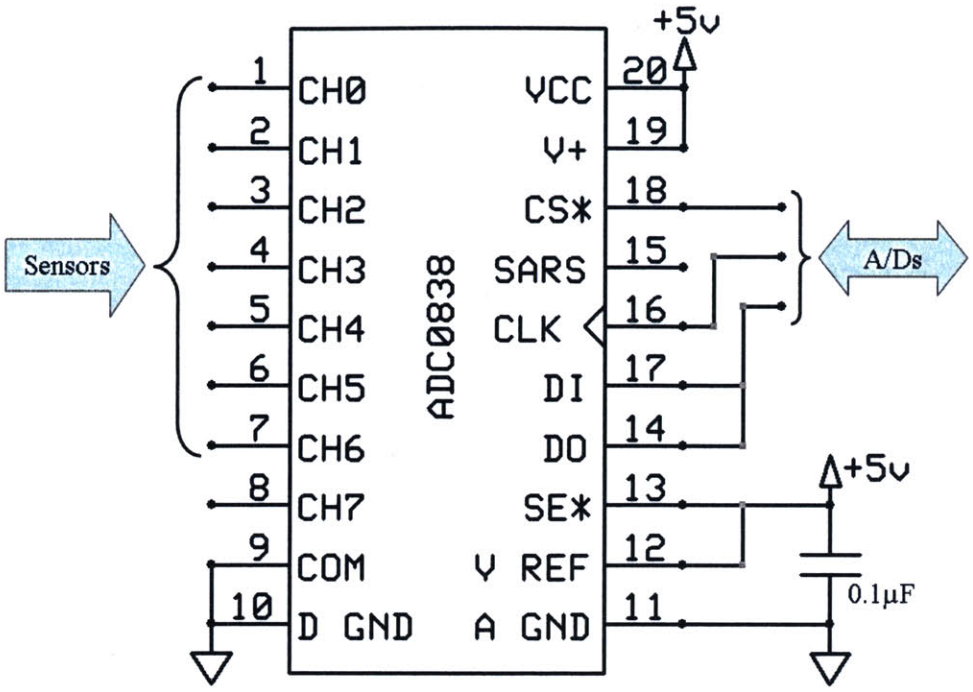

Figure 3.7.2: This configuration provides the full 256-bit resolution over a 0V-5V range.

The six Wheatstone bridge signals and the other seven sensors could cause significant signal routing issues unless the A/D conversion was consolidated. A multiplexer serves as a kind of relay station. It receives several signals as inputs and can recreate each one at its output one signal at a time. Multiplexers can communicate with external peripherals thereby allowing one to select the input channel that is relayed to the output. In this manner several signals can be consolidated into one. This relaxes the requirements on processor pins required and the number of A/D's required.

The analog to digital converter chosen was the ADC0838. This component is an 8-bit successive approximation unit. While higher resolution in the form of a 12-bit or 16-bit unit would yield more accurate torque measurements, the advantages of greater accuracy were unclear. Without the ability to control to the higher resolutions, the benefits of greater accuracy are largely lost. This component has a built in eight channel multiplexer so two of these units would satisfy all the conversion needs of the system. Additionally it is capable of supporting a reduced span with differential input. One of the A/D's can be configured to have a span of 3V-5V for the strain

readings while the other can interface with the sensors that use the full 0V-5V range. Schematics of both these configurations can be found in Fig. 3.7.1 and Fig. 3.7.2. Lastly, this model supports the digital SPI communication standard so it is easy to interface with most processors.

3.7.2 Interrupts

Interrupt capability, as the name suggests, is the ability for an event to flag the processor and interrupt its current task. The ability to support interrupts would facilitate communication as one joint would not be held up waiting to either transmit data to or receive data from another joint. When an interrupt has been triggered, the process jumps into a specified routine written to handle that event. After completion of the interrupt routine, the processor returns to its prior task. This assumes that the processor is capable of supporting interrupts which will be ensured during the processor selection.

The majority of the communication occurring in the vehicle will be among the head module and the body joints. The robot is designed to support 16 joints including the head. Allowing the head to interrupt any of the joints would therefore require a wire bus running throughout the robot connecting the head to each processor's interrupt pin. If all these connections were made directly, 15 I/O pins on the head module would be dedicated strictly for interrupt control. This would become cumbersome for larger vehicles as the head processor's pins would be usurped by the interrupts and the wire bus would become bulky.

This situation can be avoided by using a decoder like the MM74HC4514. Just like an A/D can encode 256 different states using 8 bits, an 8-bit decoder deciphers 8 bits into 256 states. For the purposes of this vehicle, only 15 states need to be decoded. A 4-bit decoder utilizes four input lines to differentiate between 16 different states. Each of the output states is tied to an output pin on the decoder. This would allow the head processor to dedicate only four lines for all the interrupts. A four line bus would then need to be wired through the vehicle and connected to each module. Additionally each joint requires a decoder whose appropriate output pin is

connected to the local processor's interrupt pin. For example, the interrupt pin for joint 13 should be connected to the decoder's output pin for state 13. Unfortunately this requires each joint's circuit board to be wired differently; specifically, each joint's processor interrupt pin connects to a different decoder output pin. Providing this connection after the board is manufactured is the only way to solve this problem. Therefore each board must allow one to easily make a connection between any decoder output pin and the interrupt pin. This connection is the white wire seen in Fig. 3.8.1A.

3.7.3 Power Supply

The power requirements of this vehicle necessitate two voltage sources, a low current source of 5V and a high current source greater than 6V. The 5V source will be used to power all of the electronic components such as the processor, A/Ds, amplifiers etc.; these devices should draw approximately 250mA - 300mA. The 6V source will be used to drive the actuators which can each draw up to 3A. This source can be greater than 6V, but the desired working torque of the selected actuators (see §4.3) require at least 6V.

As stated in §3.1.4, the source should be capable of providing power for a minimum of 10 minutes. Under proper operating conditions, none of the actuators should be exerting full torque for entire test cycle so the initial requirement of 1A-hr per joint was revised. Assume any joint of the 16 link vehicle that is in contact with an obstacle is exerting full torque. Further assume a minimum body frequency of 0.1Hz and at least three obstacle contacts at all times. Over the course of a one minute test then, each joint exerts full torque in the horizontal plane for 11 seconds. Joints however also exert torque in the vertical plane, though much less than their full range. Also, this number should be adjusted to account for the torque distribution through the vehicle. For example, if joint i is exerting full torque then we can assume that joint i+1 and i-1 are exerting 50% torque. Factoring in this distribution plus the power for the electronics leads to a power requirement of 0.3A-hr per joint with a peak supply rating of approximately 6A.

A distributed power supply was implemented where each joint had its own ded-

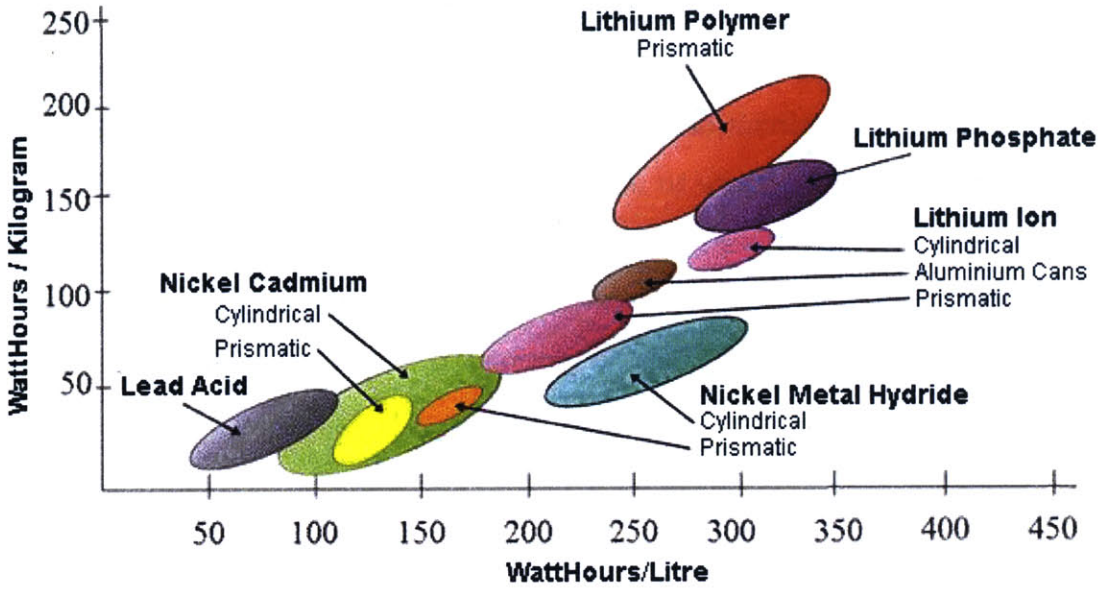

Figure 3.7.3: Lithium polymer batteries contain the most power for a given weight or volume. [42]

icated battery. This configuration was chosen because of the potential power consumption of each joint. If a central power supply was used with wires connecting to each joint, the bus cables would need to support at least 50A. Running cable through the vehicle that is able to support these high loads would add undue weight to the robot with little benefit. Not only does installing a battery on each joint eliminate bulky wiring but, one can examine the power consumption of that particular module with respect to the rest of the vehicle as well.

There are many battery technologies to choose from and, like most applications, the important features to consider are volume, weight, power and cost. Common metrics for measuring battery performance are the ratio of power output to mass and to volume. These characteristics are displayed in Fig. 3.7.3 where lithium polymer batteries are clearly superior with regard to these metrics. Another important characteristic of batteries is their discharge curve. Fig. 3.7.4 shows that this type of battery experiences a small drop in voltage during a 6A[2] discharge rate. The voltage rate of decrease is approximately a constant 1V/(A-hr) until the battery is nearly depleted when it undergoes a rapid drop in voltage. The voltage given is for a single

[2]referred to as a 5C discharge in the graph

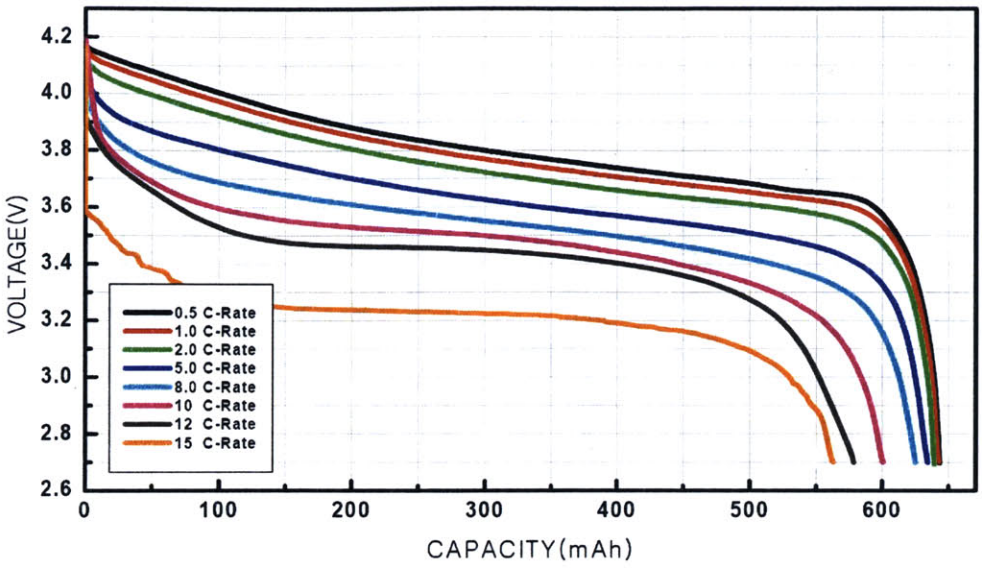

Figure 3.7.4: The voltage of lithium polymer batteries drops slowly as they are discharged. [22]

cell unit but these batteries are commercially available as two or more cells wired in series; this doubles the voltage thereby putting the batteries within the desired specifications. Though these batteries offer many benefits, they sustain permanent damage if they are discharged below 2.5V per cell. The damage can be catastrophic as the lithium can break down, release a flammable gas and combust. Therefore is important to monitor the voltage and prevent discharge into this region. Despite this problem, these batteries are still superior to others for this application; so, the Kokam 2 cell 560mA-Hr battery pack with a nominal charged voltage of 8.4V was chosen.

One can use the battery voltage to create the 5V supply needed for the electronics by using a voltage regulator. A voltage regulator converts a higher voltage into a stable lower voltage with minimum power losses. When choosing a regulator one must determine the voltage dropout, ripple and current requirements. Voltage dropout refers to the minimum supply voltage the regulator requires to maintain a stable output. A dropout voltage of 1V for a 5V regulator would mean the batteries could not discharge below 6V without disrupting the 5V supply. A higher dropout voltage means larger energy losses occur within the regulator; it also creates a narrower supply voltage operating range. Ripple is essentially the noise in the regulated voltage. If

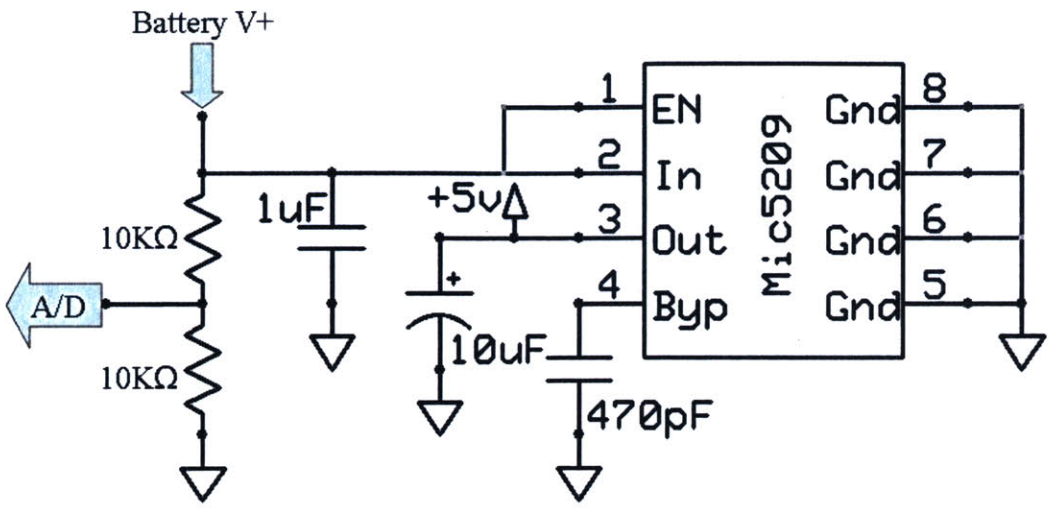

Figure 3.7.5: Wiring schematic of the voltage regulator. The battery voltage is divided by 2 to bring the fully charged voltage of 8.V within the 0V-5V range of the A/D.

the regulated voltage drops, all the analog signal voltages drop proportionally, so measurement error is not affected by ripple. The digital signals however require a minimum voltage to operate correctly. For this reason the supply voltage should stay at 5V $\pm$0.2V. Finally, the maximum current output required is between 250-300mA as determined by all the components powered by this supply. The regulator chosen is the MIC5209 which provides a 500mV maximum dropout, 1% line ripple and 500mA at the output. The thermal protection is done through the many ground pins (see Fig 3.7.5)so an external heat sink is not required.

3.7.4 Processor and Memory

The processor will need to perform some basic joint control functions and act as a communications controller. A high processor speed is desirable to facilitate high speed communication. Assuming the transmission of one bit requires three instructions, a transmission speed of 0.5Mbps would necessitate a CPU speed of at least 1.5MHz. According to Horowitz [19], the processor should be at least 20 times faster than required by communication in order to ensure proper timing within the communication standards. The processor must also support the SPI standard because the compass, A/Ds and EEPROM (discussed below) communicate in that manner.

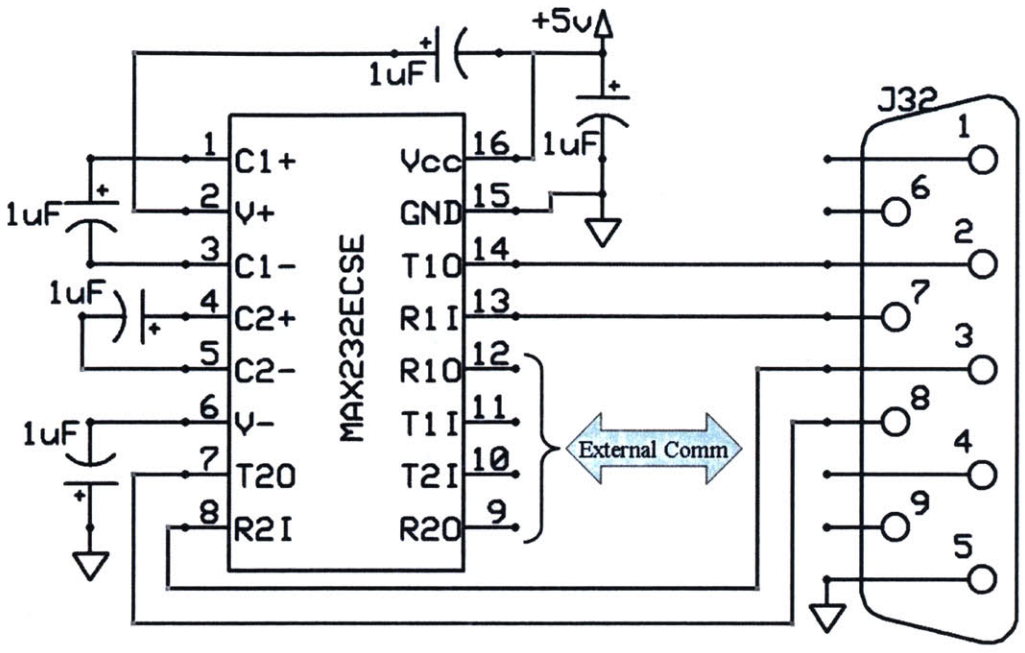

Figure 3.7.6: Wiring and pin assignments for the MAX232 serial communication converter chip.

Interfacing with Matlab requires RS-232 serial abilities; this presents an issue because the standard for RS-232 requires a voltage range from -12V to +12V. Conveniently there are ICs, such as the MAX232, that convert digital logic levels to the range required; these chips provide enough I/O pins to allow hardware flow control as well. Handshaking is desirable as it prevents one device from sending information before the other is ready to receive it. This is more important on the robot side since Matlab has a configurable input buffer size whereas the processor likely will not have an input stream buffer. Matlab supports both hardware and software handshaking but hardware is preferred because it is faster, more robust and can function well in the absence of buffers. The wiring schematic for this component is shown in Fig. 3.7.6.

The processor selected was the Ubicom SX48BD using the Parallax SX compiler. The compiler allows the processor to be programmed in S/X BASIC, an improved version of standard BASIC that has built in libraries for communication interfacing, PWM output and many other desirable functions. This processor is also available in a 48 pin Tiny PQFP (also called TQFP) surface mount package. Of these 48 pins

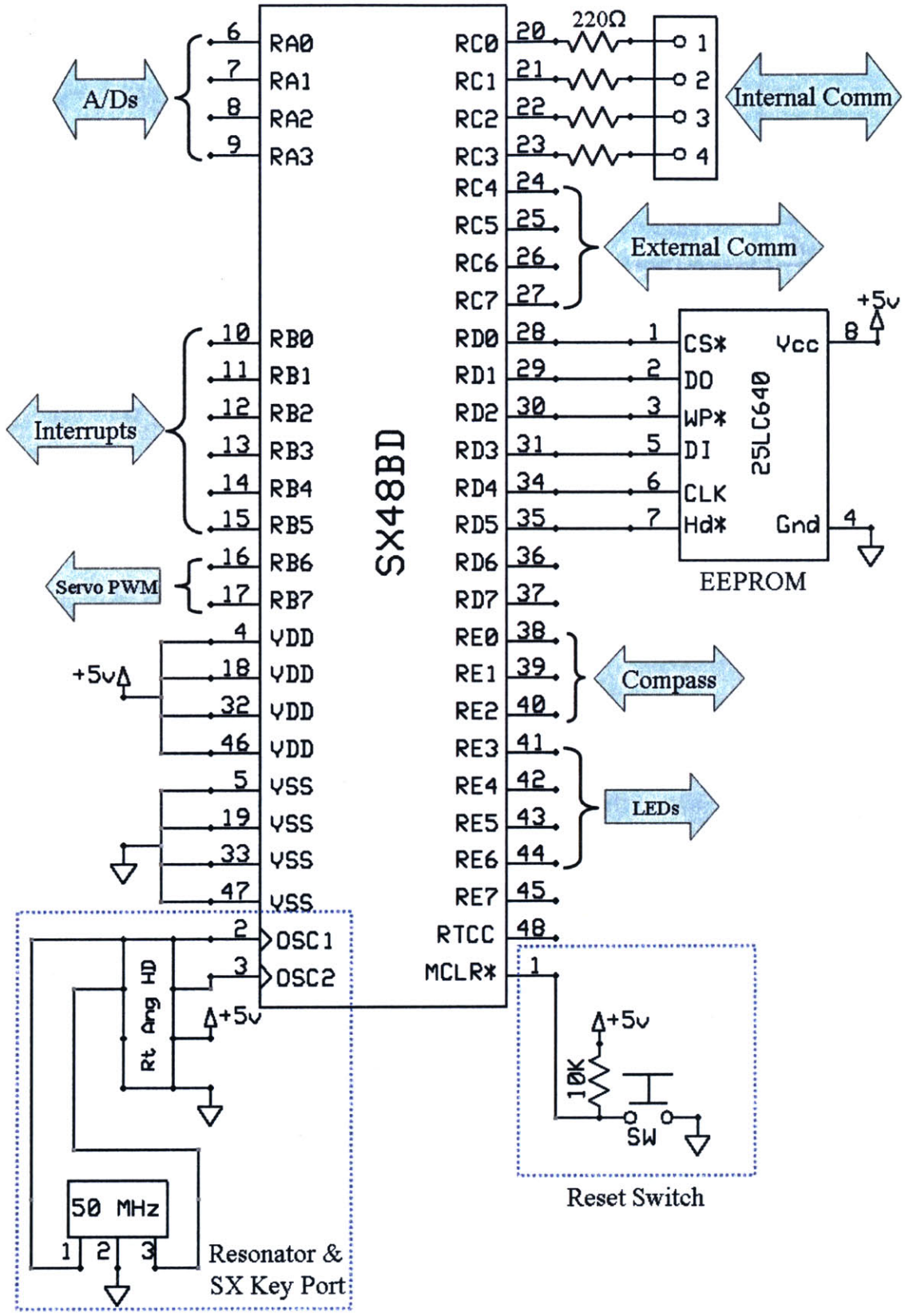

Figure 3.7.7: Wiring and pin assignments for the SX processor and EEPROM.

36 are dedicated I/O pins which are spread over four eight bit ports and one four bit port. All of the I/O pins are capable of either sourcing or sinking up to 20mA which allows a great amount of flexibility in design. Any of the pins can be used to drive multiple communication lines, LEDs or even the Wheatstone bridge if its quiescent power drain was an issue[3]. Additionally, this processor has eight pins that can trigger an interrupt so if one could implement vectored interrupts if needed.

The SX can stably run at 50MHz so no issues should arise with communication speeds. With a different external resonator this processor can stably reach speeds of 75MHz. This speed though also increases power consumption considerably, so a 50MHz resonator was used. This processor has 4K of program memory and 262 bytes of RAM which is plenty for all expected needs. However it does not fill the need for data storage of sensor values or control states. In order to record data an external memory device is needed. Towards this end the 25AA640 64K EEPROM was selected. This chip is capable of storing up to 32 bytes in its input buffer and can write at speeds of 51.2Kbps. The input buffer allows the processor to dump data on the EEPROM at will without bytes being lost. Additionally the data is static in that it is not erased when the vehicle is powered down. A wiring schematic for the processor and EEPROM is shown in Fig. 3.7.7.

3.8 PCB Layout

The layout of the printed circuit board (PCB) is very important as a good design can be corrupted by poor component and trace placement. As expected, the most important feature for any electrical system is noise prevention. By properly arranging the components and traces, one can eliminate many sources that introduce noise. One important feature to include is filter capacitors on the power supply. These prevent noise in the system from corrupting sensitive signals and should be peppered around the PCB liberally. During the layout, one should also isolate the high current components from the low current signal wires. Generally a portion of the board area

[3]This was not a concern but stated merely to emphasize the flexibility of this processor

is dedicated to high current components and the signal lines are routed away from this section. It is also advisable to avoid using the power planes for high current signals. This can be accomplished by providing a hard wired supply and return path for these lines. For components that are highly sensitive to noise, in this case the Wheatstone bridge and amplifier circuits, one can use filled ground planes. This plane connects to the board ground in a single location thereby insulating the sensitive components from the return currents of other circuitry. By implementing these minor features, one should be able to prevent common sources of noise.

As discussed in §3.1.5 the connectors must be robust to repeated movement of the cables, able to withstand vibration and shock, and able to sustain uninterrupted connection integrity. Surface mount connectors come in almost all sizes that are desired but they are not very robust. Surface mount connections are prone to breaking with repeated unplugging of the connection or with stress in the cable. Even if the connection does not completely break off, a poor solder joint could fracture and make an intermittent signal connection; this condition is very time consuming to troubleshoot. Using thru-hole connections prevents many of these issues. Since these components penetrate the thickness of the board, they are better supported and can resist much higher cable stresses. Because of the spacing of the connector pins and the board manufacturing tolerances, it is impossible to route signal traces in-between the pins. Since the connectors go through the board, they create obstacles that all traces must route around. For this reason all the connectors were placed out of the way around the edge of the board. Because of the number of connectors used, a standard 0.100" pin header was used. The mating connectors are widely available and inexpensive.

One simple rule that makes PCB layout much easier is to determine the proximity of components by the number of interconnections. This determines the majority of the layout and leaves only minor finagling of traces and pin connections to layout the board. Adding test points to the board is a good habit as they can greatly aid the debug process. The test points would ideally be big enough to attach an oscilloscope probe to but can be small enough to allow fine gage wire solder connections. Aside

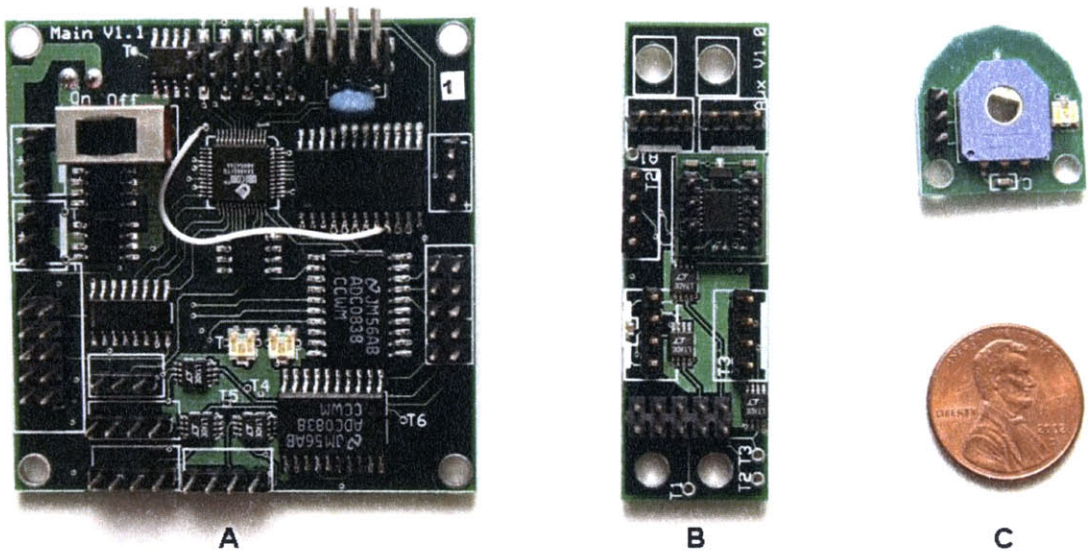

Figure 3.8.1: (A)The main PCB holds almost all the ICs. (B)This board lies in the horizontal plane and houses the compass. (C)This board mounts to the torque arm. The output shaft inserts into the potentiometer and actuates it.

from test points, indicator LEDs help with everything from debugging processor routines to determining if the module is powered correctly. Two dual LEDs were used on the board which can therefore indicate a total of nine different states.

A total of four boards were needed for each joint, one for each joint angle sensor, one for the compass, and one main board. The joint angles were determined by mounting the sensing potentiometer directly to the output shaft. The position of board for the potentiometers was allowed to move slightly during installation to prevent shaft misalignment from stressing the sensor. Since the compass is not tilt compensated, it needed to lie in the horizontal plane. The compass's board profile needed to be small so it would not interfere with the tactile sensing. As many connections as possible were located on this board to alleviate the main board. These boards are pictured in Fig. 3.8.1.

Chapter 4

Mechanical Design

4.1 Functional Requirements

The mechanical system is very dependent on the electrical system therefore many aspects of the two were designed simultaneously. The selection and placement of sensors, for example, dictate that certain features be present in the mechanical structure to allow them to be properly installed and operated. Manufacturing and assembly requirements on the other hand affect electrical characteristics such as sensor gain and operating range. This is most readily seen in the design of the strain bearing members which yield measurements to the strain gages. These members should lend themselves to easy gage installation while allowing their geometry and strain profiles to be described as a uniform cantilevered beam. The tactile sensing beams must mount to the sides of the vehicle and should protrude further than every other feature on the robot. Additionally, the construction of the robot should create a stable bottom surface for the robot. The base should prevent tipping thereby allowing lateral forces to act on the body without rotating the tactile sensors out of plane.

Martin Nilsson discusses the trade offs of designing a snake robot with torsion free joints. Though one loses control over the twisting motion in the snake, one keeps the transmission ratio of the axes constant. If joints could display relative rotations, the transmission ratio between adjacent joints would vary by $cos(\theta)$ where θ is the relative torsional angle. Additionally, allowing torsion complicates wiring in between joints.

In his paper on snake design [33], Nilsson also discusses how symmetry simplifies the kinematics of the vehicle. By ensuring that all the axes for a joint intersect at a single point, one can maximize the symmetry and reduce the number of variables needed to describe either the forward or inverse kinematics of the robot. [9]

The vehicle is designed for lateral undulation locomotion but should be able to exhibit other standard forms such as rectilinear or sidewinding motion. This requires the robot to be independently actuated in the horizontal and vertical planes which necessitates two actuators per joint. As stated above, the axis of rotation for both of the motors should intersect at a single point. Additionally, the range of motion must be at least $\pm 45^\circ$ for each axis; larger excursions up to $\pm 90^\circ$ are preferable. For lateral undulation, the goal is to maximize the force in the desired direction. If the individual joints can subtend larger angles, they can more easily manipulate the direction of their reaction force vectors. In the case of pushing against a single peg, a snake uses at least 22 vertebrae (as seen in Fig. 2.2.2) to achieve the desired reaction force vector orientation. The high number of vertebrae needed is caused by the limited range of lateral articulation the joints can display. With 22 vertebrae, a snake can exhibit up to 220° of body curvature, whereas a robot capable of $\pm 45^\circ$ could display the same curvature with five joints. By making each joint in the robot more flexible, one can imitate the body postures required without needing as many vehicle joints.

To enable different forms of locomotion, each actuator should have enough torque to lift at least two adjacent joint in the vertical plane. For lateral undulation around a single peg, one joint at time will provide the propulsive force required to overcome friction and move the snake forward. Though the propulsive force is only produced at one point, at least three points of contact are required to counteract the moment created on the body. As the robot moves forward, these points of contact progressively move to the rear of the body. In order to maintain all points of contact while demonstrating a forward progression of three link lengths, the vehicle must have a minimum of six links. Therefore, each horizontal plane actuator must supply at least enough torque to overcome the friction (F_μ) between a six link vehicle and the en-

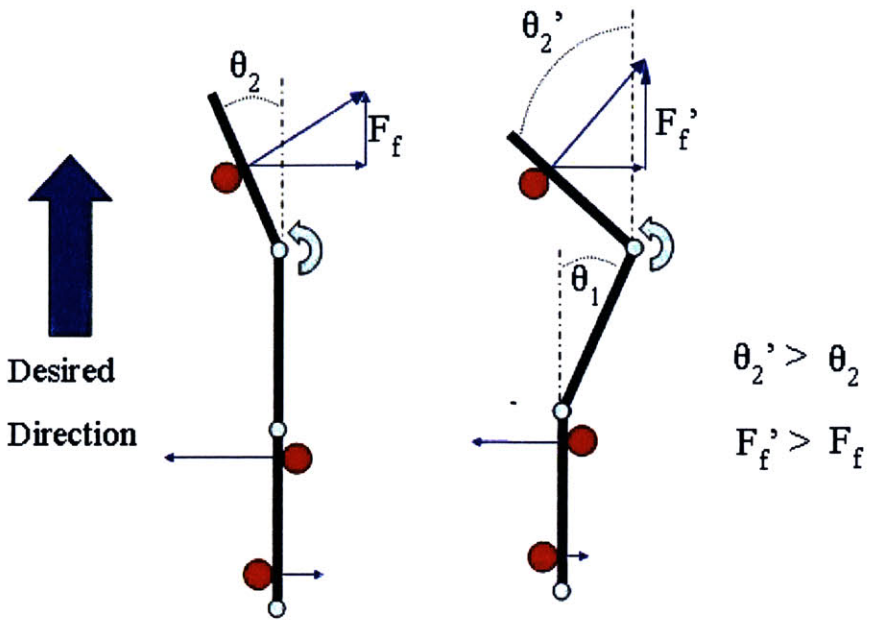

Figure 4.1.1: By adjusting the angle of adjacent joints, the robot can increase its contact angle with an obstacle thereby increasing the reaction force's component in the desired direction.

vironment. The magnitude of the force vector component in the forward direction (labeled as F_f in Fig. 4.1.1) depends on the angle of contact between the link and obstacle (θ_2). As this angle decreases, the forward force component also decreases because $F_f = F_R sin(\theta_2)$. For a single link mechanism, θ_2 would define the operating window for the joint because $F_f > F_\mu$ must be met for forward movement to occur. However, θ_2 can be changed by altering the relative angles of adjacent joints as shown in Fig. 4.1.1. For approximately the same actuator output torque, this adjustment has the effect of increasing the forward force component[1] as shown by $F_f' > F_f$. To minimize the body manipulation required, the desired operating window is $22.5° \leq \theta_2 \leq 45°$, half of the joint's range of motion. To a first degree approximation this limits the necessary manipulation to $0° \leq \theta_1 \leq 22.5°$ and gives guidelines for the actuator torque required.

While designing the parts, it is important to design around the manufacturing processes available. The geometries desired should lend themselves to simple CNC mill

[1]This assumes that the point of contact on the joint is about the same.

or lathe operations. Designing features that require an EDM, waterjet or similarly exotic tool to manufacture raises costs, increases lead time and limits outsourcing options. Additionally, tolerances should be within the expected capabilities of these machines. Components that require precise placement should utilize pins for positioning and screws for fastening. Slop in the assembly should be minimized by using locking or vibration resistant fasteners. More generally, the overall construction of the vehicle should permit easy assembly and allow simple installation or removal of modules to the vehicle.

4.2 Mechanical Overview

A model of the joint assembly as initially designed is shown in Fig. 4.2.1. The final version contains changes to correct issues discovered while testing (see §4.3). Referencing this figure, the tactile sensors mount to the bumpers which form the sides of the robot and the internal torque gages mount to the torque arms. The labeled torque arm is on the top side of the robot to prevent external frictional forces from affecting the torque measurement. The base structure was designed to have a flat bottom surface to prevent the vehicle from tipping onto its side. Without this feature the robot would be unstable during vertical motion. Additionally for lateral undulation it is important to maintain the orientation of the bumpers so they may contact the obstacles. Wiring is not shown here in order to clearly display the mechanical components. Most wires were attached to the structure by thin cable ties to prevent them from tangling or catching on something from the environment. Whenever possible commercially available parts were chosen to reduce the manufacturing effort required.

The mass of each joint is 390 grams with a distribution as shown in Table 4.2.1. The center of mass is located along center of the link 0.8cm below the bottom servo motor, as pictured in Fig. 4.2.1; the length of each link is 15.1 cm. With this information we can calculate the torque required to lift joints in the vertical plane; as Table 4.2.2 shows, the torque required grows quadratically with the number of joints lifted.

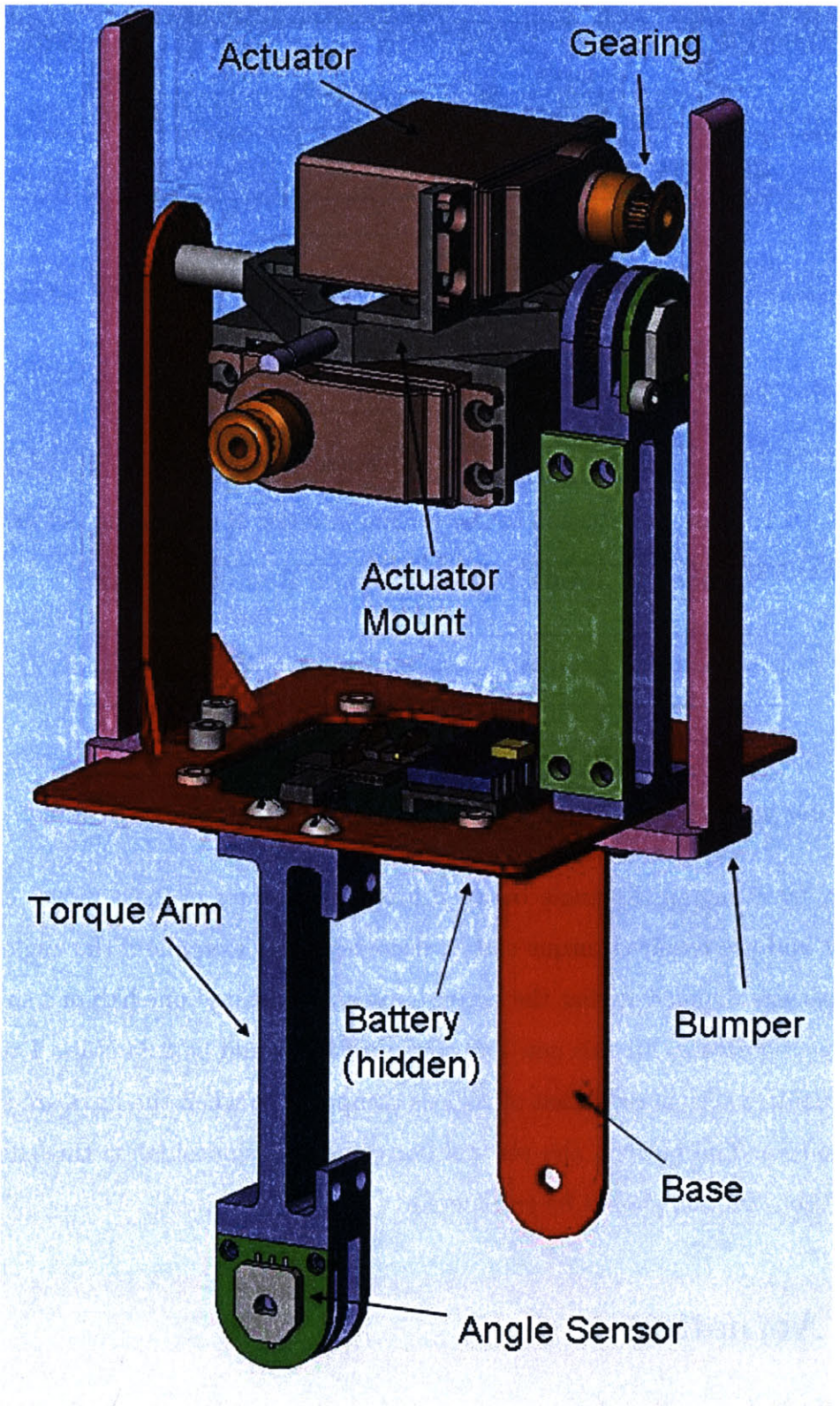

Figure 4.2.1: Link assembly shown with a belt-pulley configuration but without wires, sensors, fasteners or the felt pad.

Part	Qty/Joint	Mass [g]
Servo	2	60
Bumper	2	25
Arm	2	22
Base	1	31
Battery	1	30
Gear Set	2	15
PCBs	1	24
Fasteners + Misc	N/A	16
Joint	1	15
Servo Bracket	2	6
Cables	N/A	10
Shaft	4	2
	Total	390

Table 4.2.1: Mass distribution of the vehicle in order of decreasing net weight.

Number of Joints Lifted	Torque Required [N-m]
1	0.45
2	1.47
3	3.09
4	5.26
5	8.00

Table 4.2.2: Torque required to lift straight joints in the vertical plane.

However, by changing the angle between joints, the center of mass moves closer to the pivot and the required torque can be decreased. For example if the angle among three links was changed so that the body shape approximated one half of a sine wave, the torque required to lift this new link configuration would be 2.34 N-m. This represents a required torque reduction of 25% as compared to when the links are striaght. During sidewinding motion, the vertical body shape is sinusoidal so this effect is of practical concern and should be considered.

4.3 Actuation

The method of actuation depends on many factors, most important of which is the torque output. In order to laterally undulate, the snake must overcome its body friction to achieve forward motion. Ignoring internal joint friction, the external friction

is the only force the actuator must compensate for to progress forward. The torque required to overcome friction is:

$$\tau_r = \frac{\mu_s mgd}{sin(\theta)} \tag{4.3.1}$$

where μ_s is the coefficient of static friction between the robot and the environment, m is the mass of the robot, d is the distance from the point of actuation where the robot contacts an obstacle, and θ is the angle between the joint and the desired direction. To determine the torque required we will first assume that the robot can imitate real snakes and achieve $\mu_s = 0.2$ by using low friction materials. With a vehicle mass of 390 grams[2] one can determine the torque required as a function of d and θ. In §4.1 we placed a lower bound of $\theta > 22.5°$ to limit the range of actuation where a propulsive force is created. For a six link vehicle, Eqn. 4.3.1 reduces to $\tau_r = 12d$ where τ_r is in N-m and d is in meters. As d represents the length of the bumper plus an offset, we see that there is a direct relationship between the maximum output torque and the maximum length of the bumper.

Actuation could be performed by either a brushed or brushless motor. Brushless motors require an inner commutation control loop and are inherently more complex to work with than brushed motors. They are appropriate where high efficiency is desired as the lack of a mechanical brush reduces the internal friction; however for this application simplicity is more desirable than efficient performance. There are plenty of options within the brushed DC motor category. Typical values of maximum torque for these motor, as sold by Maxon Motors, are anywhere from 1 mN-m to 9 mN-m depending on its size[3] and the applied voltage. These motors then require a gear head and control circuitry. Using a planetary gear head about the same dimensions as the motor would allow up to a 370:1 gear ratio producing an output torque range of 0.37N-m to 3.3N-m. DC motors are generally connected to an H-bridge and driven by a pulse width modulated (PWM) signal. All this hardware can be installed as

[2]This is somewhat misleading as the design process was iterative. The actuator torques effected the maximum vehicle mass and vice versa; however, here we present it as a linear process.

[3]The diameter of the motor was limited to 25mm and its length to 40mm.

#	Make	Model	Mass [g]	Volume [cm^3]	Torque [kg-cm]
1	Airtronics	94359	62	29	14.4
2	Cirrus	CS-600	148	113	24.0
3	Expert	SL851	145	130	13.1
4	FMA	S500	153	113	21.5
5	Futaba	S3801	108	92	14.0
6	Futaba	S5301	125	92	21.1
7	Hitec	HS-815BB	152	115	24.7
8	JR	DS8550	58	25	13.6
9	KoProPo	PS-2144FET	54	31	13.0
10	Multiplex	65377	158	108	18.4
11	Tower	TS-80	152	115	24.7

Table 4.3.1: High Torque Servos.

separate components or purchased as an off-the-shelf package. To keep the design simple, a commercially available servo motor was chosen. Prepackaged servo motors are available as a single housed unit that contains the motor, transmission and control circuitry. The input is done through a three pin connection for power, ground and a PWM signal. These modules, however, do not use the PWM signal to control velocity; rather they convert the signal into a desired output position and control the motor to the desired position. While using a servo motor is much more convenient from a design perspective, one must deal with the internal position control loop on the software side.

Most of the servos commercially available are hobby servos meant for RC operation, however many meet the specifications desired. A comprehensive compilation of the available models are available online (see [8]) and the specifications for the highest torque models are included in Table 4.3.1. A variation of torque density was used to compare their performance, specifically a dimensionless metric defined as:

$$P = \frac{10 * Torque^3}{Mass^3 Volume} \tag{4.3.2}$$

where 10 is merely a factor to scale P. The form of this metric was created to reward servos for desirable traits such as output torque and penalize them for undesirable traits such as mass and volume. The powers serve to emphasize the importance of

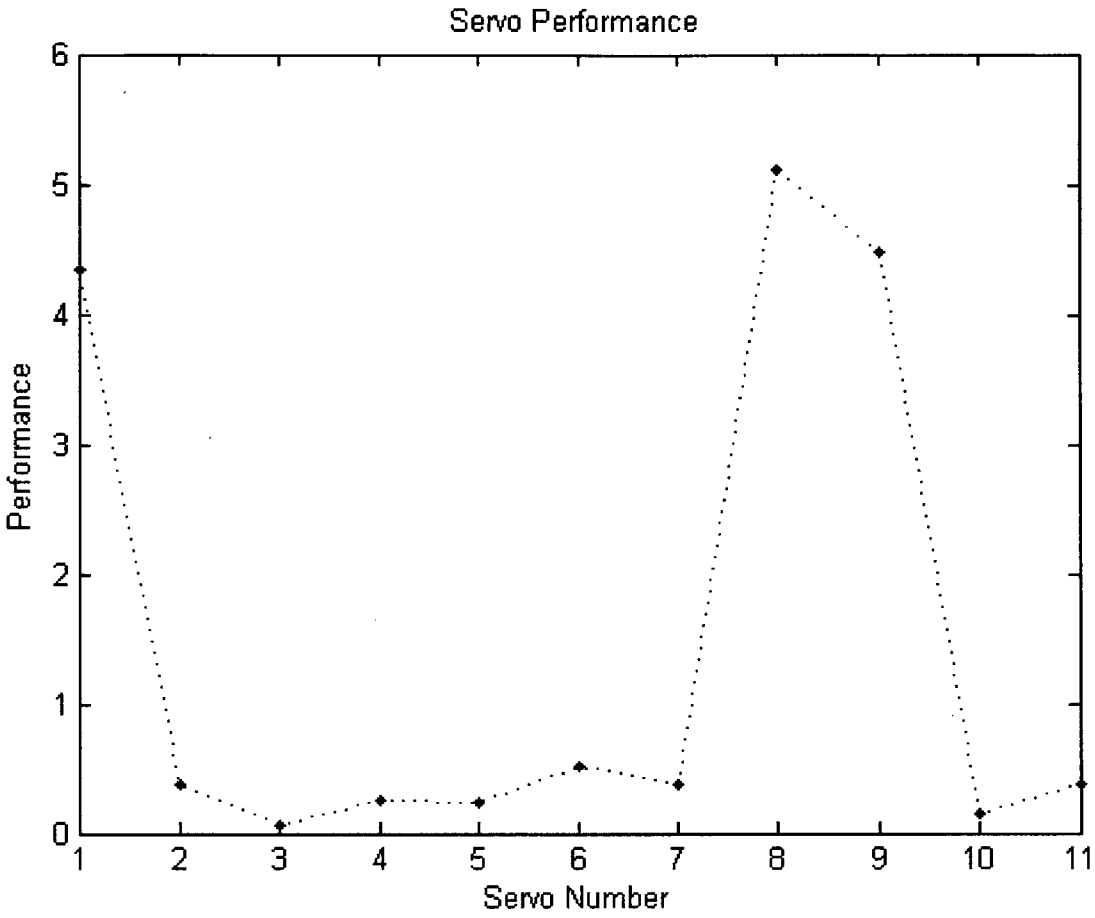

Figure 4.3.1: Servo comparison of the models in Table 4.3.1.

certain traits, here torque output and mass drive the decision much more than volume does. Fig. 4.3.1 shows the application of this metric to the servos in Table 4.3.1.

Though the KoProPo servo performance metric was higher, the servo chosen was the Aitronics 94359 because it incorporates a heat sink, internal metal gears and ball bearings. This servo has a maximum torque of 1.4 N-m and by applying Eqn. 4.3.1 the maximum bumper length is 11.7 cm. With this bumper length though, the worst case scenario would lead to no motion as the applied force would exactly equal friction. In order to produce motion and account for variations in μ_s, the torque output should be increased. The addition of a single stage gearing between the actuator and joint would accomplish this. A safety factor of two is reasonable so a 2:1 gearing on the output is the goal.

Conversely, the length of the bumper could be decreased thereby decreasing the link length. This relationship exists because the amount of empty space between bumpers should be minimized to permit continuous contact with obstacles as the snake moves. Creating a bumper of 5.8 cm would imply a link length of 8.4 cm. The space between the bumpers is necessary to provide the needed clearance for each joint to rotate by $\pm 45°$. With this configuration, the length of the torque arm would be reduced too much and would prohibit proper installation of the required strain gages. To avoid this situation, it is preferable to permit a larger link and incorporate an output transmission ratio. A transmission ratio of two is easily achievable by either a belt or gear drive system. The system was originally designed and built using a timing belt drive system because these belts virtually eliminate backlash. Additionally using a flexible member in the transmission compensates for assembly tolerances and offsets between the actuator and output.

During the testing phase the belts proved to be ineffective as they experienced ratcheting when the servo output a high torque. Ratcheting occurs when the tension in the belt is insufficient, the number of teeth in mesh is too low or the tension applied is too high. It was ultimately determined that the applied tension was out of specification for the belt thereby causing the belt's teeth to deform and skip over the grooves in the pulleys. When the belt skips, the relationship between the joint angle and the servo's position is shifted by an unknown amount. Correcting this failure required a retrofit replacing the belt-pulley system with a gear drive system. Unfortunately without an overhaul of many of the already manufactured components, it was impossible to maintain the desired gear ratio. With the center distance between the output shaft and actuator already constrained by the hardware, the only commercially available gear ratio that could be installed into this hardware was 24:23. This reduction eliminated the safety factor designed in earlier and presented certain complications during the test runs.

A model of the revised actuation assembly is shown in Fig. 4.3.2. The center joint provides a connection for both axes of actuation and allows them to intersect at the center point. This component is the connection joint between adjacent links

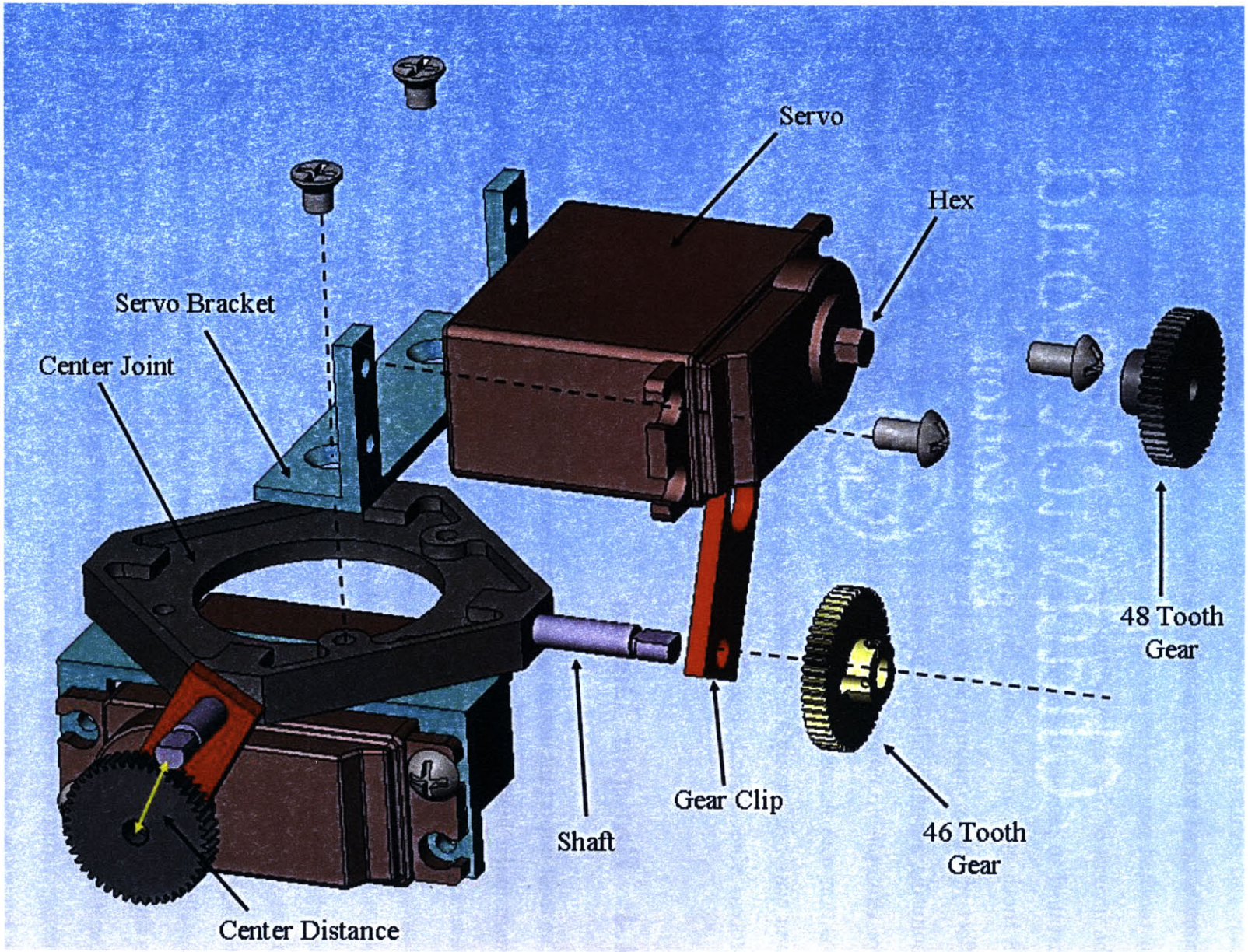

Figure 4.3.2: Exploded view of the revised servo mounting assembly with a gear drive system instead of a belt-pulley system.

and the mounting structure for the servos. The shafts are screwed into the center joint and secured with Loctite^{TM} adhesive thread locking compound. The servo is manufactured with a proprietary spline profile on the output. In order to mount the 46 toothed gear to the servo, this spline was machine into a hexagonal shape and the inverse of this was machined into the gear using a boring EDM. A gear clip was installed to prevent the applied forces from deflecting the servo shaft away from the 48 tooth gear and allowing the gear teeth to come out of mesh. The clip has the effect of dually supporting the otherwise cantilevered servo output shaft. The servo mounting assembly allows the actuator to easily be installed in a given orientation. For example, to create a symmetric maximum actuation angle from the "straight" position, the servos were installed while they were at their center position and the joint was held straight. These considerations were validated during the assembly process where installation of the servos in center position was not an issue.

4.4 Bumper Design

The most important design criterion for the bumper is that it behaves as a cantilevered beam under load. Additionally it must allow simple installation of the gages on the inner surface and the potentiometer on the outer surface. The design of bumper is shown in Fig. 4.4.1A. When the robot contacts an obstacle, the force applied will cause the bumper to deflect a small amount and develop a strain profile. Because the member is only supported at the base by four fasteners, the bumper should behave exactly like a cantilevered beam. Fig. 4.4.1C shows a finite element analysis of the stress profile on the inside surface of the beam for a force of 14.2N[4] applied at the tip. Recalling Hooke's Law, $\sigma = E\varepsilon$, one can see that the strain is linearly proportional to the stress profile. These results match the results expected of a cantilevered beam, therefore validating the general geometry of the bumper. Since the strain varies linearly along the length of the bumper, the strain applied to the strain gage over its length is not constant. This causes the resistance of the gage to vary therefore

[4]This was designed under the assumption of a 2:1 gear ratio.

calling into question the strain measurement. The question essentially concerns where the point of actual strain measurement is. Since the internal resistance of the gage varies linearly with position, it can be shown that output resistance is equal to the differential resistance at the center of the gage times a constant. Therefore the gage output corresponds to measuring the stain at the center of the gage. This is important to know as it gives the value for x in Eqn. 3.3.3.

The width of the bumper was determined by the linear potentiometer. As shown in Fig. 3.3.5, the potentiometer is constructed of a flexible membrane which is suspended over an air gap and supported on all four sides. Since the surface of the potentiometer is flush with the supports, a raised surface must be attached to the sensor to aid in actuation. An adhesive felt pad was used because it provides a soft, low friction, easy to attach raised surface (see Fig. 4.4.1A). The pad width defined the width of the conductive surface on the SoftPot^{TM}. The potentiometers were custom made for this application and with the given specifications and manufacturing constraints, the sensor was designed to be as narrow as possible. The bumper was then dimensioned to be the same width as the sensor.

The bumper was constructed from Aluminum-7075 because this alloy is light, strong and possesses good machining qualities. The Young's modulus of this alloy is up to three times higher than other alloys, which causes the beam's deformation to scale by the same factor as shown by the equation for deflection of a cantilevered beam:

$$y = \frac{Fx^2}{6EI}(3L - x). \tag{4.4.1}$$

The thickness of the beam must be defined appropriately in order to prevent the base structure from interfering with the bumper deflection. Fig. 4.4.1B shows the deformation of the beam caused by the stress profile pictured next to it. This deformation was caused by a force equal to what the robot is capable of producing. The closest point of contact between the bumper and the base structure occurs 7.5cm up the bumper's length where the clearance after deflection is 3.5mm for a beam

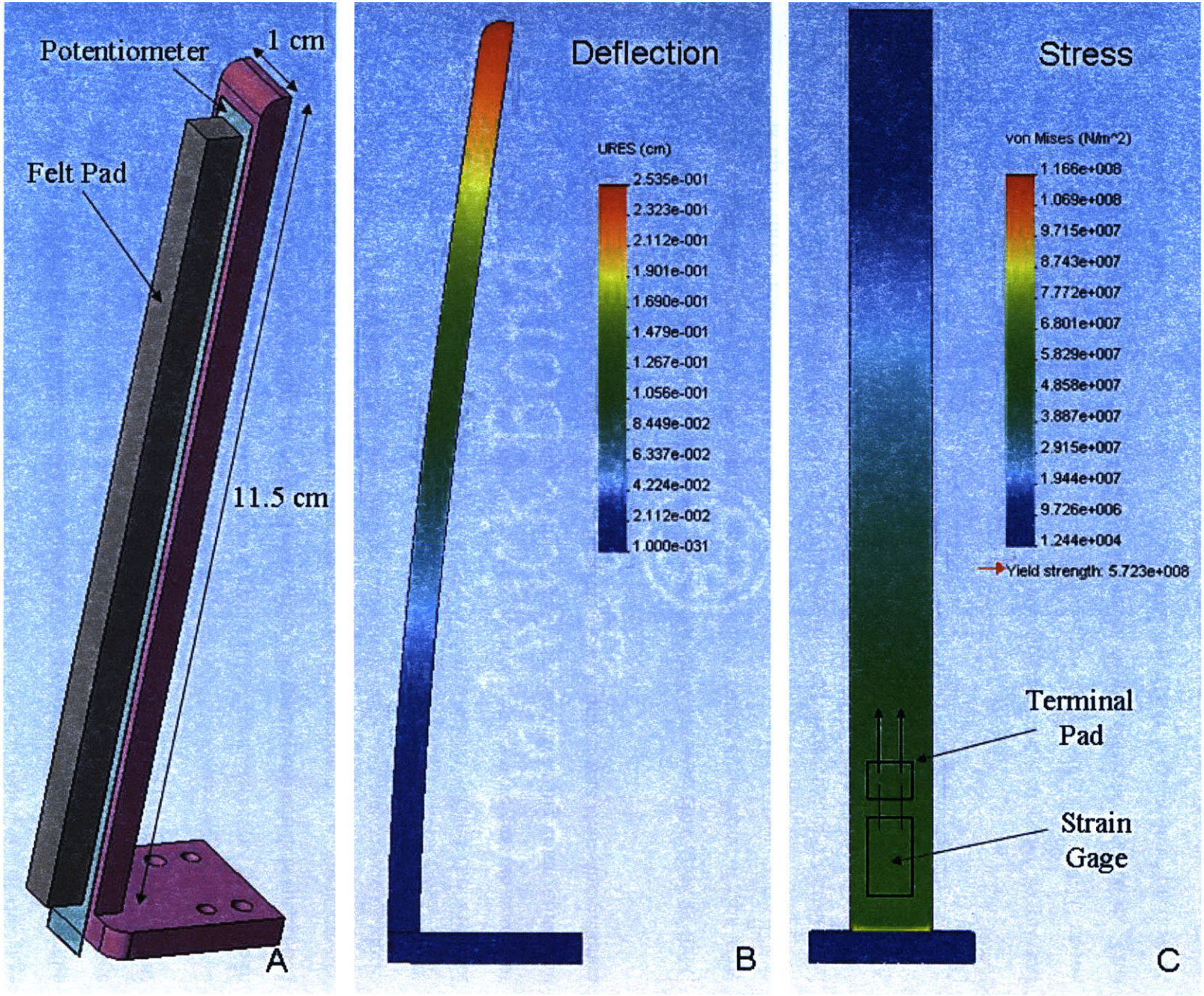

Figure 4.4.1: (A) Geometry of the bumper showing the placement of the linear potentiometer and felt pad. (B) Deformation in cm of the bumper structure caused by a a force F=14.2N applied at the tip. (C) Stress profile developed on the bumper's inner surface in relation to the strain gage placement.

thickness of 3.8mm. Strain falls off with h^3 so if the bumper was made too thick, the strain measurement would need a large amplification and therefore be more sensitive to errors and noise. To minimize this effect the thickness was defined to permit the maximum allowable deflection. The strain gages are mounted to the inside surface of the beam, as shown in Fig. 4.4.1C, by a thin cyanoacrylate glue similar to Krazy Glue. In order to protect the gage and its fine wire from stresses caused by movement of the connection, an intermediate terminal pad was used. The gage's output wires and the connectors attach to the PCB were soldered to this pad. Additionally, short lengths of the connector's insulated wires were glued to the inner surface of bumper to prevent stresses on the solder joints. This strain relief method proved to be very effective as no joints or sensors suffered any damage throughout testing.

4.5 Torque Arm

The "arm" component connects the actuator output to the joint, therefore making it the ideal location to measure the torque output of the servo. Since this component attaches to the axis of rotation it must also allow measurement of the joint output angle. Additionally, this member's lengthwise dimension lies in the horizontal plane therefore it should permit the PCB that houses the compass to mount to it.

The actuation torque acts on the arm through the dowel pins that connect the arm to the output gear. This causes a relative rotation between the servo mount and the rest of the link assembly. The shaft, which serves as the axis of rotation, screws into the servo mounting assembly and therefore rotates along with it. This allows the shaft to actuate the angle sensing potentiometer directly without the need for an intermediate coupling. In order to prevent damage to the potentiometer, the shaft must be constrained properly in both the axial and radial directions. By providing a dually supported structure for the shaft with tight tolerances, radial displacements are largely eliminated. Axial displacements can be addressed through the use of spacers and E clips as shown in the exploded view of the arm assembly (see Fig. 4.5.1). The screws that fasten the potentiometer's PCB to the arm are smaller

than the holes in the PCB. This permits the PCB's installation position to vary and accommodate assembly tolerances in both the mechanical structure and PCB construction. Also, this further reduces sources of potentially damaging stresses on the sensor. By designing the assembly in this manner, the shaft could be dimensioned to fit snugly into the potentiometer's keyed hole which is important as a tight fit minimizes the introduction of backlash.

The servo mount is attached to the base assembly by two shafts that act as pivots. Any torque output from the servo acts on the link through the gear drive. Since the gear is rigidly mounted to arm, this configuration ensures that all of the torque transmitted acts through the arm. By characterizing the strain profile induced within this member, one can then use the strain gages to determine the applied torque. This component is supported by both the base structure and the servo mount, both of which can create applied and reaction moments on the member therefore complicating its analysis as a normal cantilevered beam. While the arm behaves under stress as a cantilevered beam, the source of applied torque changes the stress profile as shown in Fig. 4.5.2 and Fig. 4.5.3. Since this member has multiple supports, one cannot be sure what end of the arm the torque is applied to without using multiple strain gages. The reason is any strain reading could be interpreted as either a lower torque applied at one end or a higher torque applied at the other. For example the strain sensed by the upper strain gage pictured in Fig. 4.5.2C could be cause by the moment pictured or by a moment of about 0.75 N-m applied at the opposite end. Attaching two gages to the arm allows one to determine the full stress profile and provides the required information to determine the magnitude of the applied torque. The gages are positioned at opposing ends of the beam and mounted in a similar manner as on the bumper.

It is desirable to minimize the deformation of arm because this deformation introduces a twisting angle between the joints. As the arm deflects, the shaft that connects to the servo mount is accordingly displaced. This manifests as a rotation of the servo mount axis, therefore creating a moderate deflection can result in significant torsion over the whole vehicle body. Increasing the thickness of the arm creates a

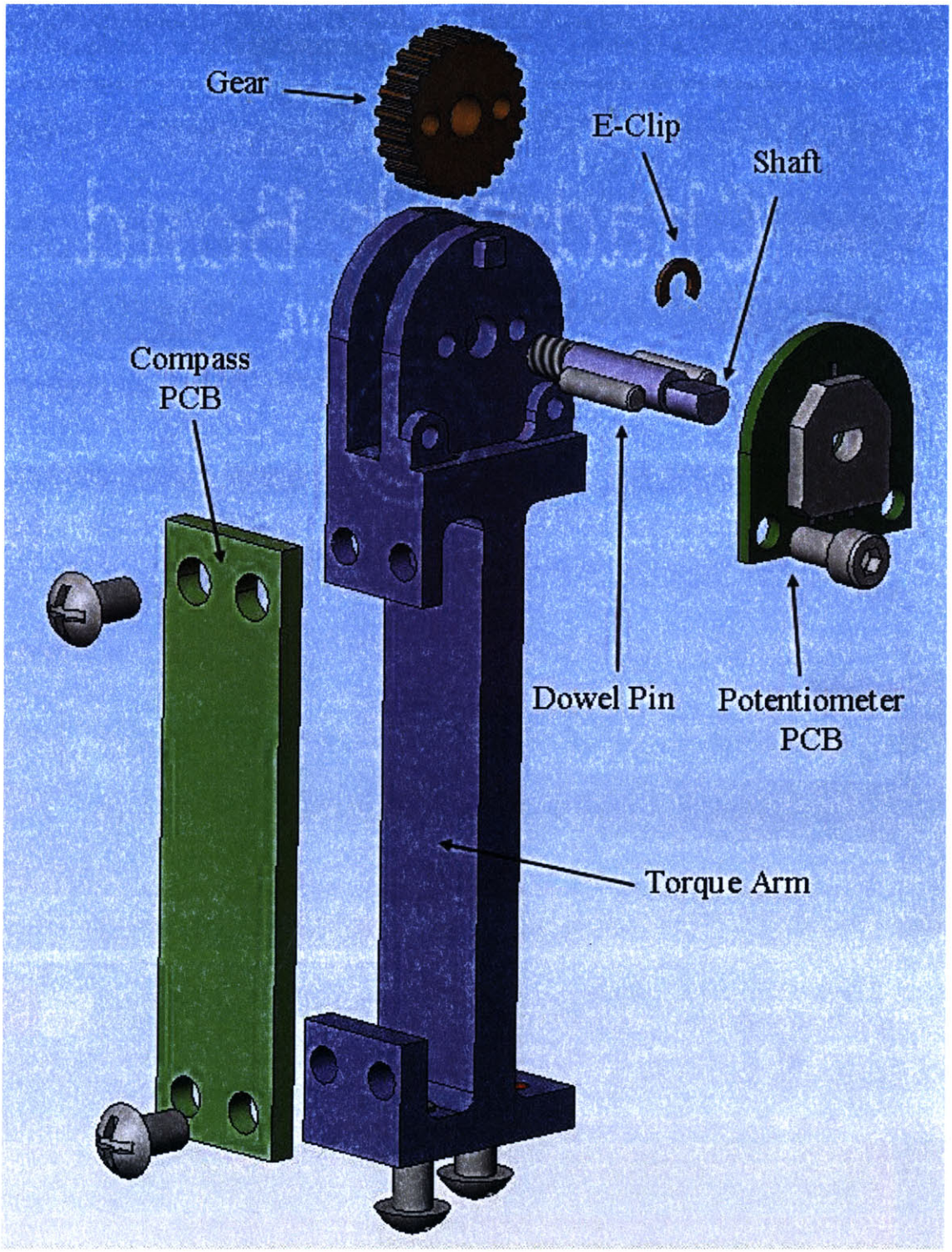

Figure 4.5.1: An exploded view of the arm assembly.

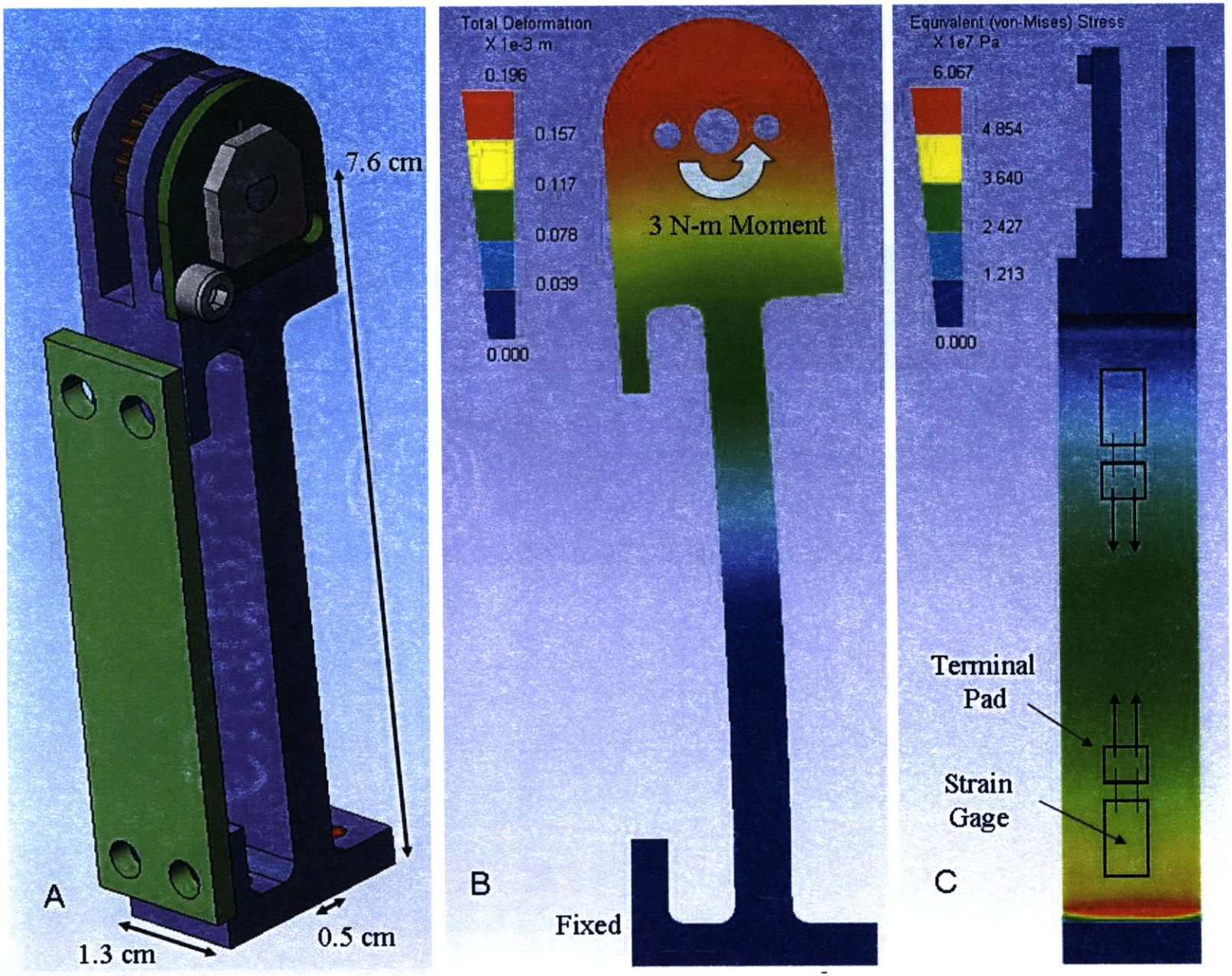

Figure 4.5.2: (A) Torque arm assembly. (B) FEA of arm deformation with displacement in meters. (C) FEA of the arm's stress profile with the applied moment at gear.

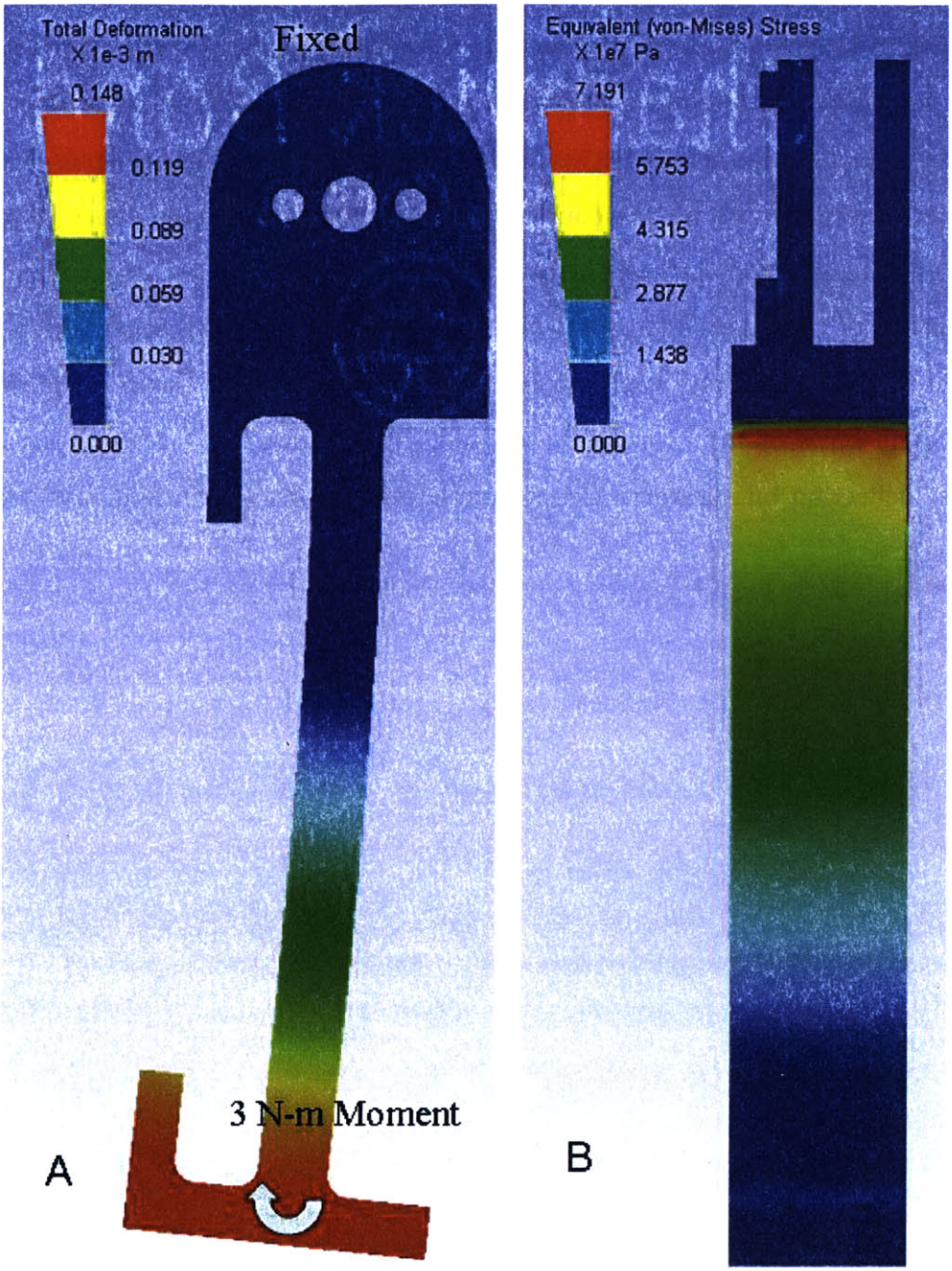

Figure 4.5.3: (A) FEA of arm deformation with displacement in meters. (B) FEA of the arm's stress profile with the applied moment at the base.

higher moment of inertia that resists the bending moment and thereby reduces the deflection and torsional angle created. The arm was made out of Aluminum 7075 and machined to a thickness of 0.5 cm. An FEA of the deformation shows a maximum deflection of 0.2mm which corresponds to a torsional angle of 0.19°. Such a small angle even when accrued over the entire vehicle is a negligible amount of torsion and does not alter the interaction between the bumper and obstacles. Despite the small deflection, the mounting for the compass's PCB incorporated a clearance to prevent any stresses transferred through the mount from damaging the board or solder joints. One surface of the board's supports is offset by 1 mm from the other which allows the arm to deflect without applying any direct bending to the board. Additionally, the through holes in the board are oversized. This allows the screws to move with the arm deflection but prevents forces from being transferred through the screws to the board.

Chapter 5

Testing and Discussion of Results

5.1 Bumper Force Validation

Before we can examine how the snake functions on a vehicle level, we must first properly characterize the systems and validate the measurements taken. The first step of this process requires us to ensure that the force sensing scheme proposed functions as expected. One module of the robot was clamped such that the bumpers were in the vertical plane instead of in the horizontal plane as designed. Various masses were then suspended from the bumper one at a time. The position of these masses on the bumper was varied in order to test the efficacy of using the potentiometer and strain gage readings to measure applied force. During this test, 255 measurements were taken at each test position by the SX at a frequency of 100Hz. As can be seen by Fig. 5.1.1, the sensed force was within the specifications outlined in the functional requirements (see §4.1). Table 5.1.1 summarizes the accuracy of the force sensing scheme. The error is independent of the location of the contact along the bumper's length but it does increase with larger contact forces. As the force of interaction grew larger, so did the maximum error and the standard deviation from the true value. The relative error, however, decreased with increasing force. Since the Wheatstone bridge is not balanced, its nominal output is greater than zero. After amplification, this leads to a quiescent digital value for strain measurement. All strain measurements must use the quiescent value as the zero point in order to determine the amount of strain sensed

by the gages. Calculation of the applied force showed a large degree of sensitivity to this quiescent value. Noise in the system can alter the nominal gage reading which in turn corrupts the measured strain value. The resulting measurement error would grow linearly with applied force as seen from the data collected. To minimize this effect, the zero point is periodically measured and reset. By averaging the force measurement over many samples, this error is virtually eliminated as shown by the mean error being constant with respect to applied load.

Applied Force [N]	7.5	15	30
Average Measured Force [N]	7.2	14.6	29.6
Max Error [N]	0.7	0.8	1.2
Max % Error	9.3%	5.3%	4%
Standard Deviation [N]	0.15	0.2	0.3
Mean Error [N]	0.34	0.28	0.36

Table 5.1.1: Analysis of the measured force applied onto the bumper to test the accuracy of the proposed force detection scheme.

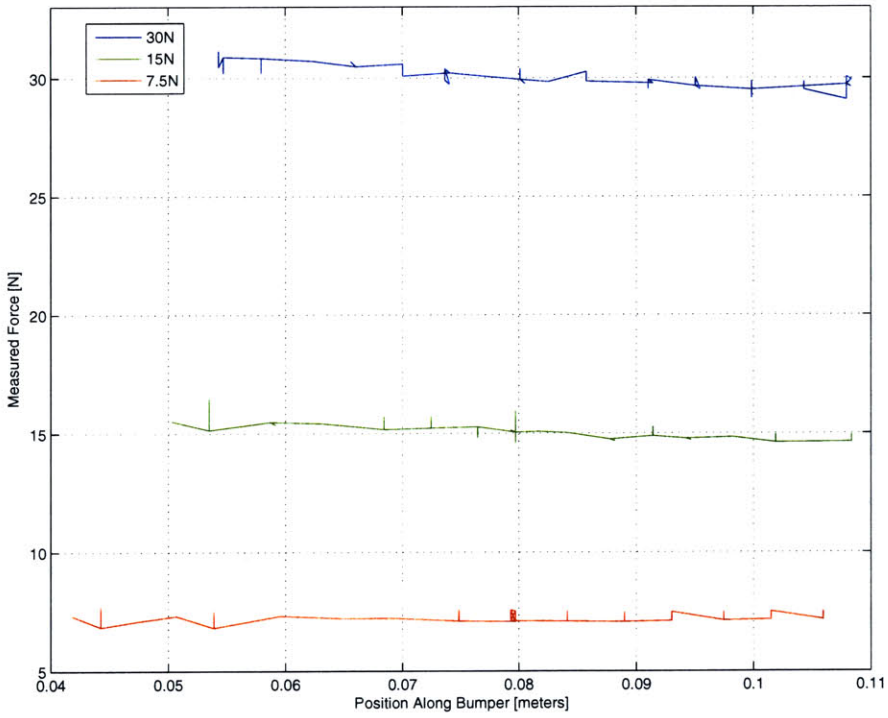

Figure 5.1.1: The measured force on the bumper as a the location of the applied force is varied.

5.2 Friction

The loss of the 2:1 gear ratio places additional constraints on the snake's ability to locomote. In order to decrease the torque required for forward motion, one must minimize the friction between the vehicle and the environment. The coefficient of friction was determined using the inclined plane method whereby the robot was placed on a horizontal platform. The angle of the platform was slowly increased until motion was observed. In this manner the coefficient of friction, μ_S is determined by $\mu_S = tan(\alpha)$ where α is the angle between the platform and the horizontal plane. The friction was varied by attaching PTFE push-on edge trim molding to the edges of the base structure and covering the surfaces that contact the ground with an adhesive backed Teflon film. These combinations were then tested on various substrates readily available; the results are summarized in Table 5.2.1. The configuration used was the edge trim with the Teflon film on the polished wood surface. This frictional coefficient is lower than that encountered by real snakes but necessitated by the absence of the gear ratio. Ball casters could have been added to the modules, similar to Hirose's work, to further reduce the friction. In an environment where the snake can move freely, this addition does not imitate wheels but rather an overall reduction in friction. This approach would be similar to snakes moving on ice as studied in [20]. Ball casters would make the vehicle more sensitive to applied forces. This would require higher force control resolution in order to maintain stability of the controller. Though friction requires higher actuator torques, it also provides dissipative reaction forces that serve to stabilize the vehicle.

	Bare	**PTFE Edge Trim**	**Trim + Teflon**
Bare Plywood	.55	.40	.34
Linoleum Tile	.46	.27	.20
Polished Wood	.31	.18	.12

Table 5.2.1: Coefficient of static friction μ_S on different substrates.

5.3 Servo Characterization

The servo is inherently a position control system where the PWM input signal is converted to a desired position. The output of the servo is connected to a potentiometer which is used as the output position sensor. Servos generally implement a PD control loop with a high proportional term in order to maintain position in the presence of external forces. The controller regulates the torque output until the difference between the actual output and the desired state is zero. In order to regulate the torque output, the relationship between the error signal and commanded torque must be determined. One can then control the output torque by reading the current position and manipulating the desired position. By examining the voltage on the internal potentiometer at different commanded positions, it was found that the wiper voltage was roughly equal to the pulse width in milliseconds as shown in Table 5.3.1. The differences between the values are well within the signal noise observed. This implies that the pulsed command is converted to a voltage from which the potentiometer voltage is subtracted to create the error signal. Given this data it seems reasonable to assume $x_d = C * t_{pwm}$ where $C = 1\text{V/ms}$ and t_{pwm} is the length of the PWM signal in milliseconds. The servo's control law can be expressed as:

$$\tau_{\text{out}} = K_P(x_d - x) + K_D(\dot{x}_d - \dot{x}) \tag{5.3.1}$$

where x_d is the desired commanded position and x is the current position. The K_D coefficient acts on the time derivative of these signals. For a slowly varying signal, this term can be ignored yielding the torque output as a linear function of the error signal. As the error signal grows, the torque generated will scale accordingly until the torque saturates at its maximum value.

To test the torque output of the servo as a function of the error signal an arm was attached to a servo. The servo was commanded to a position where the arm was horizontal. While in this position, a large mass was attached to the arm by a string. The mass was placed on a digital force plate to measure its weight. An inelastic string was then tied taught between the weight and the horizontal arm thereby preventing

Pulse Width [ms]	Potentiometer Voltage [V]	Angle [Deg]
0.63	0.631	0°
1.00	1.010	35°
1.09	1.110	45°
1.24	1.262	56°
1.55	1.571	90°

Table 5.3.1: The voltage of the servo's internal potentiometer equals the pulse width in milliseconds under no load conditions.

the arm from rotating upward without lifting the weight completely off the scale. The weight was large enough to prevent the servo from lifting it completely. This set up constrained the servo to freely move in the downward direction but prevented movement in the upward direction from the horizontal position. Therefore any torque created to move the arm upward would decrease the force between the mass and the force plate by a measurable quantity. From this measurement, the torque output of the servo could be determined. At the horizontal position the torque exerted was equal to the moment created by the arm's weight. However since x was constrained, as the servo was commanded to move upward, the error signal, $x_d - x$, would grow.

The results of this test are shown in Fig. 5.3.1. Examining the data, we see that the torque output scales linearly with the error signal until it reaches its maximum value. While the error is small the torque output is shallow compared to a larger error signal. This is likely caused by the internal stiction of the servo. The servo contains a 165:1 gearing supported by ball bearings. In order to create torque at the output, the servo must overcome the internal resisting torque. After the stiction dominated region, the torque output follows the expected trend. While the friction does change the initial area of the curve, the slope of the area we are interested in is unaffected. For the 100Hz test, the slope of the data is 5.9N-m/ms; using the conversion factor C, this indicates K_P = 5.9N-m/V[1]. This data also shows that torque output can only be controlled if the error signal is below 0.2V. While this result severely limits the ability to control the force applied another equally negative result is uncovered. The maximum torque output is 0.89N-m, well below the manufacturer specification

[1]An alternative method of characterizing the servo's controller parameters is presented in [12].

of 1.41N-m. During this test the frequency of the commanded state was varied as well. The servo manufactures recommend an input frequency of 50Hz, however it was found that a higher torque saturation occurred with a frequency of 100Hz. Attempts to increase the maximum torque by increasing the frequency of the command signal further than 142Hz resulted in the servo going unstable.

During these tests, the servo was powered by a battery kept between 7.5V-8.4V, well above the required minimum of 6V. Lowering the applied voltage to the published testing conditions did not improve servo performance but rather decreased the maximum output torque. Additional testing showed that while the working torque of the servo was much lower than expected, the servos were able to provide a larger resisting torque. In a subsequent test the servo was commanded to a constant position and a slowly increasing force was applied perpendicular to the arm. In this situation the servo was able to resist rotation caused by a maximum load of 1.76N-m. In this scenario the motor output is acting in the same direction as the internal friction so this result is expected.

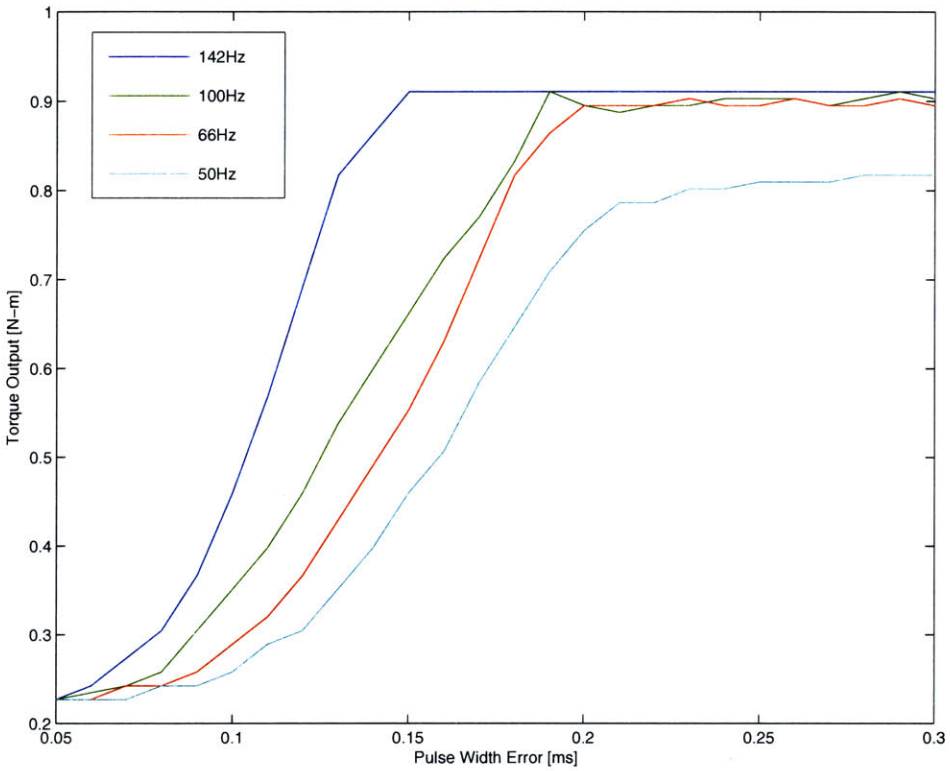

Figure 5.3.1: The torque output of the servo varies with the error signal and the frequency of the command signal.

5.4 Lateral Undulation

5.4.1 Experimental Setup

A six link vehicle was assembled to test with a lateral undulation gait. The goal is to show that this vehicle can exert a controlled force to produce motion. The snake robot will be placed in a structured obstacle environment that will provide ample contact points. As obstacle searching is outside the scope of this project, the robot will be placed in a known starting position and orientation. In this case it will start with its body length parallel to the desired direction. The obstacles are smooth and circular to provide reaction forces that are perpendicular and simple to calculate. Additionally the obstacles are spaced to allow the snake to easily lie in-between them. The ground surface is a smooth polished wood table top that was tested to have low friction with the robot. The configuration is shown in Fig. 5.4.1.

5.4.2 Results

Because the torque output of the actuators is 37% less than the stated specification, we must reexamine the operating range of the vehicle. Referring once again to Eq. 4.3.1 with $\tau_r \leq 0.80$N-m and $\mu_S = 0.12$, we find that $\theta \geq 40°$. Unfortunately this requires the vehicle to operate near the stall torque which would imply slow speeds. The amount of force applied to the obstacles can be increased by using inertial effects of the links. If a joint has rotational momentum before it contacts an obstacle, then upon impact with the obstacle, this rotational momentum will contribute to a forward impulse. Additionally, the motion of adjacent joints can be leveraged for added force. For example if joint i is pushing against an obstacle, the applied force can be increased by moving joint i-1 in the opposite direction. This creates a reaction moment on joint i which imparts a larger force on the obstacle as shown in Fig. 5.4.2.

While testing the gait, communication with Matlab occurred too slowly because Matlab's serial communication package did not respond quickly enough for real time control. Since the SX does not have an input buffer, hardware handshaking was

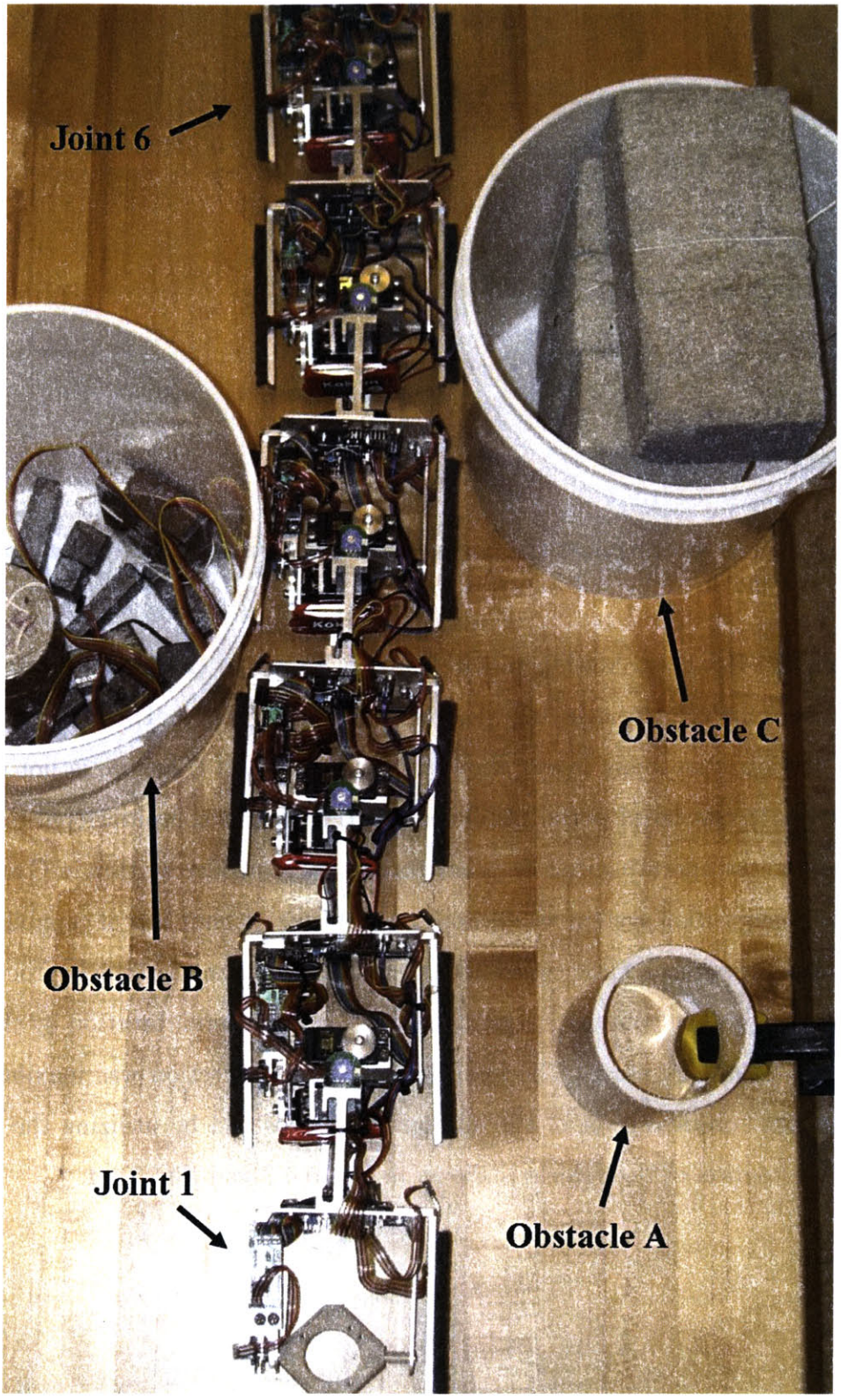

Figure 5.4.1: The robot will use obstacle A to provide the forward propulsive forces and obstacles B and C to provide reaction forces and moments.

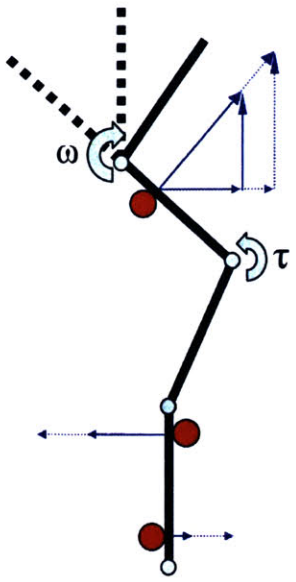

Figure 5.4.2: The force against the obstacle can be increased by the reaction torque created from moving adjacent joints.

implemented. However, Matlab required up to 500ms to change the state of the handshaking pins thereby delaying the communication greatly. This delay is caused because Matlab runs many layers above the hardware and therefore is not granted direct access to the serial ports. Additionally, the Matlab computational processes are subject to the operating system prioritization. A controller written in C and used with a data acquisition system would work much faster without loss of capability. For this situation however, a basic controller was implemented on the vehicle processor to prove the design. The controller regulates torque in the lateral direction by changing the position command error. The force in the forward direction was maximized by saturating the torque output of the appropriate servos and by utilizing the inertial effects. The motion of the vehicle is shown in Fig. 5.4.3 and Fig. 5.4.4.

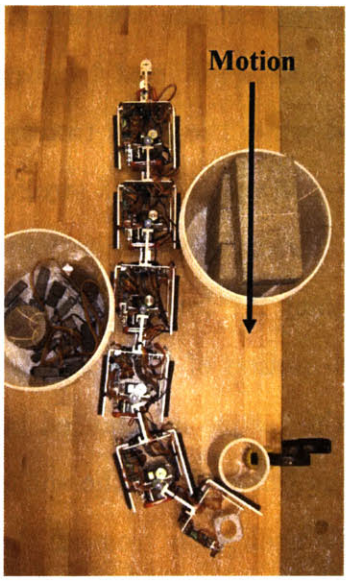

(a) Joint 1 Swings and imparts an impulse onto obstacle A.

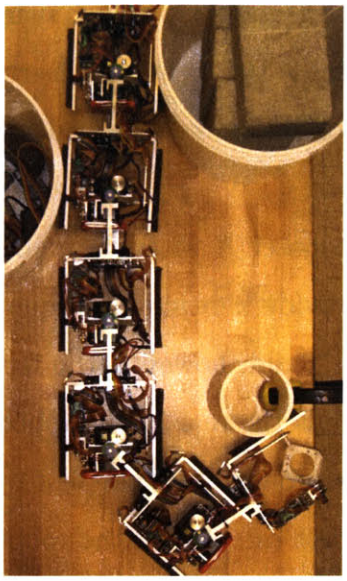

(b) Joint 1 continues to apply a force until it reaches the desired position.

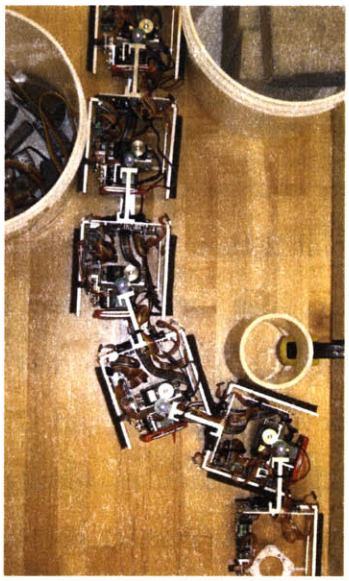

(c) Joint 1 swings clockwise while Joint 2 imparts an impulse.

Figure 5.4.3: Lateral undulation motion I.

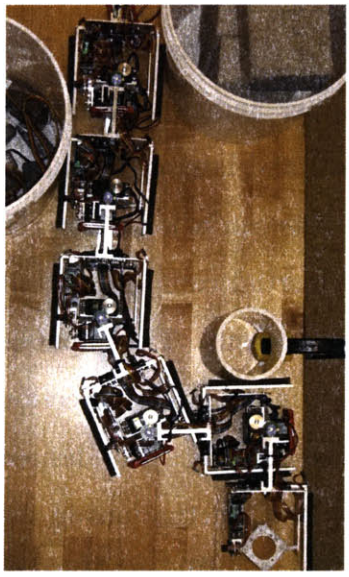

(a) Joint 2 applies a force until Joint 3 is in the proper location.

(b) Joint 2 swings clockwise while Joint 2 imparts an impulse.

(c) The snake has progressed forward and contact with obstacles B & C are lost.

Figure 5.4.4: Lateral undulation motion II.

As shown in the motion stills, joint 1 initially swings to contact the obstacle A. Joint 2 aids the motion to increase the rotational inertia of joint 1. As joint 1 moves through its motion the body of the snake is pulled forward while the body torques are countered by contacts B and C. When joint 1 has moved through its full stroke, joint 2 then swings towards contact A aided by joint 3. During this motion joint 1 rotates the other way to provide a reaction torque on joint 2. Joint 2 contacts obstacle A the same way joint 1 did; however, the forward motion of the body has moved contacts B and C towards the rear of the robot so the torque is balanced by different modules. Ideally this process would repeat over the full body of the snake but as new contact points are not established the robot pulls itself away from all the preset obstacles. The motion of joint 3 completes the process and the final position of the snake is the result of the absence of obstacles remaining in contact with the robot. The motion could not continue because this gait requires a least three contact points for locomotion to occur. Torque output limitations prevented the addition of other joints to continue the motion.

Fig. 5.4.5 shows the net forces on the vehicle during the entire motion. This was calculated by summing the forces sensed by each bumper and using the joint angle data to determine the force components in the forward and lateral directions. The large spikes correlate to the points of initial contact between a joint and the forward obstacle. This force is an impulse because of the inertial components but then diminishes to the force created by the servo's maximum torque. The impulses are seen in both directions though they are about 40% smaller in the lateral direction because of the angle between the joint and obstacle. This angle has the desired effect of creating more force in the forward direction. These large fluctuations in the forward direction force however, have a negative impact on the controller's ability to balance the lateral forces to zero. During the period from 1.2 seconds to 2.2 seconds, the force in the forward direction was about constant and therefore the lateral forces were balanced to nearly zero. However during seconds 3 - 4.5, the forward force is almost constant but does show small oscillations around a single value; in this period, the lateral forces are once again nearly zero except for similar oscillations.

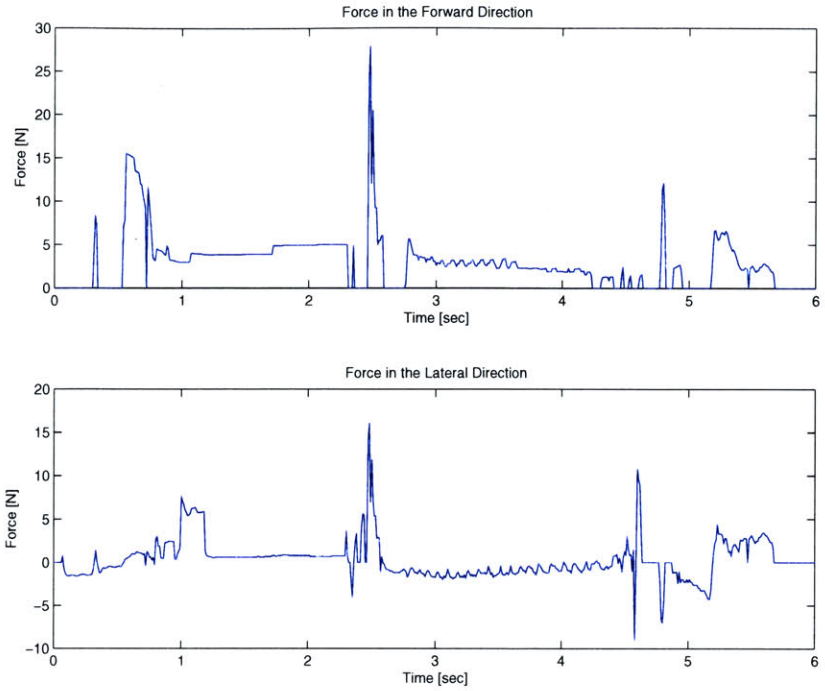

Figure 5.4.5: Net forces over the robot body during lateral undulation. The lateral forces largely cancel to remain close to zero while the forward force is maximized.

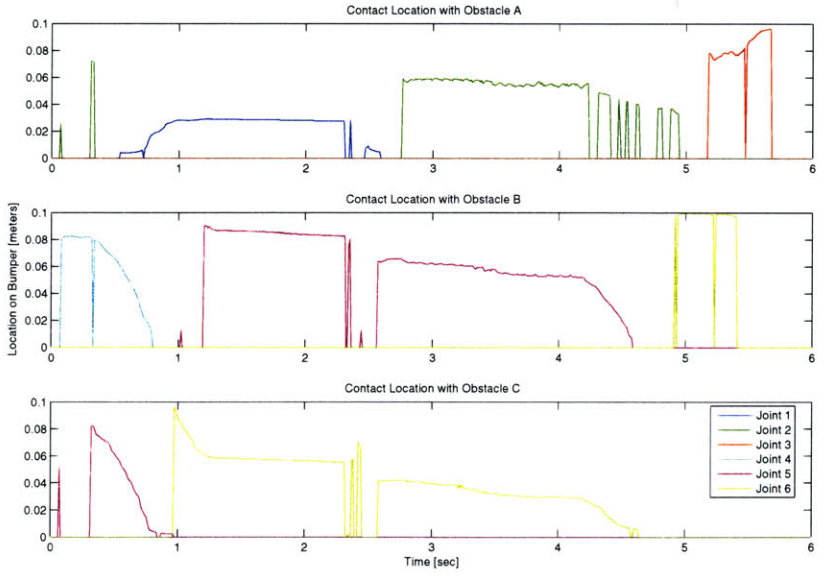

Figure 5.4.6: The location of contact with Obstacle A stays relatively constant on each joint but Obstacles B and C are moved down the length of the body.

One unexpected result was that the point of contact between a particular joint and obstacle A was relatively constant. As shown in Fig. 5.4.6, the point of contact with obstacle A remained stationary with respect to each joint instead of changing as the joint angle increased. Additionally the forward progression was largely due to the impulses imparted onto the obstacles. The points of contact with obstacle B and C move towards the rear of the vehicle as the robot progresses forward and the plot of their location does indeed show this trend. However, during the periods of constant forward force there was little forward progression. The majority of the movement occurred during or directly after the impulse contacts. This shows that the maximum actuator torque output was insufficient to provide a propulsive force, a claim that was proven during tests without the inertial input. If the vehicle was controlled to move slowly then forward progress would not occur except in a very limited set of cases. Through careful placement of the obstacles and initial orientation of the robot, forward motion could be achieved but was not robust. Adding the inertial factor greatly increased the window of operation that yielded positive results. This allowed the joint angle, θ_1, to be smaller and reduced the sensitivity of the placement of obstacles B and C. The same result could be accomplished with higher torque actuators.

Chapter 6

Conclusion

6.1 Design Evaluation

This thesis outlined the design process for constructing a robotic snake capable of tactile and force sensing. While this design was targeted towards performing lateral undulation, this does not prevent it from implementing other gaits. During the design process a great deal of time was spent on the electrical system which proved well spent as the electronics performed very well. Communication with the sensors was seamless and the processor was able to handle all the variables without issue. Using the interrupts proved vital for inter-joint communication and the common system ground prevented problems with signal reference levels. No problems were encountered with the force measurement resolution. The force sensing scheme results were very encouraging towards its ability to perform well in a more complex controller.

The attention paid to proper cable fastening and strain relieving paid off. Almost no time was spent debugging problems related to faulty sensor readings caused by poor or broken connections. While the cable assembly is somewhat chaotic it isolated the connection points from failure inducing forces and strains.

The biggest fault in the design process was the absence of a prototype construction phase for the hardware. All the electronic subsystems were tested and proved out on a breadboard to verify performance and wiring. The mechanical system, however, moved directly from design to manufacturing. Had a prototype phase been incorpo-

rated, the issue with the belt drive system would have been discovered. This would have initiated a redesign to lower the mass of the vehicle, reduce the link length, or install another method of producing the desired gear reduction. Using a 1:1 gear ratio did enable each joint to actuate by $\pm 90°$ which showed to be an important attribute for joints of this size. This highlighted the fundamental trade off between joint size and possible angle excursion. Larger joints are able to subtend bigger angles but the increased angular displacement also becomes a necessity.

During testing it became apparent that the servo's large K_P term presented significant barriers to effective control. The high proportional term causes the torque to saturate with a small error. This reduces the number of controllable states as the PWM signal can only be controlled to an accuracy of 10us. Additionally the frequency of actuation limit on the servo could potentially constrain more advanced controllers. A more appropriate actuation solution would have been to incorporate a DC motor and planetary gear head. Though it would have been more expensive, voluminous, and complicated to integrate, the reduced output torque and controllable states prevent meaningful controller from being implemented. Though a large number of snake robots utilize commercial servo motors, it has been discovered that they are not suitable for a force controlled vehicle.

6.2 Improvements

There are a handful of potential improvements to this vehicle. Aside from general improvements such as reduce the mass, size and increase actuator output torque; there are some that are more specific to this particular design. The design of the Wheatstone bridge, amplifier, A/D system was overly complicated by the resistor tolerance issue. A more appropriate solution would have been to incorporate trimming potentiometers to level out each bridge to the desired quiescent voltage. This was not initially done because of fears that joint vibration would change the setting on the potentiometer. Additionally the number of extra components required would have made the PCB layout much harder. In retrospect though, implementing po-

tentiometers would have allowed one to detect the applied strain over the full A/D range thereby increasing the resolution by a factor of 3. Though periodic recalibration would be needed, each joint could detect when this is needed by identifying a change in the quiescent levels.

Other improvements are a bit more subtle. The battery voltage at each joint was monitored by the joint local processor to prevent damage from excessive discharge. However spikes in current draw would cause the voltage to drop suddenly. Occasionally the voltage would dip below the minimum required for the voltage regulator to function properly. This would cause the processor to shut off. Since the processor controlled the servo, this would cause the servo to spasm and behave erratically until the voltage rose back to a level which allowed the processor to function. Instead of using a software based battery protection scheme, it would be better to use a hardware one. Even a simple circuit like a crowbar would suffice and prevent this behavior.

The lines for inter-joint communication connect directly to the processor and decoder. These components however have over current protection in which the input and output pins are connected to the power and ground pins through diodes. This has the effect of allowing current to travel from the I/O pins to the ground and power planes. If a particular joint connected to the vehicle is turned off while signals are sent over the inter-joint bus lines, the disabled joint may draw power and exhibit signs of being active. This has the effect of loading the communication line and corrupting the signal. This can be prevented by placing small resistors between the I/O pins and communication bus which would limit the current flow.

6.3 Future Work

There is much work yet to be done on snake robots. The dynamics associated with lateral undulation are very complex and computationally intensive. Performing the required inverse kinematics is not currently an option for real time control. Any controllers that rely on inverse dynamics or kinematics must be applied to a small robot with low degrees of freedom. As far as hardware though, the basic design of this

system provides an appropriate platform for a force controlled laterally undulating snake. The next step is to develop controllers with achievable goals. Currently the snake creates propulsive forces at a single point. By increasing the actuator torque, additional modules could be connected. This would provide the freedom needed to manipulate the body shape and exert propulsive forces at many locations. As the robot progresses forward, it will need to leverage new obstacles which would require the ability to search for and properly take advantage of new points of contact. This can be done strictly from tactile input however would be aided by a vision system. Though success with these goals would be an achievement, lateral undulation will not be successful without the development of a position-force hybrid controller scheme that can stably handle multiple points of contact. Further efforts in this field should be directed to controlling snakes with one or two propulsive force creating contacts with the hope of gaining a better insight that would lead to the development of a more flexible scheme.

Bibliography

[1] Zeki Bayraktaroglu, Fabienne Butel, and Viviane Pasqui. Snake-like locomotion: Integration of geometry and kineto-statics. *Advanced Robotics*, 14(6):447–458, 2000.

[2] Zeki Y. Bayraktaroglu, Fabienne Butel, Pierre Blazevic, and Viviane Pasqui. Geometrical approach to the trajectory planning of a snake-like mechanism. *IEEE International Conference on Intelligent Robots and Systems*, 3:1322 – 1327, 1999.

[3] Z.Y. Bayraktaroglu and P. Blazevic. Understanding snakelike locomotion through a novel push-point approach. *Transactions of the ASME. Journal of Dynamic Systems, Measurement and Control*, 127(1):146 – 52, 2005.

[4] Z.Y. Bayraktaroglu, P. Blazevic, V. Pasqui, and P. Coiffet. Towards a convivial control interface for a snake-like robot. *8th IEEE International Workshop on Robot and Human Interaction*, pages 119–123, 1999.

[5] Z.Y. Bayraktaroglu, A. Kilicarslan, and A. Kuzucu. Design and control of biologically inspired wheel-less snake-like robot. *2006 1st IEEE RAS & EMBS International Conference on Biomedical Robotics and Biomechatronics*, pages 6 pp. –, 2006.

[6] S. Bennet, T. McConnell, and S. L. Trubatch. Quantitative analysis of the speed of snakes as a function of peg spacing. *Journal of Experimental Biology*, 60:161–165, 1974.

[7] J. W. Burdick, J. Radford, and G. S Chirikjian. A 'sidewinding' locomotion gait for hyper-redundant robots. *Advanced Robotics*, 9:195–216, 1995.

[8] Randy Carr. The gigantic servo chart. 2003. Spring 2005. http://www.fatlion.com/sailplanes/servochart.html.

[9] J. J. Craig. *Introduction to Robotics 2nd Ed.* Addison-Wesley, 1989.

[10] H. Date, Y. Hoshi, and M. Sampei. Dynamic manipulability of a snake-like robot with consideration of side force and its application to locomotion control. *Proc. Int. Sympo. Adaptive Motion of Animals and Machines*, 2000.

[11] Hisashi Date, Mitsuji Sampei, and Shigeki Nakaura. Control of a snake robot in consideration of constraint force. *IEEE Conference on Control Applications - Proceedings*, pages 966 – 971, 2001.

[12] Kevin J. Dowling. *Limbless Locomotion.* PhD thesis, Carnegie Mellon University, 1997.

[13] Carl Gans. *Biomechanics Approach to Vertebrate Biology.* The University of Michigan Press, 1980.

[14] J. P. Gasc, D. Cattaert, C. Chasserat, and F. Clarac. Propulsive action of a snake against a single site: its combined analysis. *Journal of Morphology*, 201:315–329, 1989.

[15] M. Gevher, A.M. Erkmen, and I. Erkmen. Sensor based online path planning for serpentine robots. *Proceedings - IEEE International Conference on Robotics and Automation*, 1:674 – 679, 2001.

[16] J. Gray and H. W. Lissmann. The kinetics of locomotion of the grass-snake. *Journal of Experimental Biology*, 26:354–367, 1950.

[17] S. Hirose and Y. Umetani. Kinematic control of active cord mechanism with tactile sensors. *International Symposium on the Theory and Practice of Robots and Manipulators*, pages 241–252, 1977.

[18] Shigeo Hirose. *Biologically Insired Robots: Snake-Like Locomotors and Manipulators.* Oxford University Press, 1993.

[19] Paul Horowitz and Winfield Hill. *The Art of Electronics.* Cambridge University Press, 1989.

[20] Jianghai Hu, S.N. Simic, and S. Sastry. How should a snake turn on ice: a case study of the asymptotic isoholonomic problem. *42nd IEEE International Conference on Decision and Control (IEEE Cat. No.03CH37475)*, Vol.3:2908 – 13, 2003.

[21] Yan-Bin Jia. Constact sensing for parts localization: Sensor design and experiments. *Proceedings of the 2003 IEEE Intl. Conference on Intelligent Robots and Systems*, pages 516–522, 2003.

[22] Kokam. Specification for slpb 393459h3. 2004. Spring 2005. http://www.fmadirect.com/tech_data/pdfs/KOK640_15C.pdf.

[23] Sam Lewis. Lateral undulation of a robotic snake. Master's thesis, Texas Tech University, 2005.

[24] S. Ma. Analysis of creeping locomotion of a snake-like robot. *Advanced Robotics*, 15(2):205 – 224, 2001.

[25] Shugen Ma, H. Araya, and Li Li. Development of a creeping snake-robot. *Proceedings 2001 IEEE International Symposium on Computational Intelligence in Robotics and Automation (Cat. No.01EX515)*, pages 77 – 82, 2001.

[26] Shugen Ma, W.J. Li, and Yuechao Wang. A simulator to analyze creeping locomotion of a snake-like robot. *Proceedings 2001 ICRA. IEEE International Conference on Robotics and Automation (Cat. No.01CH37164)*, vol.4:3656 – 61, 2001.

[27] F. Matsuno and K. Suenaga. Control of redundant 3d snake robot based on kinematic model. *2003 IEEE International Conference on Robotics and Automation (Cat. No.03CH37422)*, vol.2:2061 – 6, 2003.

[28] Brad Moon. Testing an inference of function from structure: Snake vertebrae do the twist. *Journal of Morphology*, 241:217–245, 1999.

[29] Brad R. Moon. *Structural and Functional Integration of the Snake Axial System.* PhD thesis, University of Michigan, 1998.

[30] Brad R. Moon and Carl Gans. Kinematics, muscular activity and propulsion in gopher snakes. *The Journal of Experimental Biology*, 201:2669–2684, 1998.

[31] Holly Nash. Snake anatomy and physiology. *Online*, 1997. Fall 2006. http://www.peteducation.com/article.cfm?cls=17&cat=1831&articleid=2974.

[32] M. Nilsson. Serpentine locomotion on surfaces with uniform friction. *2004 IEEE/RSJ International Conference on Intelligent Robots and Systems (IROS) (IEEE Cat. No.04CH37566)*, vol.2:1451 - 5, 2004.

[33] Martin Nilsson. Why snake robots need torsion-free joints and how to design them. *Proceedings of the 1998 IEEE International Conference on Robotics & Automation*, pages 412–417, 1998.

[34] Karl Paap, Michael Dehlwisch, and Bernhard Klaassen. Gmd-snake: A semi-autonomous snake-like robot. *3rd International Symposium on Distrubuted Autonomous Robotic Systems*, 1996.

[35] P. Prautsch and T. Mita. Control and analysis of the gait of snake robots. *Proceedings of the IEEE International Conference on Control Applications*, pages 502–507, 1999.

[36] William Riley, Leroy Sturges, and Don Morris. *Statics and Mechanics of Materials.* John Wiley & Sons, Inc., 1995.

[37] M. Saito, M. Fukaya, and T. Iwasaki. Serpentine locomotion with robotic snakes. *IEEE Control Systems Magazine*, 22(1):64 - 81, 2002.

[38] Michael Sfakiotakis and Dimitris P. Tsakiris. A simulation environment for undulatory locomotion. *Proceedings of the IASTED International Conference on Applied Simulation and Modelling*, pages 154 – 159, 2004.

[39] Yansong Shan and Yoram Koren. Design and motion planning of a mechanical snake. *IEEE Transactions on Systems, Man, and Cybernetics*, 23(4):1091–1100, July/August 1993.

[40] Yansong Shan and Yoram Koren. Obstacle accommodation motion planning. *IEEE Transactions on Robotics and Automation*, 11(1):36 – 49, 1995.

[41] Sandra Sinclair. *How Animals See: Other Visions of Our World.* Croom Helm, 1985.

[42] Custom Power Solutions. Cell chemistries. 2005. Spring 2005. http://www.mpoweruk.com/chemistries.htm.

[43] Tamara Stephas. A physically-based model of snake locomotion using environmental obstacles. Master's thesis, University of Toronto, 1997.

[44] Y. Umetani and S. Hirose. Biomechanical study of active cord-mechanism with tactile sensors. *3rd Conference on Industrial Robot Technology*, 1976.

[45] Michael Walton, Bruce Jayne, and Albert Bennett. The energetic cost of limbless locomotion. *Science*, 249:524–527, 1990.

[46] Rainer Worst and Ralf Linnemann. Construction and operation of a snake-like robot. *IEEE Internation Joint Symposia on Intelligence and Systems*, 1996.